4 HYDRLOGY AND HYHRAULICS FLOW EXAMPLES

In this chapter, we are to present a total of 17 problems to demonstrate the design capability of WASH123D, to show the needs of various approaches to simulate flow river network and overland flow problems, and to illustrate some realistic problems using WASH123D. Section 4.1 present 7 examples to demonstrate the design capability and flexibility of seven flow modules in WASH123D. Section 4.2 includes four simple example problems to show possible differences in simulations using the kinematics-wave, diffusive-wave, and fully dynamic-wave approaches. Section 4.3 include six realistic-real world examples to illustrate the types of flow problems WASH123D can deal with.

4.1 Design Capability of WASH123D

Seven examples are used in this section to demonstrate the design flexibility to simulate hydrology and hydraulics in WASH123D. Example 1 is to simulate hydraulics in one-dimensional flows in river/stream/canal networks. Example 2 is to simulate two-dimensional overland flows in a complex topography. Example 3 is to model three-dimensional variably saturated flows in subsurface media. Example 4 is to simulate coupled one-dimensional river flow and two-dimensional overland flow. Example 5 is to model coupled two-dimensional overland and three-dimensional subsurface flow. Example 6 is to simulate coupled three-dimensional subsurface and one-dimensional river flows. Example 7 is to simulate one-dimensional river, two-dimensional overland, and three-dimensional subsurface flow problems.

4.1.1 One-Dimensional Flows in River/Stream/Canal Networks

This example simulates water flow in a channel network system in order to investigate how the change of upstream headwater would affect the downstream flow at various locations. The system was composed of five channel reaches that were connected via two junctions (Fig. 4.1.1-1). Reaches 1, 2, and 4 were 100 m long, and each was discretized with 11 nodes and 10 elements: Nodes 1 through 11 for Reach 1, 12 through 22 for Reach 2, and 44 through 54 for Reach 4. Reaches 3 and 5 were 200 m long, and each was discretized with 21 nodes and 20 elements: Nodes 23 through 43 for Reach 3, and 55 through 75 for Reach 5. In this case, Nodes 11, 12, and 23 were associated with with Junction 1, while Nodes 43, 54, and 55 with Junction 2, where zero capacity was assumed for both junctions.

Reaches 1 and 3 had a uniform channel width of 10 m, a uniform bottom elevation slope of -0.001 along the downstream direction, and a constant Manning's roughness of 0.03. Reaches 2, 4, and 5 had a narrower channel width of 5 m, same bottom elevation slope at -0.001, and a higher Manning's roughness of 0.035. Initially, the network was dry everywhere. As the simulation starts, a uniform rainfall of 10-4 m/s was applied on all Reaches. At Nodes 1 and 44, both served as upstream boundary nodes, water stage was controlled. Figures 4.1.1-2 and 4.1.1-3 depicted the time-dependent water depth controlled at Nodes 1 (single hump) and 44 (double humps), respectively. A depth-dependent outgoing normal flux, as shown in Figure 4.1.1-4, was applied at the two

downstream boundary nodes (i.e., Nodes 22 and 75). No infiltration was considered. A two-hour simulation was performed with a fixed time step size of 0.002 and 0.001 second used for time periods of 0 through 10 min and 10 min through 2 hrs, respectively. The semi-Lagrangian approach was used to solve the 1-D diffusion flow equation.

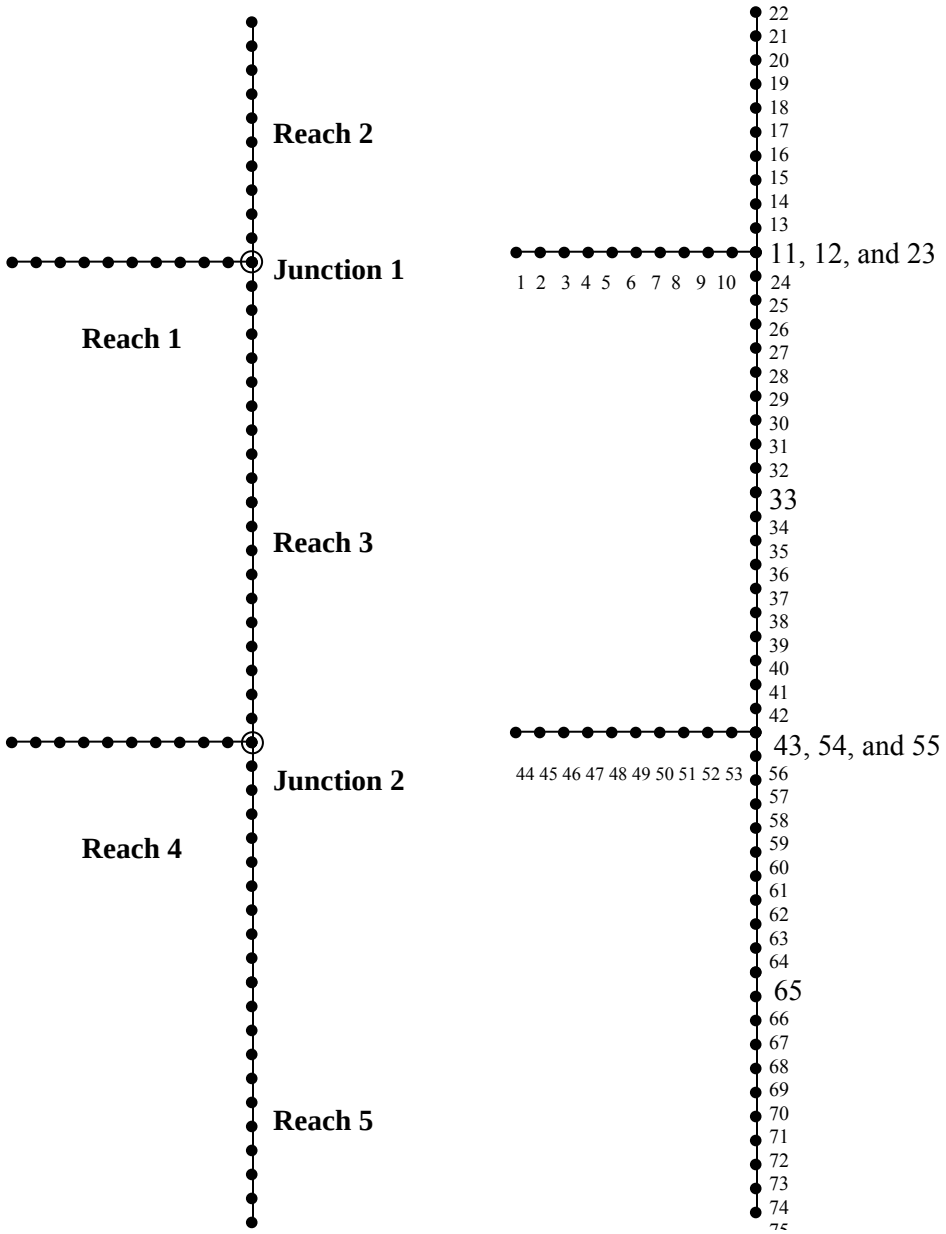

Fig. 4.1.1-1. Channel Network Configuration of Example 4.1.1

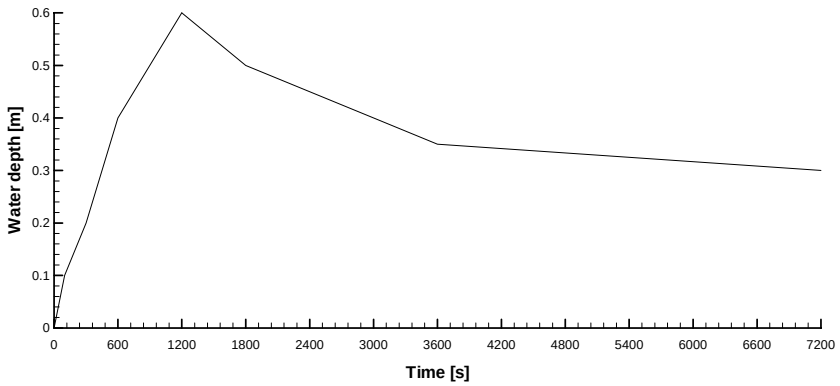

Fig. 4.1.1-2. Water Depth at Node 1 for Example 4.1.1

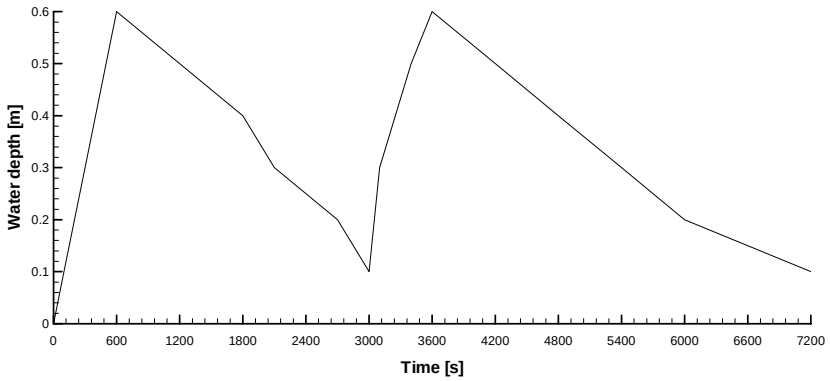

Fig. 4.1.1-3. Water Depth at Node 44 for Example 4.1.1

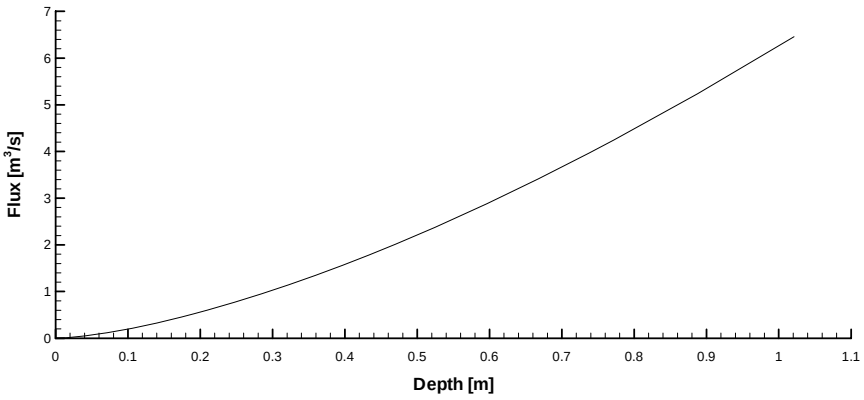

Fig. 4.1.1-4. Water Depth Dependent Outgoing Normal Flux for Example 4.1.1

Figure 4.1.1-5 plots the water stage change at nodes 5, 17, 26, 40, 48, and 70 during the simulation period. It is observed that the change of headwater at Node 44 at time = 3,000 s (i.e., the second hump) not only affected nearby downstream locations (Nodes 48, 40, and 70) but also had influence on those far-away location (Nodes 26, 17, and 5), even some of them were upstream nodes (e.g., Node 5). This result demonstrates how headwater control may impact the flow in the whole channel network system when the bottom elevation slope of the system is small (0.001 in this case). It also indicates that WASH123D can be used to deal with water management issues on a design level. Table 4.1.1-1 presents partial numerical results of water depth at Time = 7,200 s.

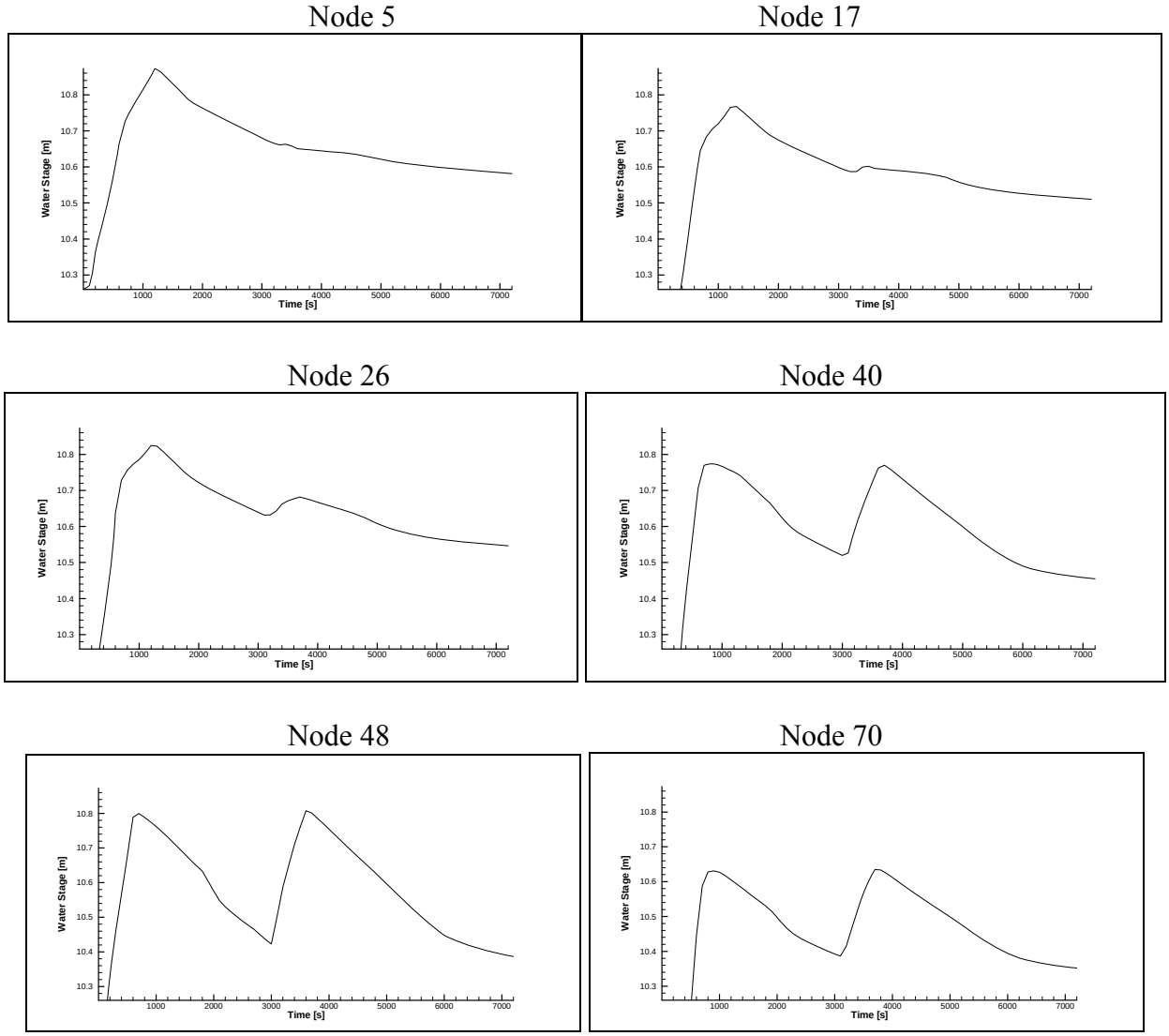

Fig. 4.1.1-5. Water Stages at Various Locations for Example 4.1.1

Table 4.1.1-1 Partial numerical results of water depth distribution at Time = 7,200 s

Node ID	Water Depth [m]
1	0.30000000E+000
2	0.30500313E+000
3	0.31027116E+000
4	0.31560379E+000
5	0.32115150E+000
6	0.32679867E+000
7	0.33262904E+000
8	0.33857747E+000
9	0.34468589E+000
10	0.35092209E+000
11	0.35729881E+000
12	0.35729881E+000
13	0.35044212E+000
14	0.34308253E+000
15	0.33470995E+000
16	0.32577832E+000
17	0.31517319E+000
18	0.30385018E+000
19	0.28953972E+000
20	0.27406891E+000
.	.
.	.
41	0.26021083E+000
42	0.24632798E+000
43	0.22884521E+000
44	0.10000000E+000
45	0.13593196E+000
46	0.14919869E+000
47	0.16705594E+000
48	0.17672218E+000
49	0.18889280E+000
50	0.19708776E+000
.	.
.	.
70	0.18695757E+000
71	0.17995510E+000
72	0.16943911E+000
73	0.15877223E+000
74	0.13962945E+000
75	0.11806921E+000

4.1.2 Two-Dimensional Overland Flows Complex Topography.

TIn this example, 2-D overland flow on a region of non-uniform slope was computed by solving the

2-D depth-average diffusion wave equation with the semi-Lagrangian approach. The computational domain embraces a rectangular area of 800 m wide (in the y direction) and 1,500 m long (in the x direction), which was discretized with 24,022 triangular elements and 12,242 nodes (Fig. 4.1.2-1).

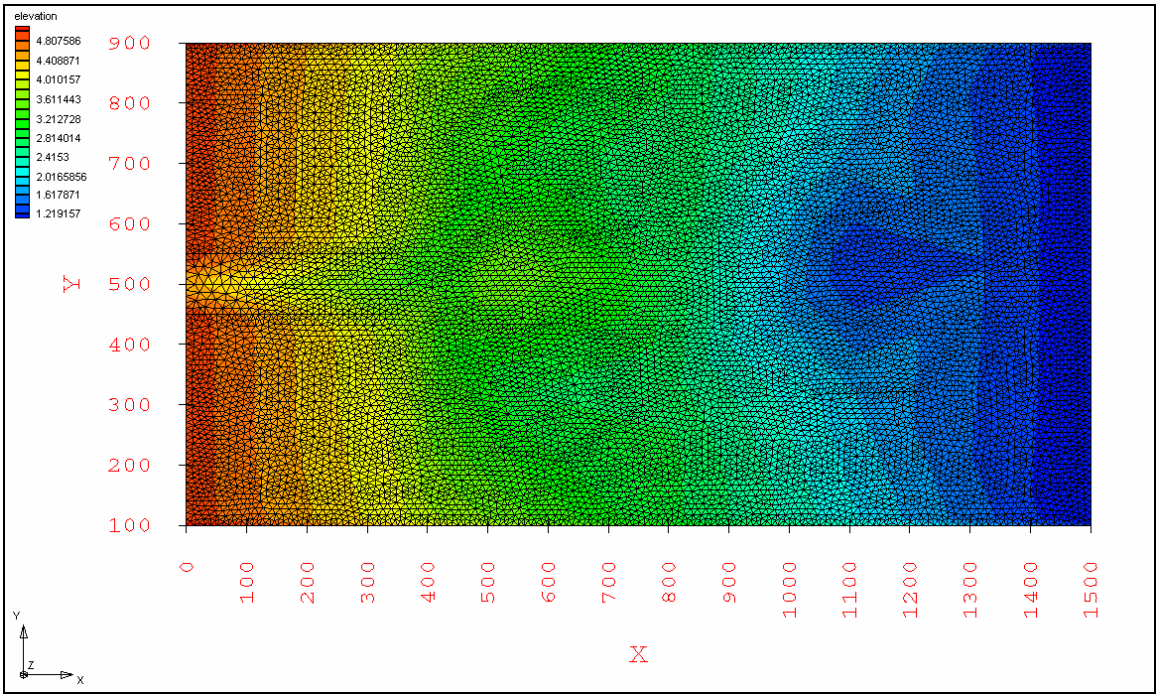

Fig. 4.1.2-1. Domain Discretization of Example 4.1.2

The Manning's roughness was set to 0.025 throughout the entire domain. A time-dependent rainfall rate was applied to the whole region and is given in Figure 4.1.2-2. For a computation, a time-dependent water stage boundary condition (Fig. 4.1.2-3) was applied to the boundary nodes on the left side (i.e., x = 0 m), a water depth-dependent outgoing normal flux boundary condition (Fig. 4.1.2-4) was applied to the downstream boundary element sides (i.e., x = 1,500 m), and a zero water depth boundary condition was applied to the other two sides (i.e., y = 100 m and 900 m).

Water depth was set to 0.001m initially throughout the region. Variable time step sizes of 0.1 s, 0.2 second, and 0.1 second were used from time periods of 0 through 600 seconds, 600 through 2,400 seconds, and 2,400 through 3,600 seconds, respectively. Simulation results of water depth and flow velocity were shown in Figures 4.1.2-5 and 4.1.2-6, respectively. The reasonable result shown in this example demonstrates the capability of WASH123D in computing overland flow with complex terrain. Table 4.1.2-1 also lists partial numerical results of water depth at Time = 1,800 seconds and 3,600 seconds, respectively.

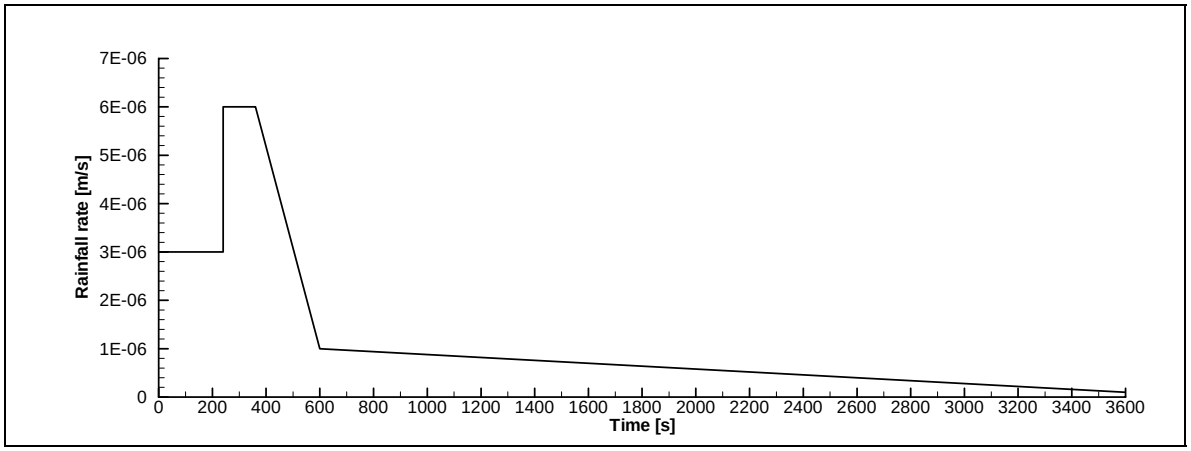

Fig. 4.1.2-2. Time-dependent Rainfall for Example 4.1.2

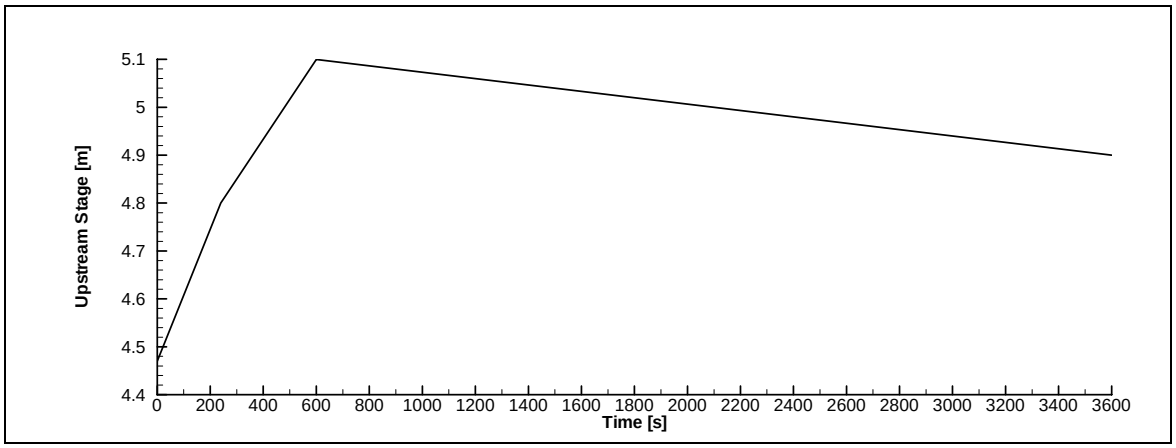

Fig. 4.1.2-3. Time-dependent Upstream Water Stage for Example 4.1.2

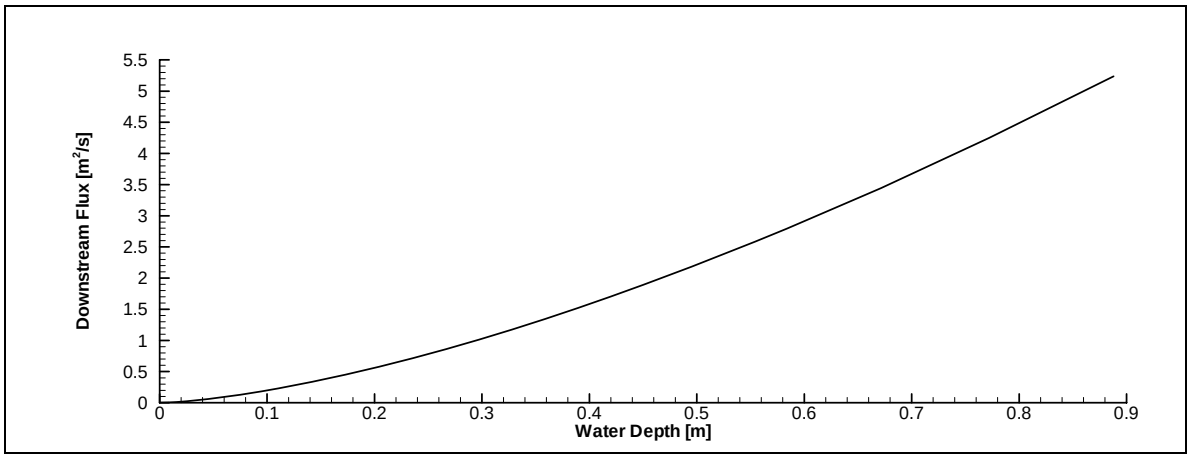

Fig. 4.1.2-4. Water Depth-Dependent Downstream Flux Rate for Example 4.1.2

Time = 600 s

Time = 1,200 s

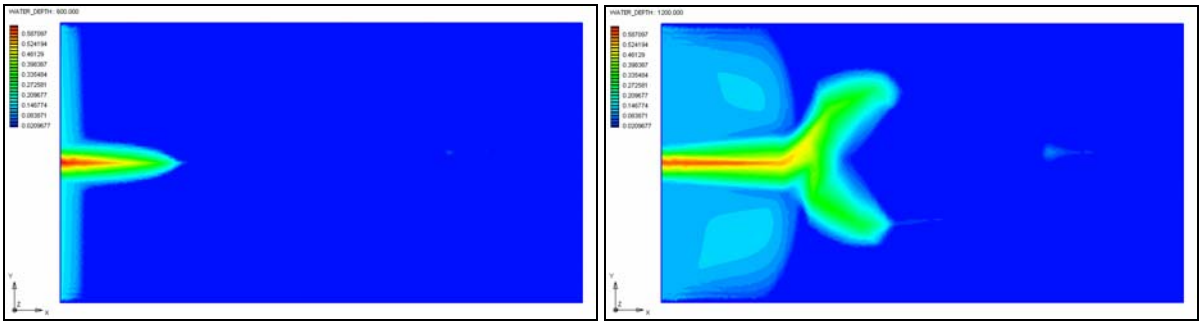

Time = 1,800 s

Time = 2,400 s

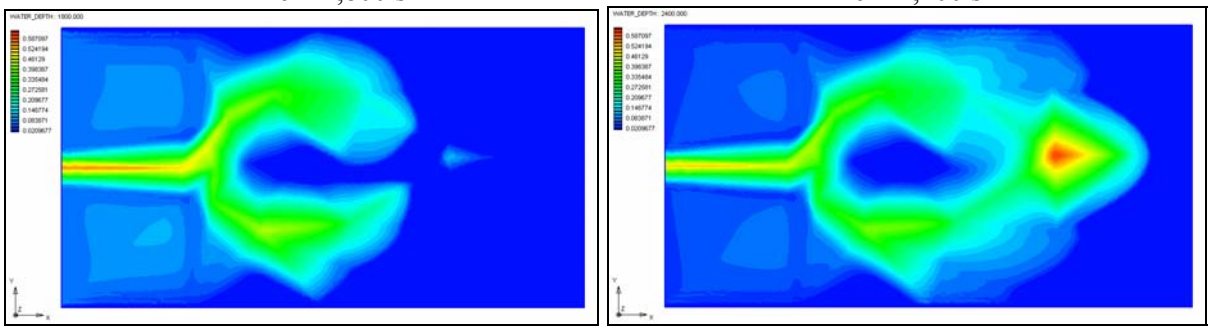

Time = 3,000 s

Time = 3,600 s

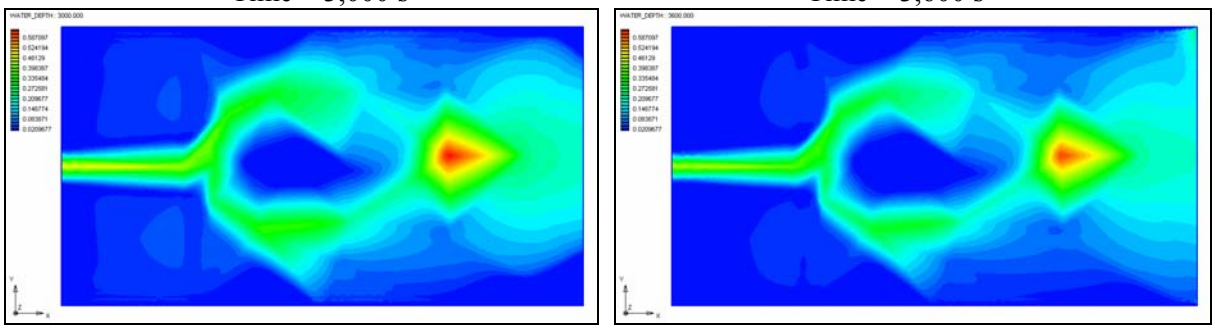

Fig. 4.1.2-5. Water Depth Distribution at Various Times for Example 4.1.2

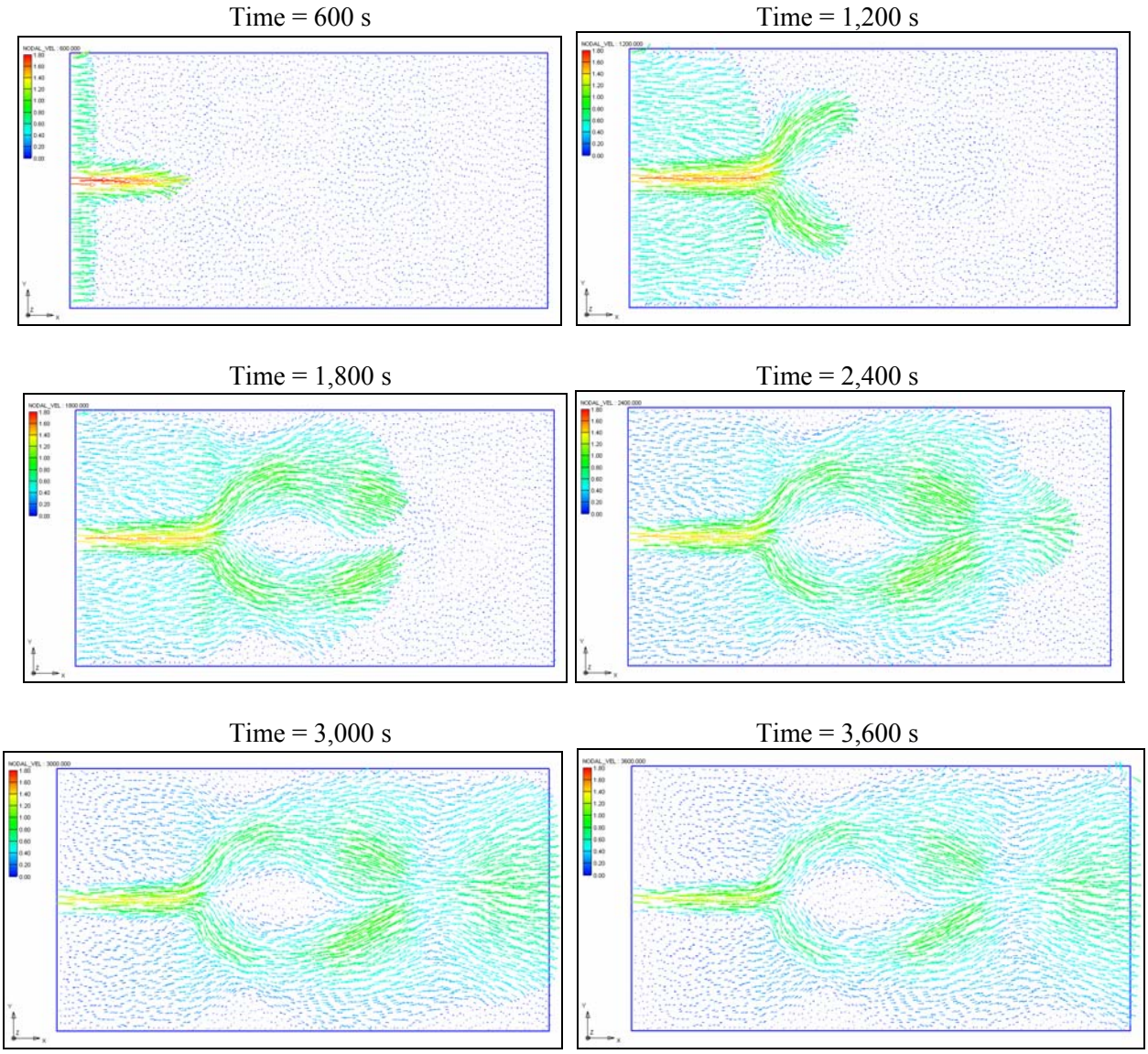

Fig. 4.1.2-6. Flow Velocity Distribution at Various Times for Example 4.1.2

Table 4.1.2-1 Partial numerical results of water depth at Time = 1,800 s and 3,600 s

Time [s]		1,800	3,600
Water Depth [m]	Node 1	0.00000000E+000	0.00000000E+000
	Node 2	0.26090607E-002	0.10483699E-002
	Node 3	0.96222901E-002	0.10416206E-002
	Node 4	0.49737288E-002	0.10289529E-002
	Node 5	0.51648537E-002	0.10290203E-002
	Node 6	0.49025188E-002	0.10295436E-002
	Node 7	0.44320597E-002	0.10298545E-002
	Node 8	0.41718356E-002	0.10299471E-002
	Node 9	0.40598833E-002	0.10300189E-002
	Node 10	0.39577560E-002	0.10299620E-002
	Node 11	0.39489289E-002	0.10299892E-002
	Node 12	0.39715800E-002	0.10299585E-002
	Node 13	0.39699679E-002	0.10299746E-002
	Node 14	0.39984312E-002	0.10301055E-002
	Node 15	0.40032635E-002	0.10300571E-002
	Node 16	0.39609258E-002	0.10298948E-002
	Node 17	0.40035252E-002	0.10300201E-002
	Node 18	0.40222042E-002	0.10300089E-002
	Node 19	0.40323242E-002	0.10299806E-002
	Node 20	0.40586892E-002	0.10299574E-002
	Node 21	0.40794709E-002	0.10300354E-002
	Node 22	0.40799779E-002	0.10300547E-002
	Node 23	0.41178206E-002	0.10300545E-002
	Node 24	0.40928576E-002	0.10299279E-002
	Node 25	0.41204993E-002	0.10299628E-002
	Node 26	0.41837656E-002	0.10300589E-002
	Node 27	0.41255215E-002	0.10298985E-002
	Node 28	0.41787453E-002	0.10300411E-002
	Node 29	0.41646828E-002	0.10299727E-002
	Node 30	0.41751149E-002	0.10299484E-002

4.1.3 Three-Dimensional Variably Saturated Flows in Subsurface Media.

This example was designed to demonstrate a 3-D flow simulation with the 3DFEMWATER model (Yeh, 1987). Since the computational results from our watershed model matches that from 3DFEMWATER perfectly, the 3-D subsurface flow module of WASH123D is verified with this example.

The dimension and discretization of the domain of interest are depicted in Figures 4.1.3-1 and 4.1.3-2, respectively. It was bounded on the left (x = 0 m) and right (x = 1,000 m) by hydraulically connected rivers; on the front (y = -400 m), back (y = 400 m), and bottom (z = 0 m) by impervious aquifuges; and on the top (z = 72 m) by an air-soil interface. A pumping well was placed at (x,y) = (540,0), and the screen of the well was from z = 0 through 30 m. Water table was assumed to be horizontal and was 60 m above the bottom of the aquifer before pumping. The saturated hydraulic conductivity has components K_{xx} = 5 m/d (= 0.208 m/hr), K_{yy} = 0.5 m/d (= 0.0208 m/hr), and K_{zz} = 2 m/d (= 0.083 m/hr). The porosity of the medium was 0.25 and the field capacity was 0.0125. The following three equations were employed to describe the unsaturated hydraulic properties. They were translated into x-y series that can be used in the WASH123D input file to represent pressure head-dependent moisture content, relative conductivity, and water capacity, respectively (i.e., θ vs. h, K_r vs. h, and dθ/dh vs. h).

$$\theta = \theta_r + (\theta_s - \theta_r)\frac{1}{1+\left(\alpha\left|h_a - h\right|\right)^{\beta}} = 0.0125 + \frac{0.2375}{1+0.25h^2} \qquad \textbf{(4.1.3.1)}$$

$$K_r = \left[\frac{\theta - \theta_r}{\theta_s - \theta_r}\right]^2 = \frac{(\theta - 0.0125)^2}{0.2375^2} \qquad \textbf{(4.1.3.2)}$$

$$\frac{d\theta}{dh} = -(\theta_s - \theta_r)\frac{\beta\left(\alpha\left|h_a - h\right|\right)^{\beta-1}\cdot\alpha}{\left[1+\left(\alpha\left|h_a - h\right|\right)^{\beta}\right]^2} = -0.2375\frac{0.5h}{(1+0.25h^2)^2} \qquad \textbf{(4.1.3.3)}$$

where θ_s (= 0.25) is the porosity; θ_r (= 0.0125) is the minimum moisture content that is associated with the minimum pressure head h_a (= 0.0); α (= 0.5) and β (= 2.0) are the parameters used to compute the moisture content and relative hydraulic conductivity.

Because the example problem was symmetric about the pumping well in the y direction, the computational domain was taken as x ∈ [0 m, 1000 m], y ∈ [0 m, 400 m], z ∈ [0 m, 72 m]. The boundary conditions were given as shown in Figure 4.1.3-3: pressure head maintained at 30 m at the pumping well during pumping; pressure head assumed hydrostatic on two vertical planes at (1) x = 0 m and z ∈ [0 m, 60 m] and (2) x = 1000 m and z ∈ [0 m, 60 m]; no flux imposed on all other boundary faces.

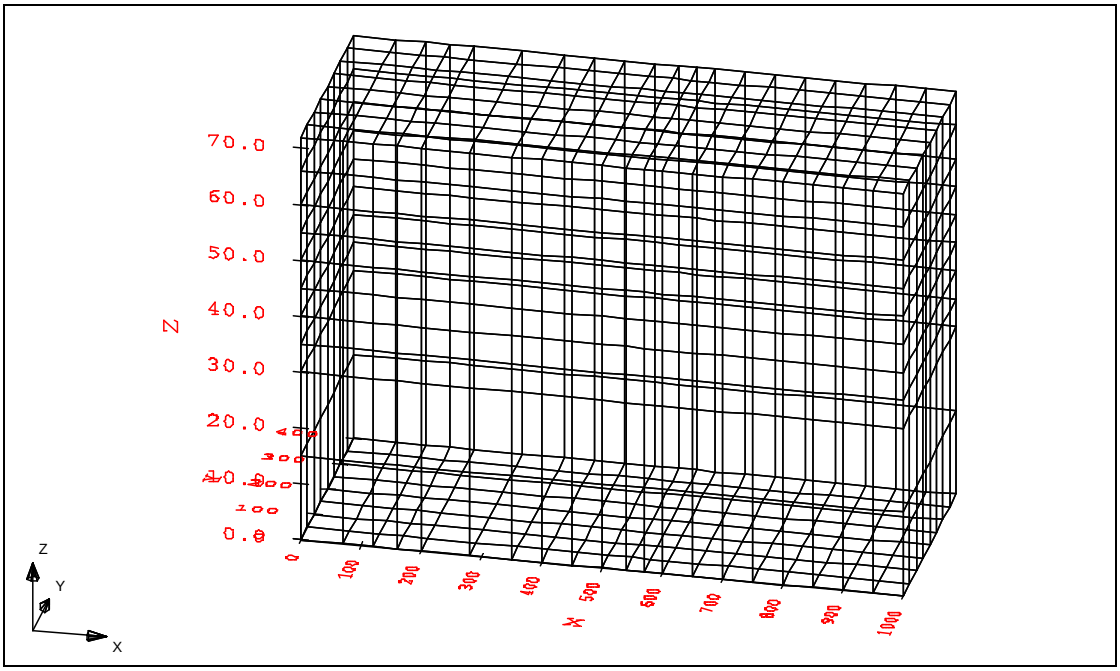

Fig. 4.1.3-1. Domain and Descretization of Example 4.1.3

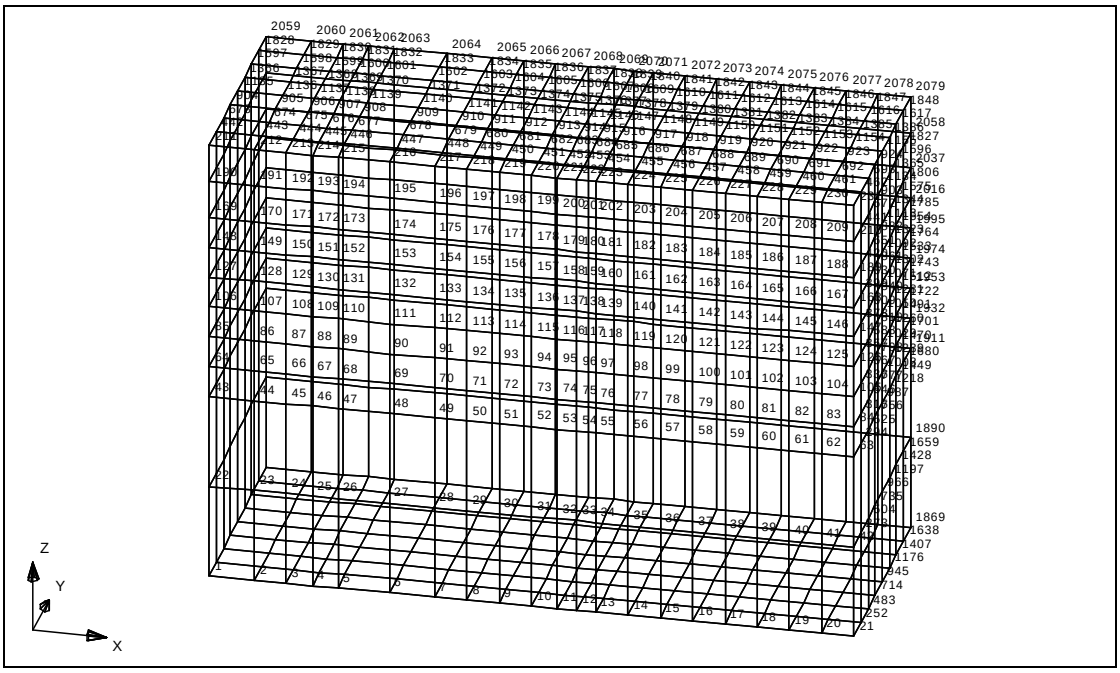

Fig. 4.1.3-2. Node Numbering for Example 4.1.3

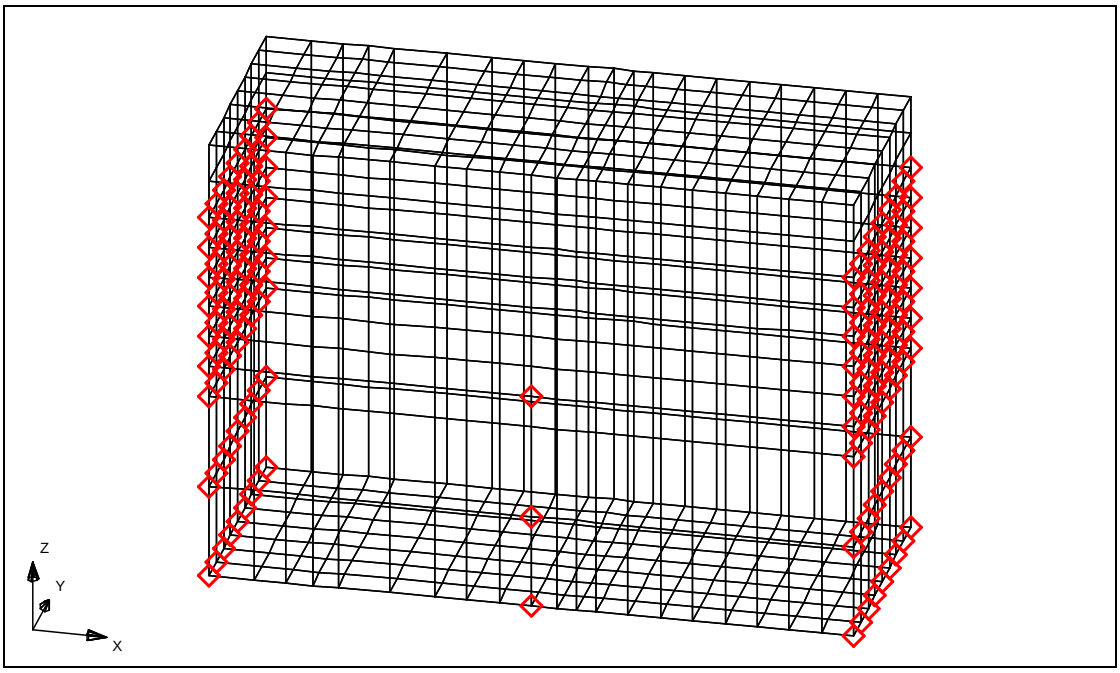

Fig. 4.1.3-3. Dirichlet Boundary Conditions for Example 4.1.3

The steady-state solution was determined with the absolute error tolerance of pressure head of 0.01 m and 0.00001 m for nonlinear iterations and linear matrix solvers, respectively. Simulation results of total head and flow velocity were shown in Figure 4.1.3-4 and Figure 4.1.3-5, respectively. Table 4.1.3-1 shows partial numerical results of pressure head that are corresponding to Figure 4.1.3-4.

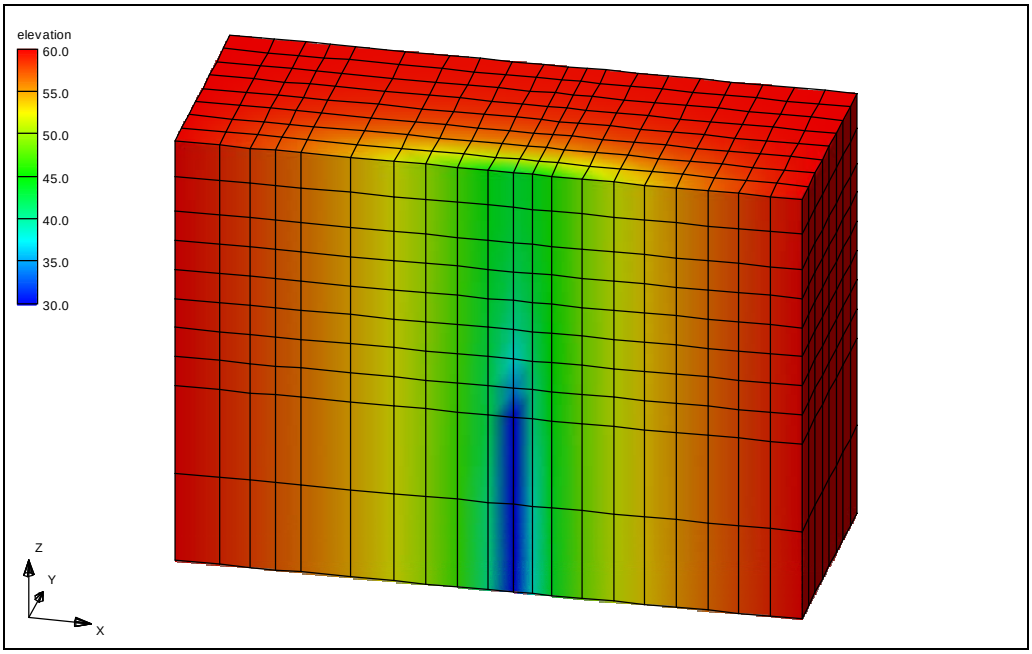

Fig. 4.1.3-4. Total Head Distribution for Example 4.1.3

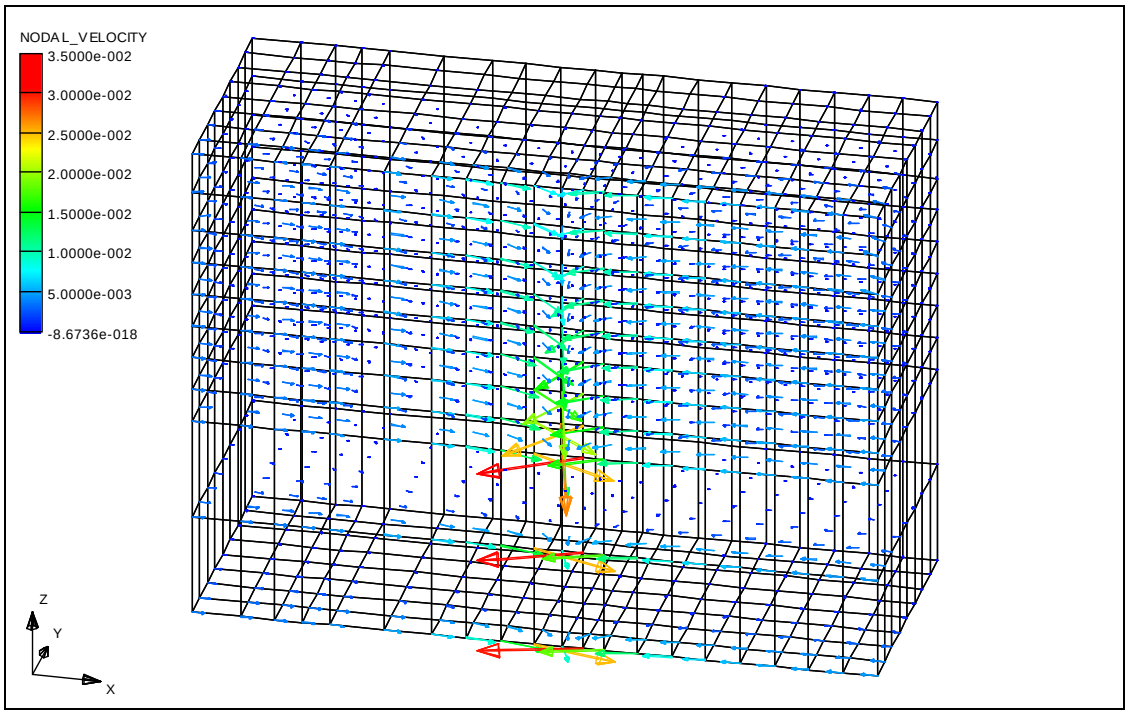

Fig. 4.1.3-5. Flow Velocity Distribution for Example 4.1.3

Table 4.1.3-1 Partial Numerical Results of Pressure Head

Node ID	Pressure Head [m]	Node ID	Pressure Head [m]
1	0.60000000E+002	211	-0.12140085E+002
2	0.58755458E+002	212	-0.13229426E+002
3	0.57839757E+002	213	-0.14165134E+002
4	0.57072146E+002	214	-0.14927611E+002
5	0.56255441E+002	215	-0.15744612E+002
6	0.54376744E+002	216	-0.17622228E+002
7	0.52233408E+002	217	-0.19744420E+002
8	0.50117077E+002	218	-0.21763400E+002
9	0.46862747E+002	219	-0.24469933E+002
10	0.40317625E+002	220	-0.27569262E+002
11	0.30000000E+002	221	-0.28751296E+002
12	0.38291482E+002	222	-0.27948658E+002
13	0.43660431E+002	223	-0.26172644E+002
14	0.48621638E+002	224	-0.23011554E+002
15	0.51443050E+002	225	-0.20489174E+002
16	0.53448674E+002	226	-0.18539230E+002

4.1.4 Coupled One-Dimensional and Two-Dimensional Flows.

This example demonstrates the capability of WASH123D in handling coupled 1-D channel and 2-D overland flow problems. Here we considered a spreader canal that was expected to distribute water to its downstream overland regime. The 2-D overland domain was discretized with 151 elements and 171 nodes, and the 1-D spreader canal was composed of 11 elements and 12 nodes (Fig.4.1.4-1). In WASH123D, all 2-D elements that are connected to 1-D nodes are defined as channel-related elements, and they are not included in 2-D overland computation. Therefore, the 2-D computational domain contained 127 (= 151 - 24) 2-D elements and 159 (= 171 - 12) 2-D nodes. The canal was 2 m wide and its cross-sectional area was proportional to its depth. The canal was as deep as 0.1 m at the entrance (i.e. the first 1-D node, marked in red in Fig. 4.1.4-1) and as shallow as 0.025 m at the turning point near Node 123 (i.e., the 6-th 1-D node).

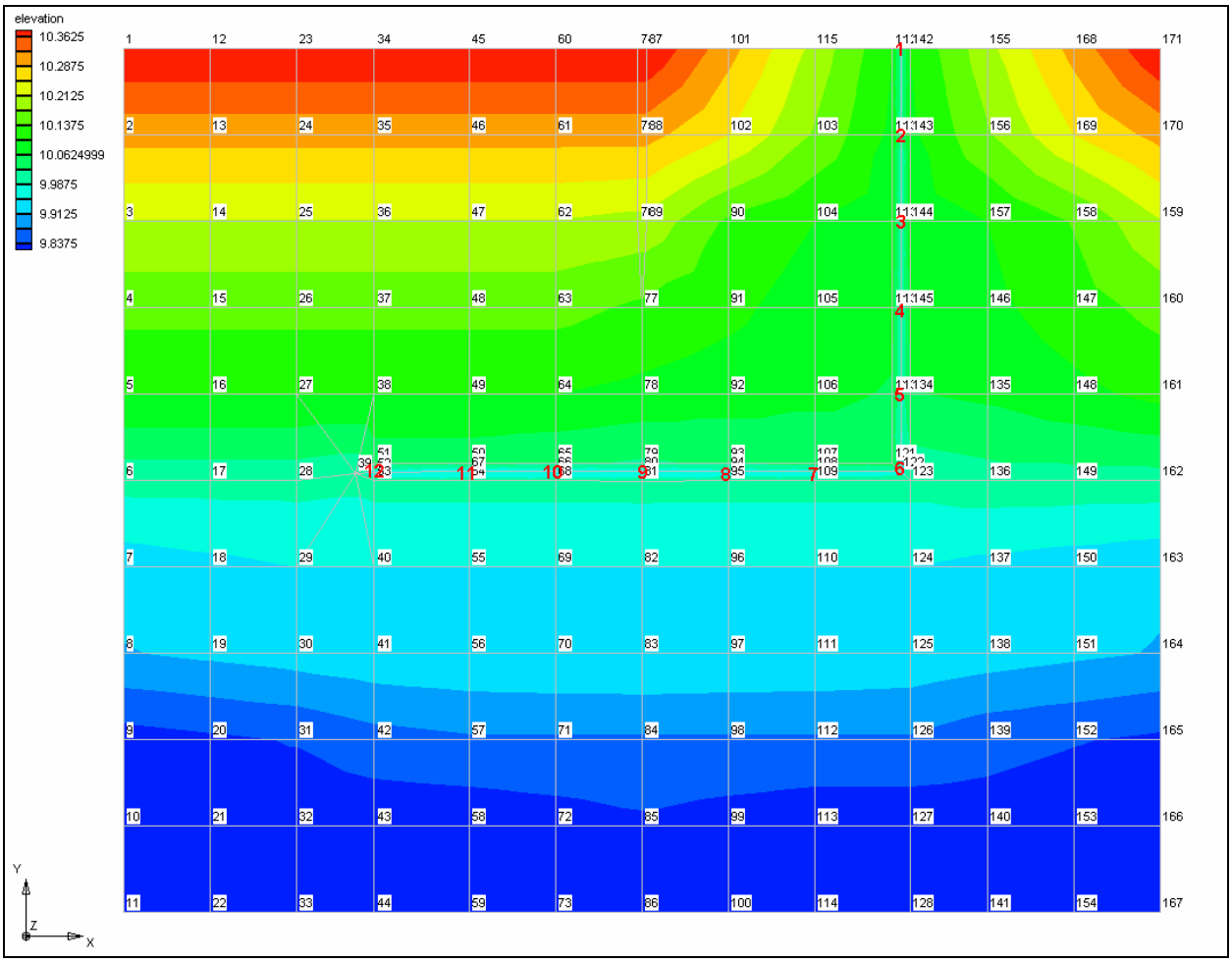

Fig. 4.1.4-1. Discretization and Surface Elevation of Example 4.1.4

The Manning's roughness was set to 0.01 for both 2-D overland and 1-D canal flow. In computing 2-D overland flow, a Dirichlet boundary condition of zero depth was specified for Nodes 1, 12, 23, 34, 45, 60, 74, 87, and 171; a depth-dependent flux boundary condition was given on the bottom

boundary (i.e., the boundary that emprises Nodes 11, 22, 33, …, 167); and a channel-overland interaction boundary condition was specified for the channel-related overland boundary sides, which included a depth-dependent flux when flow was from overland to canal and a canal stage condition when flooding occurred. A time-dependent water depth was controlled at the upstream 1-D node (i.e., the entrance, Fig. 4.1.4-2), and a zero-velocity condition was applied at the downstream dead-end node.

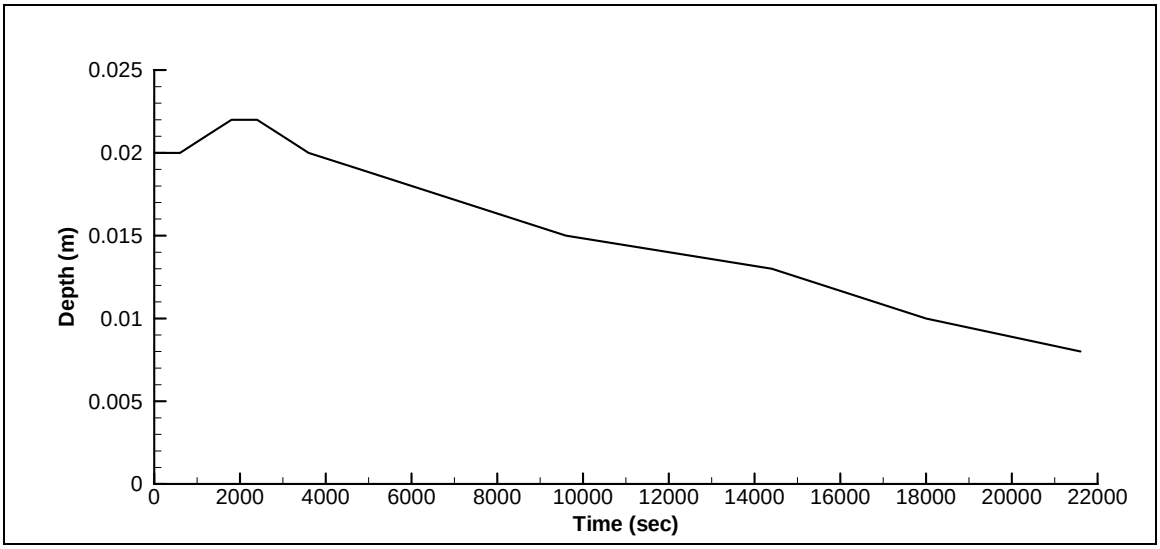

Fig. 4.1.4-2. Time-dependent Water Depth at the Upstream Canal Node for Example 4.1.4

Initially, the overland domain was completely dry, while a constant depth of 0.02 m was given for the 1-D spreader canal so that water flow from the spreader canal to its downstream overland regime can be expected within a short period of time, which allowed us to verify the algorithm of coupling 1-D channel and 2-D overland flow effectively. A constant rainfall rate of 10^{-8} m/s was then applied throughout the entire simulation period of 21,600 seconds (6 hours). The time-step size for computing 2-D overland flow was 4 seconds, and each 2-D time step contained four 1-D time steps.

Figure 4.1.4-3 plots the variation of water depth with time at four 1-D canal nodes: 3, 6, 9, and 12. Also, a dash line that represents the bank height over which canal water will overflow to the downstream overland regime is given as reference for each node (marked with respective colors), except for Node 3 where the associated bank height is 0.09 m (see the first plot in Figure 4.1.4-5 also). Figure 4.1.4-4 provides a zoom-in plot of Figure 4.1.4-3 for the period of time from 0 through 750 s, where the three plus symbols indicate the moments that water started to flow from canal to overland at Nodes 6, 9, and 12. It is consistent with what is plotted in Figure 4.1.4-5, where the computed water depth and flow direction distribution of overland flow is given. The first plot in Figure 4.1.4-44 also provides the information of bank height of each channel-related overland boundary nodes.

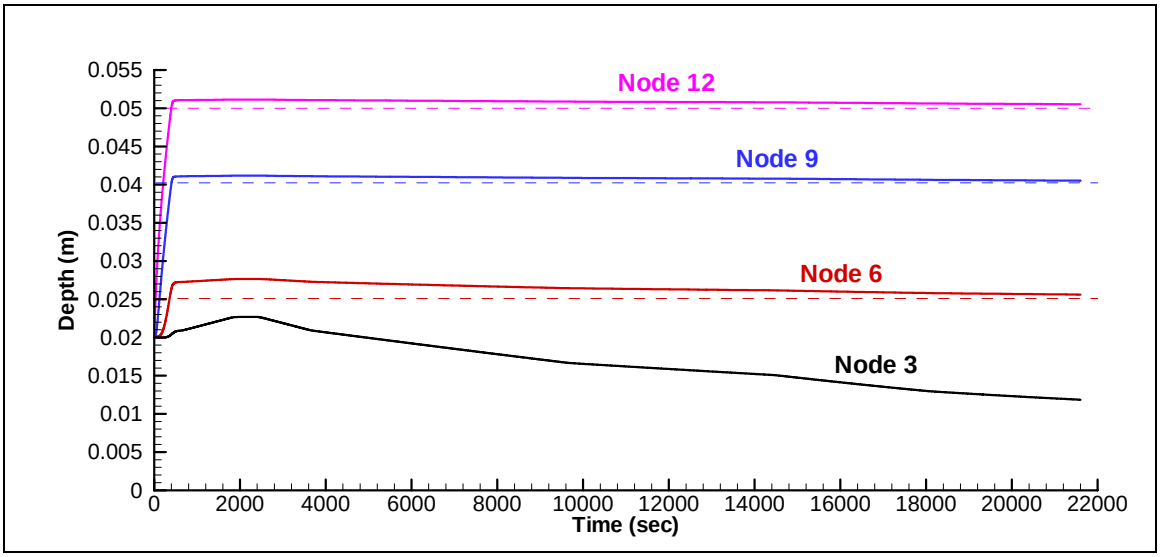

Fig. 4.1.4-3. Computed Water Depth at Various 1-D Canal Locations for Example 4.1.4 (Time = 0 through 21,600 s)

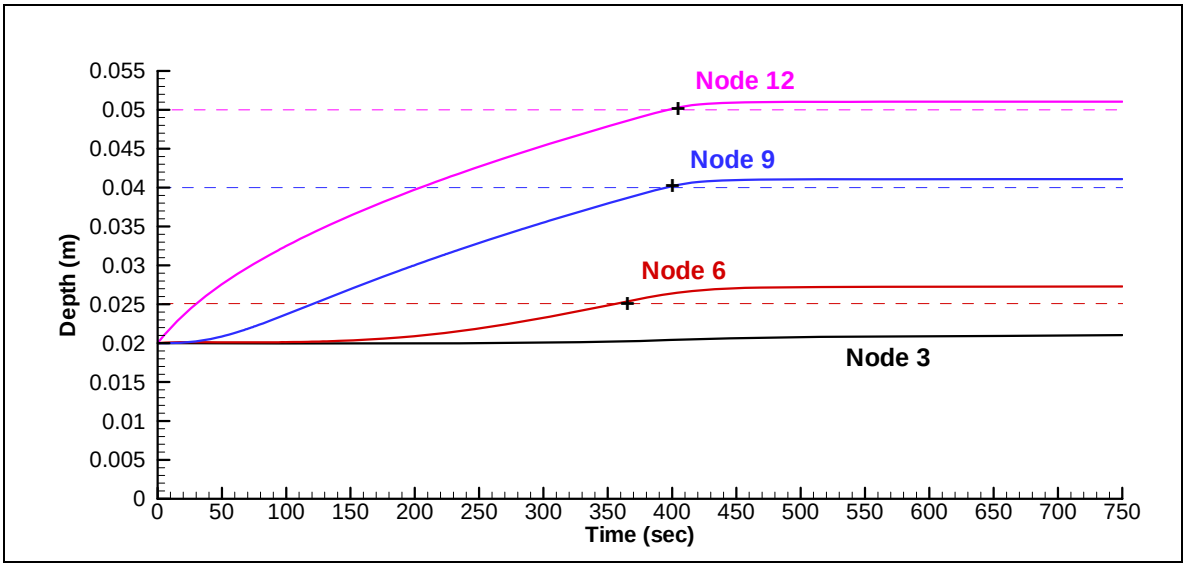

Fig. 4.1.4-4. Computed Water Depth at Various 1-D Canal Locations for Example 4.1.4 (Time = 0 through 750 s).

Time = 400 s

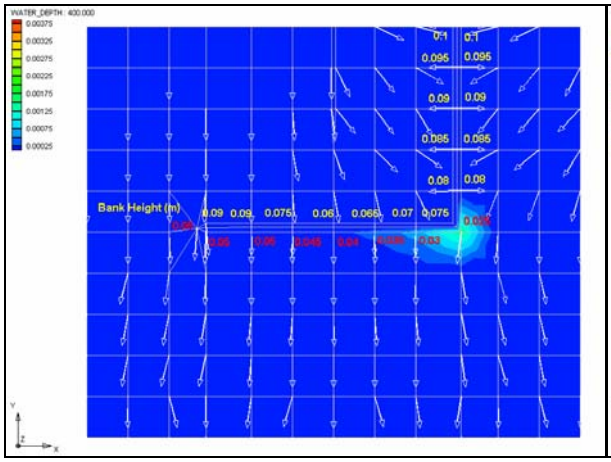

Time = 600 s

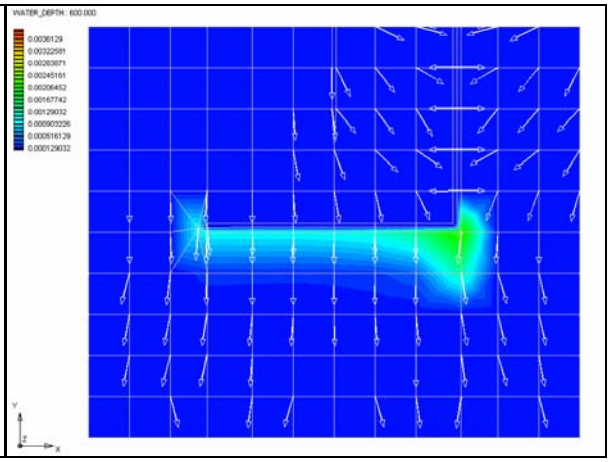

Time = 1,200 s

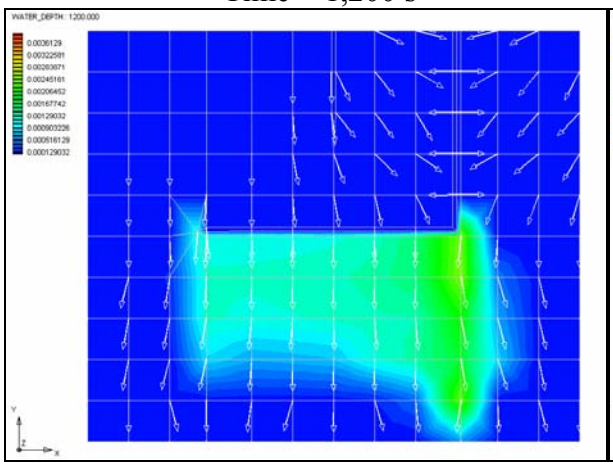

Time = 2,400 s

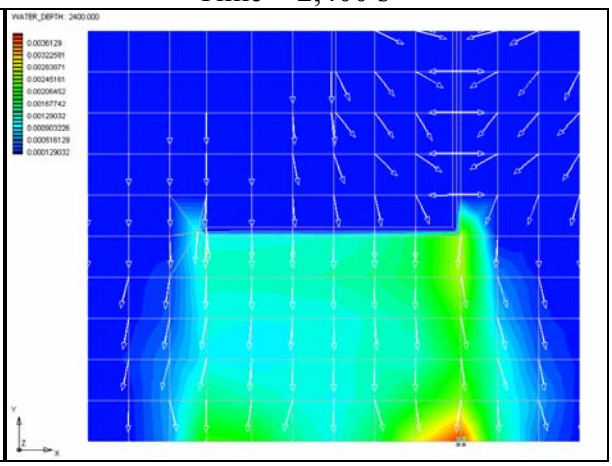

Time = 3,600 s

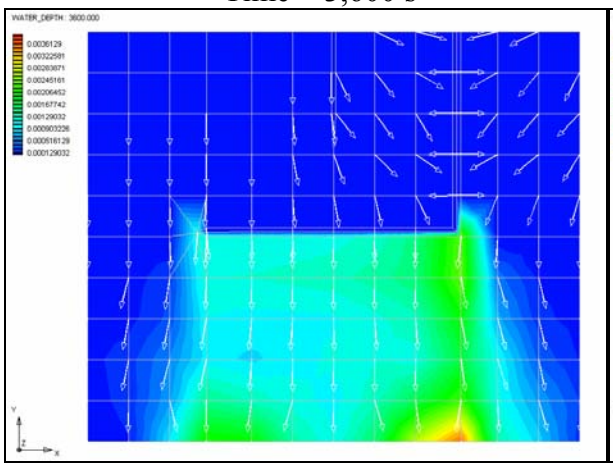

Time = 7,200 s

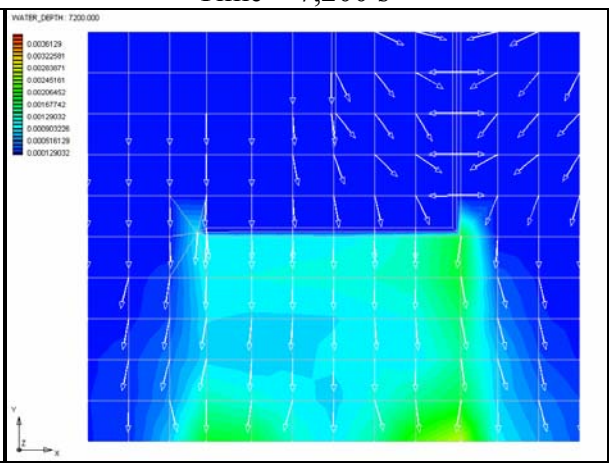

Time = 10,800 s

Time = 16,200 s

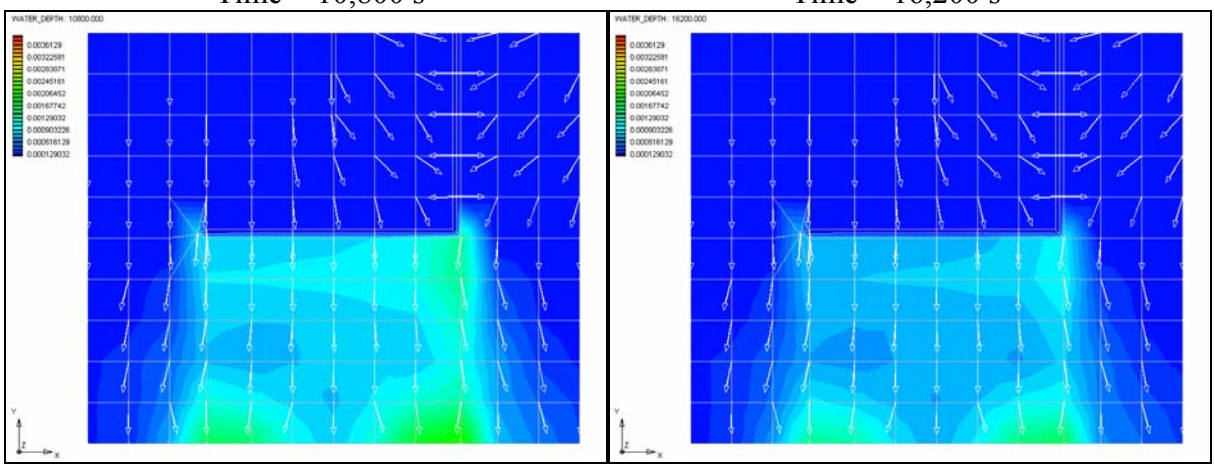

Time = 21,600 s

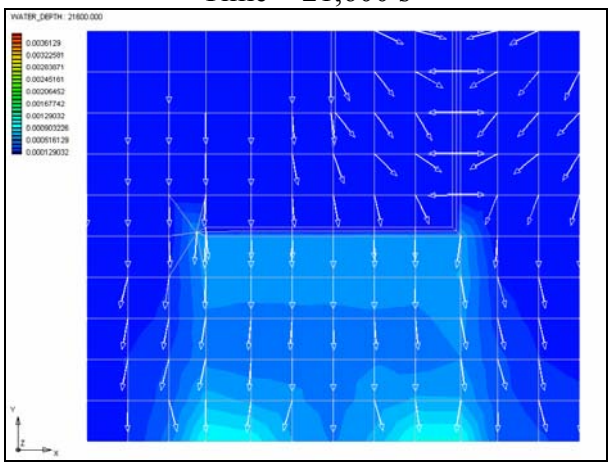

Fig. 4.1.4-5. Distribution of Water Depth and Flow Direction in the Land Surface at Various Times for Example 4.1.4

4.1.5 Coupled Two-Dimensional and Three-Dimensional Flows.

This example is designed to test coupled overland/subsurface flow within a hypothetic domain, where ground surface has a gradually changing slope in the x-direction (Fig. 4.1.5-1). Figure 4.5-1 depicts the simulation domain, dimension, and discretization of the example, where the dimension in the z direction is magnified five times for better visualization.

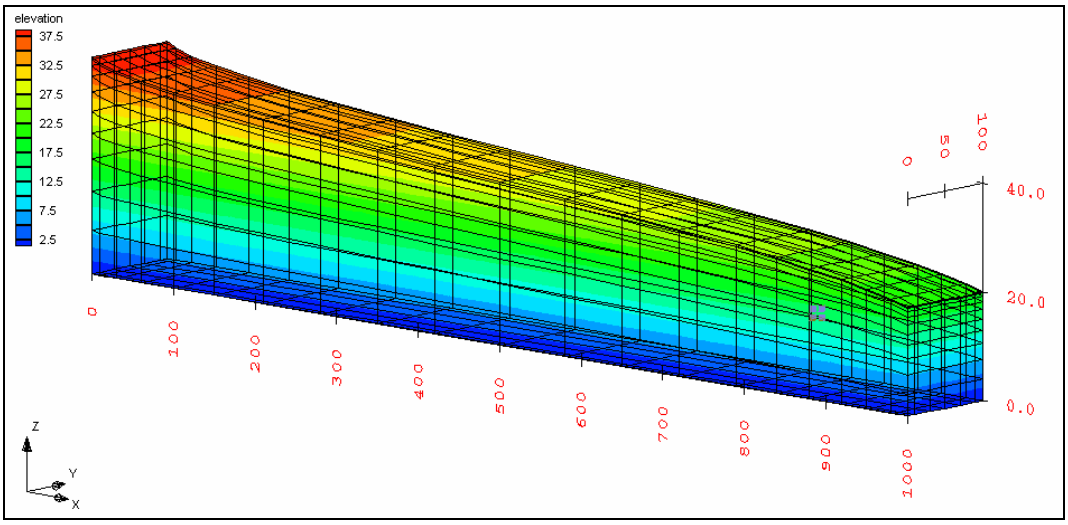

Fig. 4.1.5-1. Domain, Dimension, and Discretization of Example 4.1.5-1

The subsurface porous medium is uniformly distributed throughout the entire domain and the corresponding saturated hydraulic conductivity has components $K_{xx} = 2\text{x}10^{-4}$ m/s, $K_{yy} = 10^{-5}$ m/s, and $K_{zz} = 10^{-5}$ m/s. The following soil characteristic equations are used to describe the hydraulic properties in unsaturated zones.

$$\begin{aligned} &\theta = 0.3 && if\ \ 0 < h \\ &\theta = 0.15 + 0.0015(h+100) && if\ \ -100 < h < 0 \\ &\theta = 0.15 && if\ \ h < -100 \end{aligned} \qquad \textbf{(4.1.5.1)}$$

$$\begin{aligned} &K_r = 1 && if\ \ 0 < h \\ &K_r = \frac{h+100}{100} && if\ \ -100 < h < 0 \\ &K_r = 0 && if\ \ h < -100 \end{aligned} \qquad \textbf{(4.1.5.2)}$$

$$\frac{d\theta}{dh} = 0.0 \quad if\ \ 0 < h \quad \text{or} \quad if\ \ h < -100; \quad \frac{d\theta}{dh} = 0.0015 \quad if\ \ -100 < h < 0 \qquad \textbf{(4.1.5.3)}$$

In this example, the initial flow condition was computed by solving the steady-state flow governing equation based on the given boundary conditions: an impermeable boundary condition applied to the front (y = 0 m), back (y = 100 m), and bottom (z = 0 m) boundaries; a total head of 26 m specified

on the lower part of the left boundary (x = 0 m and z ≤ 26 m); a total head of 13 m specified on the lower part of the right boundary (x = 1000 m and z ≤ 13 m); a variable boundary condition of a zero ponding depth and a zero rainfall rate used for the top boundary (i.e., the ground surface, Figure 4.1.5-2).

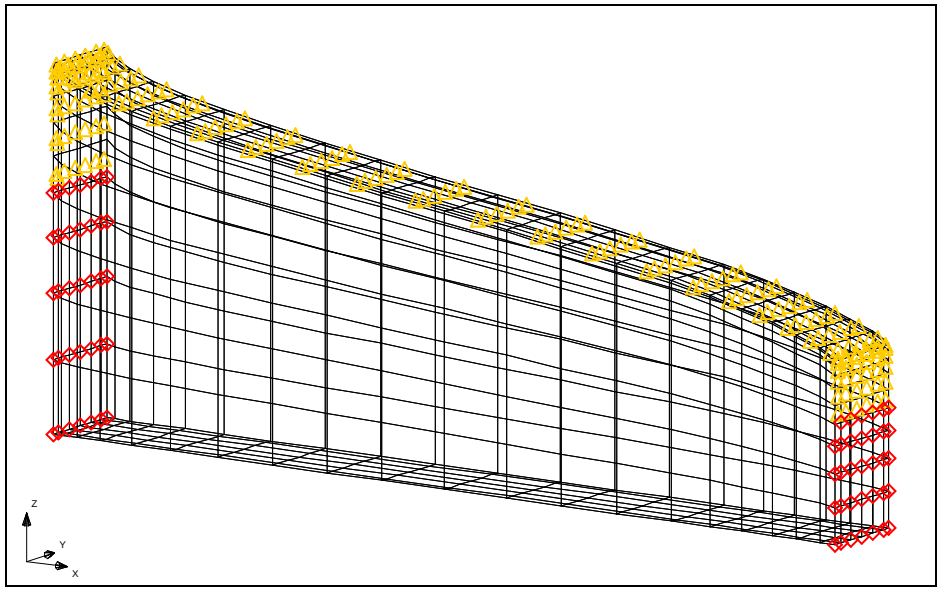

Fig. 4.1.5-2. The Setup of Boundary Conditions for Example 4.1.5
(Dirichlet boundary nodes are marked in red and variable-boundary sides are marked in yellow)

As the six-hour transient simulation began, we had a rainfall of 2×10^{-5} m/s during the first twenty minutes, followed by a no-rain period of one hour, a rain of 10^{-5} m/s for 1 hour, and 1.5×10^{-5} m/s afterwards till the end of the simulation (time = 6 hours). The overland water depth was set to zero on the highest location (i.e., at x = 0 m) to mimic a water divide, while a depth-dependent flux was given as the boundary condition to characterize water flow at the lowest location (i.e., at x = 1,000 m). The rest of the overland boundary (i.e., at y = 0 m and y = 100 m) was assumed streamline boundary and no-through flux boundary condition was applied. During the transient simulation, the computed overland water depth was used as the ponding depth for implementing the variable boundary condition on the top boundary in computing 3-D subsurface flow. The remaining boundary conditions for computed 3-D subsurface flow were set identical to those mentioned above for the initial steady-state simulation. The Manning's roughness was 0.02. The diffusion wave model was used to compute overland flow. An absolute error of 10^{-4} m was used to determine convergence for 2-D overland flow, and absolute errors of 10^{-3} m and 10^{-6} m were employed to settle nonlinear convergent solutions and linearized convergent solutions, respectively, in computing 3-D subsurface flow. The time step sizes for 3-D and 2-D computation were 10 seconds and 2 seconds, respectively.

Simulation results of subsurface pressure head/flow velocity and overland water depth are plotted in Figures 4.1.5-3 and 4.1.5-4, respectively. In Figure 4.1.5-3, the unsaturated zone is highlighted with white color. Although there was no water observed on ground surface from Time = 0 through 7,200 seconds due to infiltration, the time-dependent rainfall has changed the elevation of water table during this period of time. The constant rainfall rate after Time = 4,800 seconds not only raised

water table but also generated surface runoff after the soil could no longer take all the rainfall, and we observed water depth on ground surface at both Time = 10,800 seconds and 21,600 second. Figures 4.1.5-3 and 4.1.5-4 show consistent results for this coupled 2-D/3-D example. Table 1 gives the numerical results of water depth along the x direction that are corresponding to Figure 4.1.5-4.

Time = 0 s

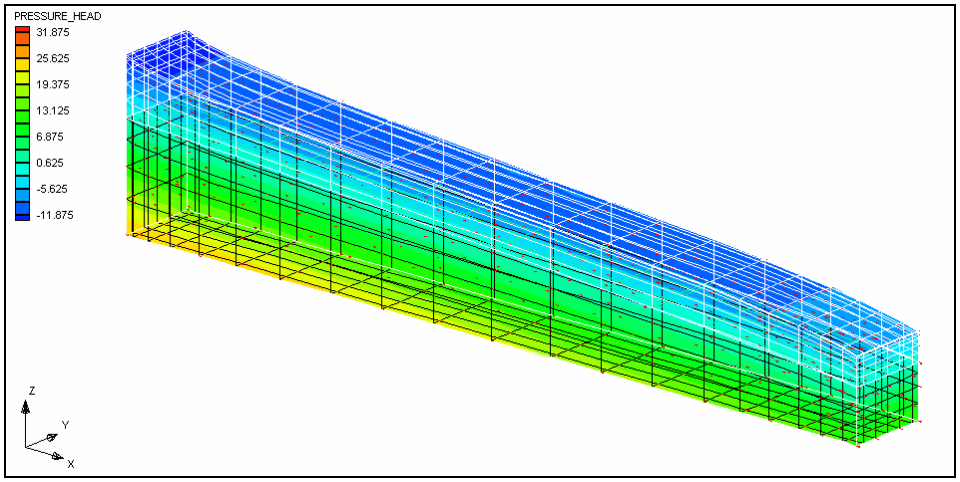

Time = 1,200 s

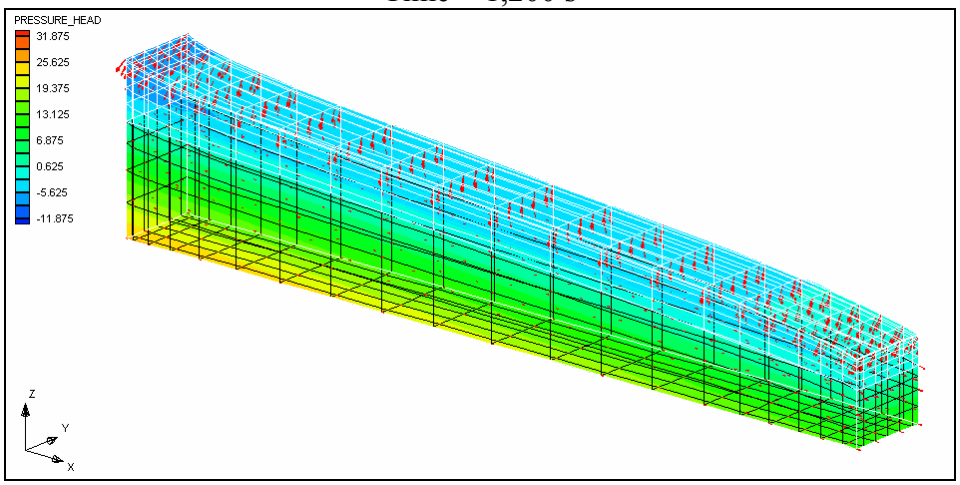

Time = 4,800 s

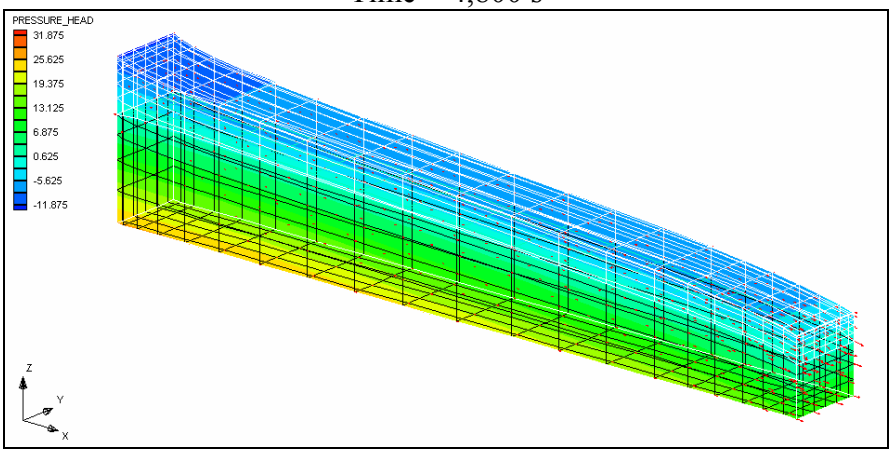

Time = 7,200 s

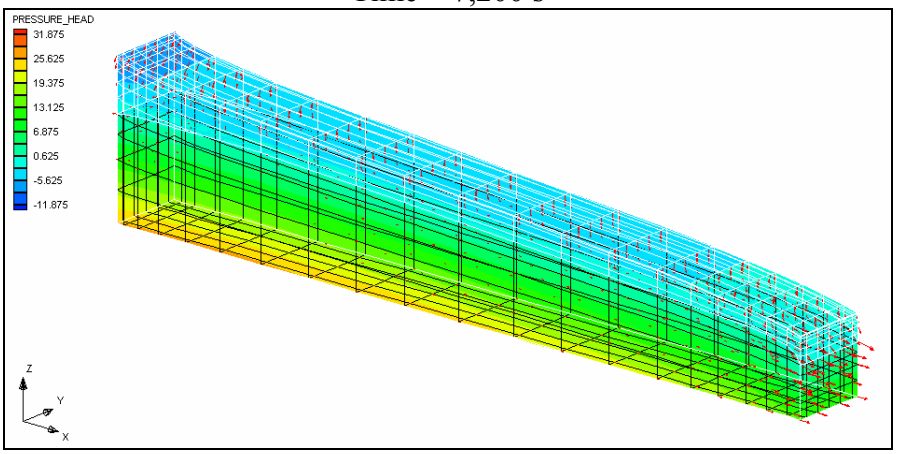

Time = 10,800 s

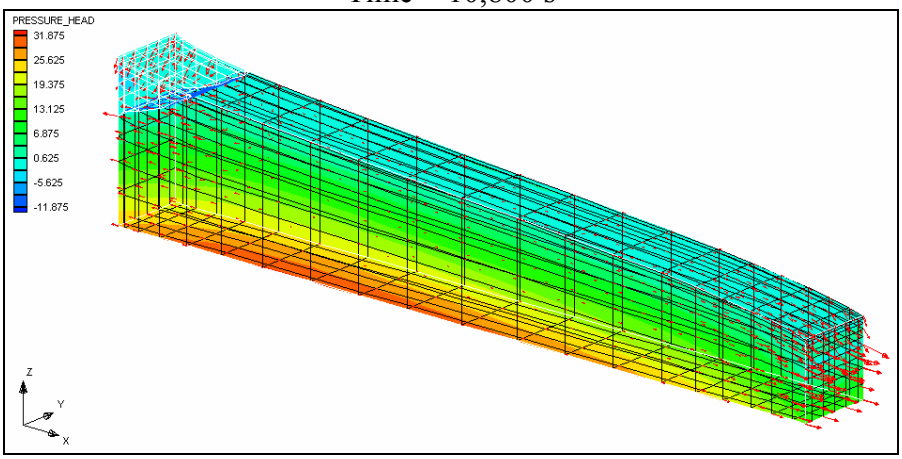

Time = 21,600 s

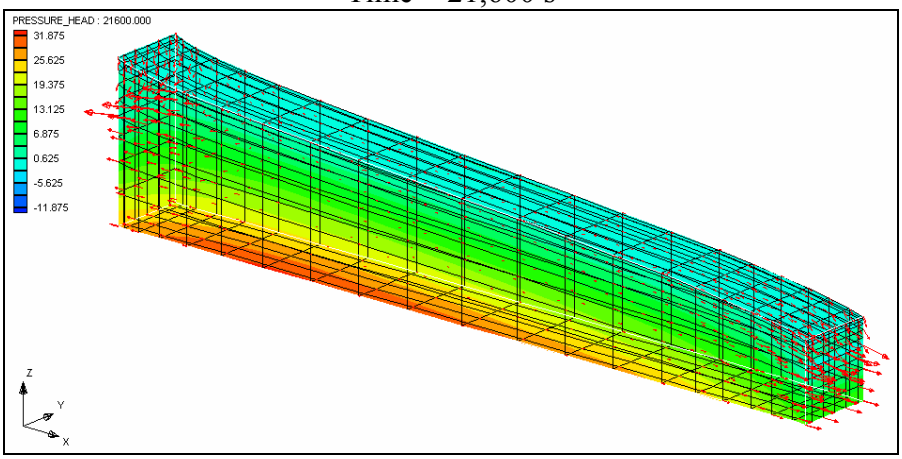

Fig. 4.1.5-3. Pressure Head Distribution at Various Times for Example 4.1.5

Time = 1,200 s

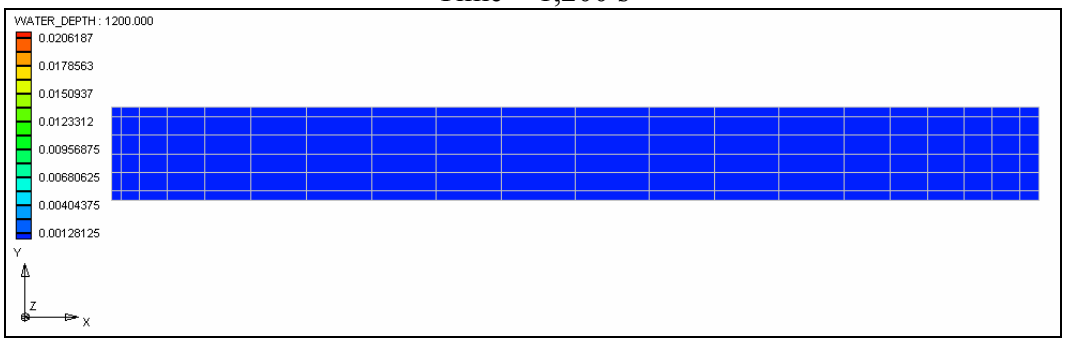

Time = 4,800 s

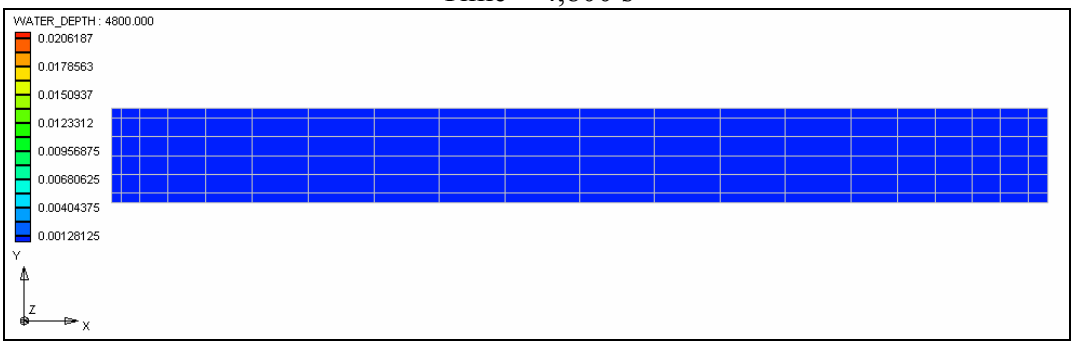

Time = 7,200 s

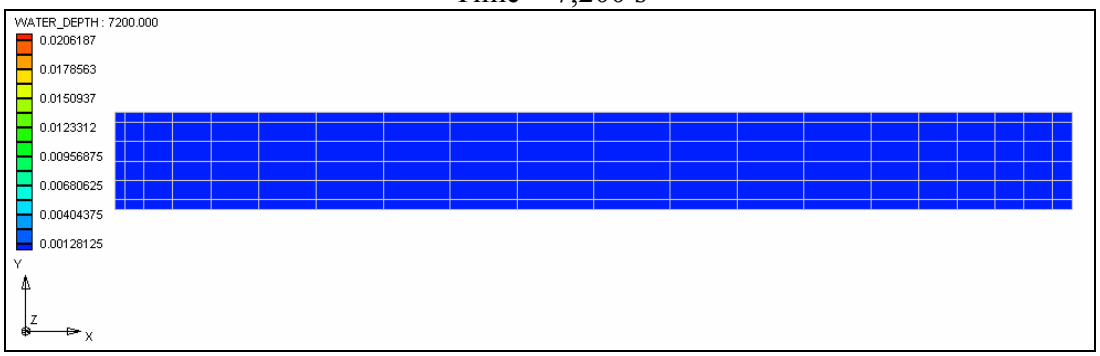

Time = 10,800 s

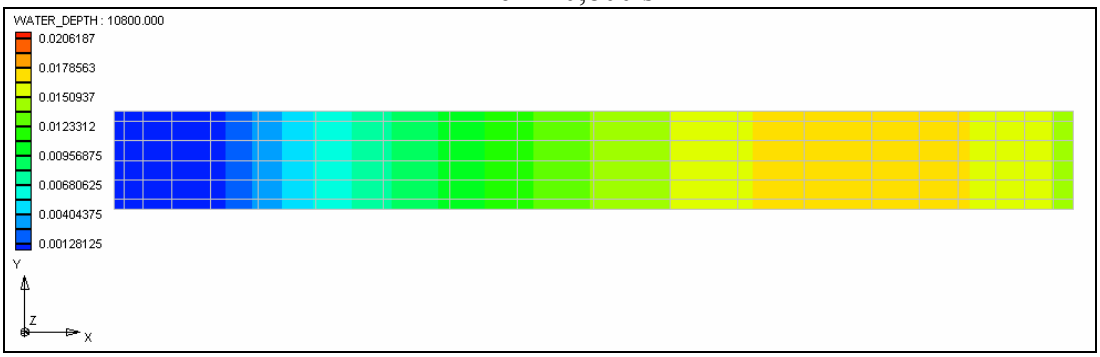

Time = 21,600 s

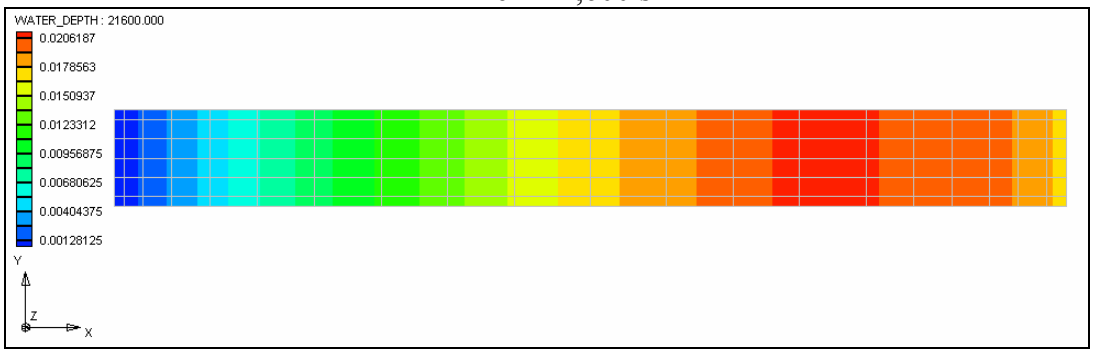

Fig. 4.1.5-4. Overland Water Depth Distribution at Various Times for Example 4.1.5

Table 4.1.5-1 Partial Results of Water Depth along the x-Direction for Example 4.1.5

Time [s]		1,200	4,800	7,200	10,800	21,600
Water Depth [m]	X = 0	0.000000E+00	0.000000E+00	0.000000E+00	0.000000E+000	0.000000E+000
	X = 10	0.000000E+00	0.000000E+00	0.000000E+00	0.000000E+000	0.566370E-003
	X = 30	0.000000E+00	0.000000E+00	0.000000E+00	0.000000E+000	0.150968E-002
	X = 60	0.000000E+00	0.000000E+00	0.000000E+00	0.000000E+000	0.285450E-002
	X = 100	0.000000E+00	0.000000E+00	0.000000E+00	0.494521E-003	0.458664E-002
	X = 150	0.000000E+00	0.000000E+00	0.000000E+00	0.295229E-002	0.665658E-002
	X = 210	0.000000E+00	0.000000E+00	0.000000E+00	0.552909E-002	0.894692E-002
	X = 280	0.000000E+00	0.000000E+00	0.000000E+00	0.790493E-002	0.111607E-001
	X = 350	0.000000E+00	0.000000E+00	0.000000E+00	0.991641E-002	0.131597E-001
	X = 420	0.000000E+00	0.000000E+00	0.000000E+00	0.119154E-001	0.152891E-001
	X = 500	0.000000E+00	0.000000E+00	0.000000E+00	0.137984E-001	0.173210E-001
	X = 580	0.000000E+00	0.000000E+00	0.000000E+00	0.150824E-001	0.186713E-001
	X = 650	0.000000E+00	0.000000E+00	0.000000E+00	0.162323E-001	0.199247E-001
	X = 720	0.000000E+00	0.000000E+00	0.000000E+00	0.172655E-001	0.210734E-001
	X = 790	0.000000E+00	0.000000E+00	0.000000E+00	0.170996E-001	0.207789E-001
	X = 840	0.000000E+00	0.000000E+00	0.000000E+00	0.166321E-001	0.201513E-001
	X = 880	0.000000E+00	0.000000E+00	0.000000E+00	0.165685E-001	0.200295E-001
	X = 920	0.000000E+00	0.000000E+00	0.000000E+00	0.162621E-001	0.196289E-001
	X = 950	0.000000E+00	0.000000E+00	0.000000E+00	0.158421E-001	0.191035E-001
	X = 980	0.000000E+00	0.000000E+00	0.000000E+00	0.150275E-001	0.181227E-001
	X = 1000	0.000000E+00	0.000000E+00	0.000000E+00	0.142089E-001	0.171431E-001

4.1.6 Coupled Three-Dimensional and One-Dimensional Flows.

This example is designed to simulate a losing stream passing through an underlying unconfined aquifer. The 3-D subsurface domain is represented by a 900 m x 800 m x 50 m area with a sloped land surface and the porous media extends to 50 m below land surface. A stream is located at the center of the domain (Fig.4.1.6-1). The saturated hydraulic conductivity of the soil is $K_{xx}=1.0^{-4}$ m/s, $K_{yy}=1.0^{-5}$ m/s and $K_{zz}=5.0^{-6}$ m/s. The effective porosity is 0.3. The unsaturated characteristic functions are linear.

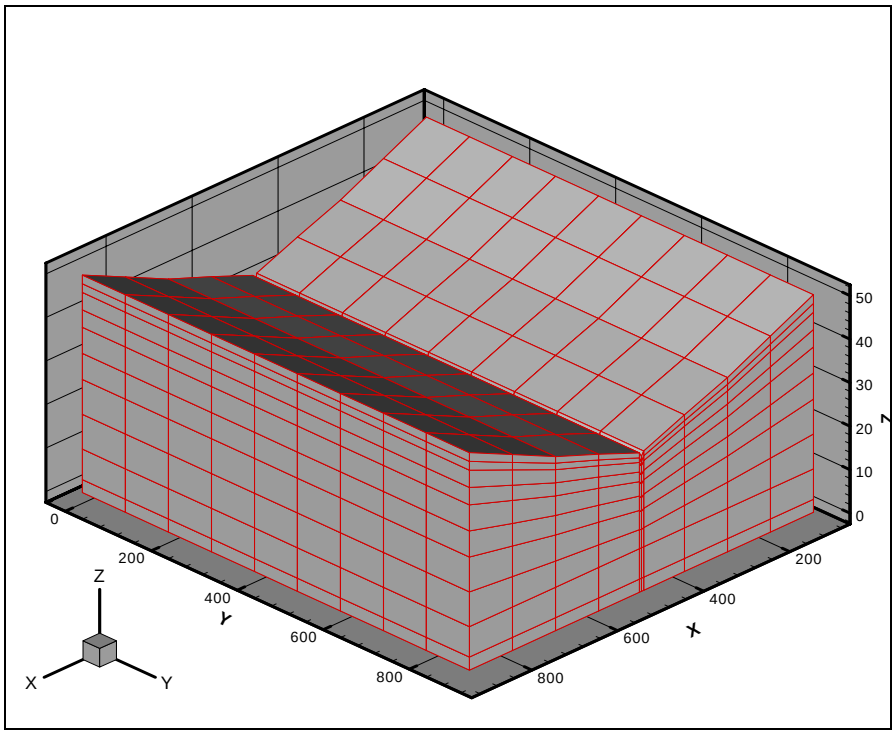

Fig. 4.1.6-1. 3-D Finite Element Mesh of Example 4.1.6

At the beginning of the simulation, a constant total head of 35 m is applied to the aquifer. A total head of 35 m was also applied as specified head boundary conditions to the lower part of the subsurface boundaries at the location of both stream ends. Other subsurface boundary surfaces were either variable boundary (top surface) or impermeable (other sides).

The stream is initially dry. An unsaturated zone hydraulically separates the stream and the aquifer. The length of the stream is 900 m. It was divided into 9 elements and 10 nodes. The bottom slope is 5/1,000. The cross-section is rectangular. The Manning's n is 0.03.

A discharge hydrograph is applied at the upstream end of the stream (Fig.4.1.6-2). The inflow hydrograph has a peak discharge of 40 m^3/s and duration of 7,200 seconds (2 hours). A rating curve was applied at the stream outlet. The total simulation time is 14,200 seconds (4 hours). A time step of 600 sec and 10 sec were used for 3-D subsurface and channel flows, respectively.

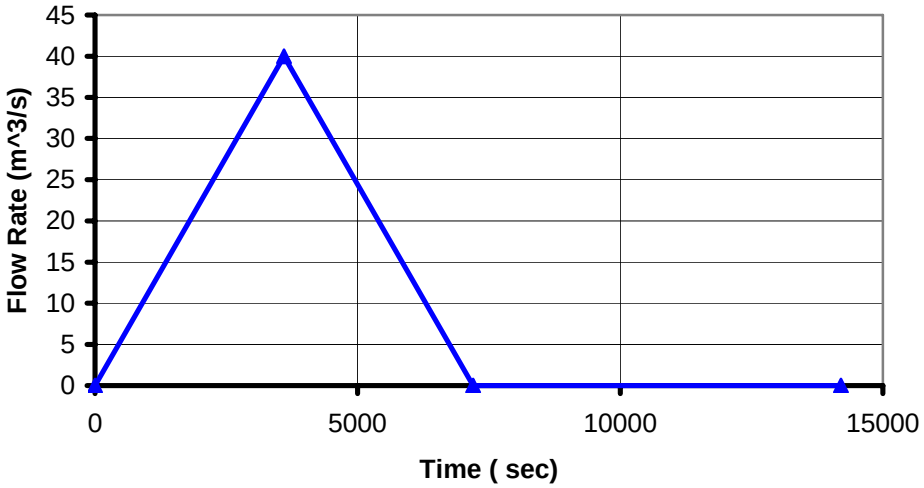

Fig. 4.1.6-2. Inflow Hydrograph for Example 4.1.6

The simulation results show that the saturated area in the subsurface domain expanded along the stream due to seepage from the channel (Fig. 4.1.6-4 and 4.1.6-5). The outflow hydrograph was modified by the infiltration into the subsurface. The peak discharge at x=600.0 m was less than the peak value without infiltration. And the time to peak was also delayed (Fig. 4.1.6-3).

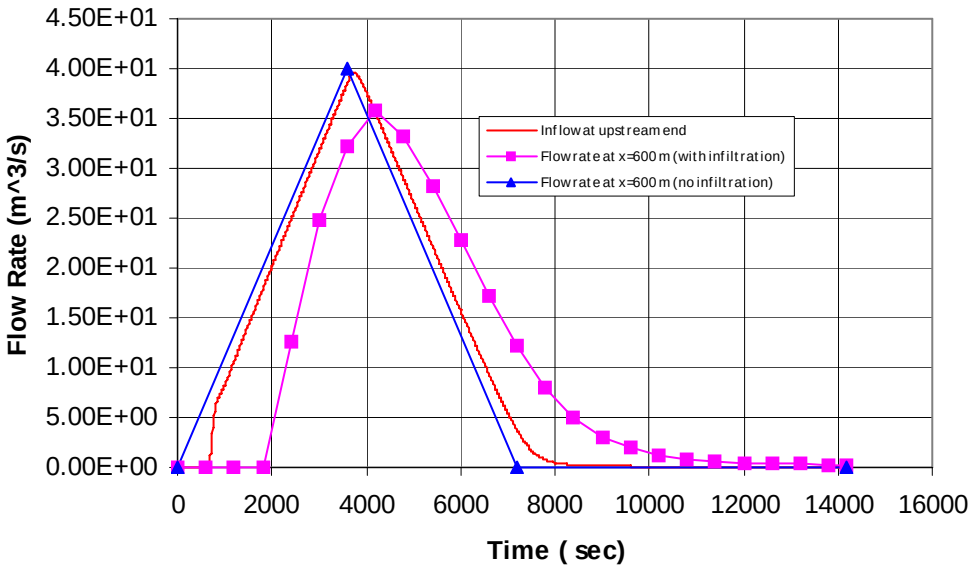

Fig. 4.1.6-3. Discharge Hydrograph (x = 0 and x = 600 m) for Example 4.1.6

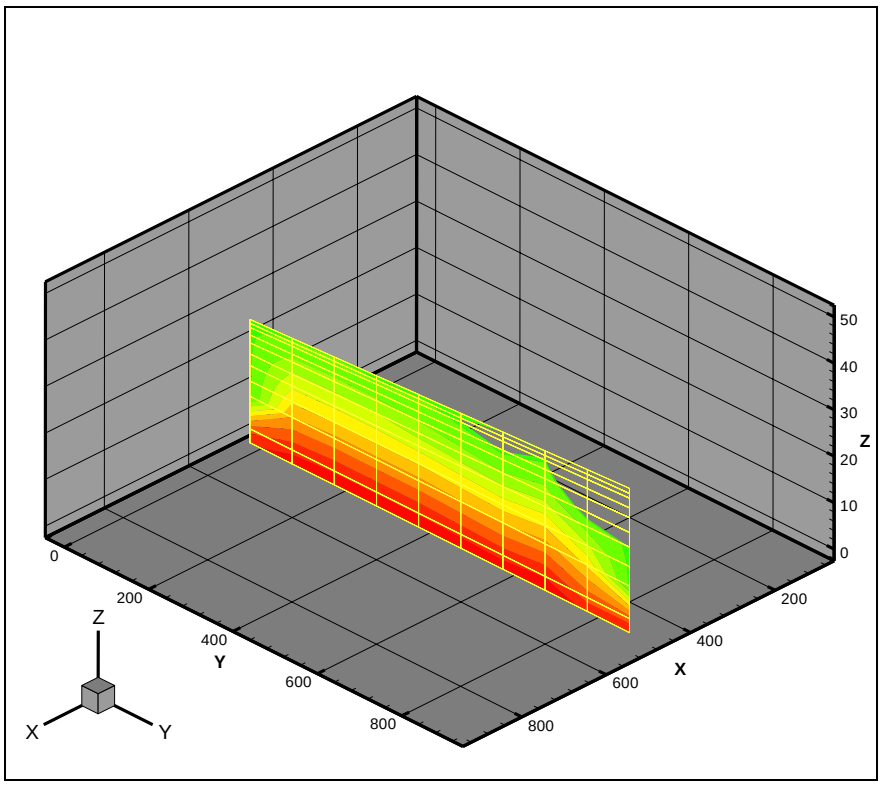

Fig. 4.1.6-4. Pressure Head Distribution at X = 500 m (Time=14,200 seconds)

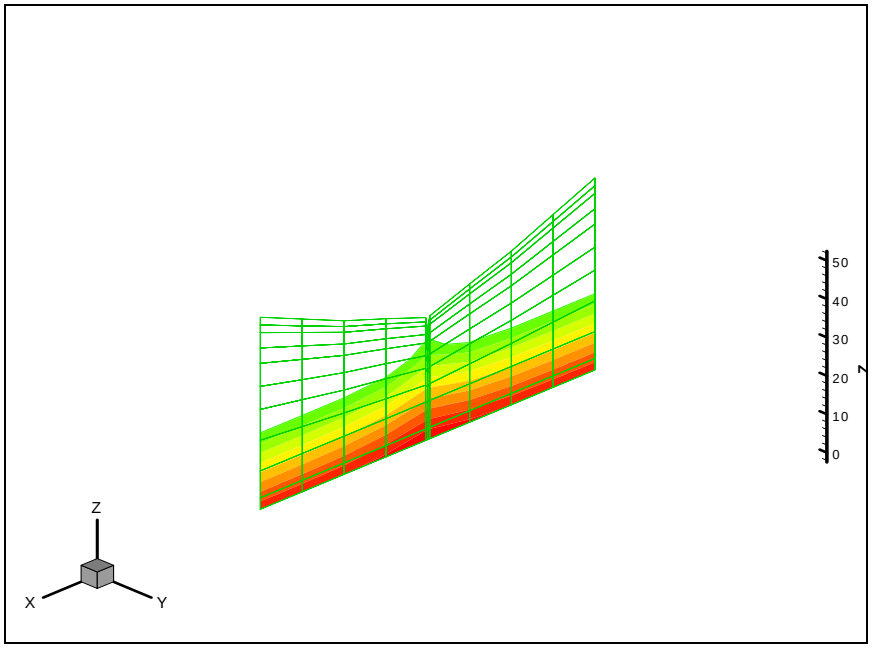

Fig. 4.1.6-5. Pressure Head Distribution at Y=430 m (time=14,200 seconds)

4.1.7 Coupled One-Dimensional, Two-Dimensional, and Three-Dimensional Flows.

This example demonstrates the capability of WASH123D in handling coupled 1-D channel, 2-D overland, and 3-D variably saturated subsurface flow problems. A spreader canal that was consisted of an upstream boundary node, a downstream boundary node, a junction, and a dead end was assumed in a hypothetic watershed. The 2-D overland domain was discretized with 154 elements and 175 nodes, and the 1-D spreader canal was composed of 14 elements and 17 nodes, where 1-D Nodes 1 through 6 were included in the first reach, 7 through 13 in the second reach, 14 through 17 in the third reach, and 1-D Nodes 6, 7, and 14 connected at the junction (Fig. 4.1.7-1). By excluding those 2-D nodes that coincided with 1-D nodes, the 2-D computational domain contained 124 (= 154 - 30) 2-D elements and 160 (= 175 - 15) 2-D nodes. The canal was 4 m wide for the first reach, 2 m wide for the second and third reaches, and its cross-sectional area was proportional to its depth. The canal was as deep as 0.1 m at the entrance (i.e. the first 1-D node, written in red in Fig. 4.1.7-1) and as shallow as 0.025 m at the junction. Figure 4.1.7-1 also provides the figures of bank height for all channel-related overland nodes (written in dark blue). The 3-D domain contained 1,050 nodes and 770 elements (Fig. 4.1.7-2), where the overland/canal domain coincided with its top boundary (i.e., ground surface).

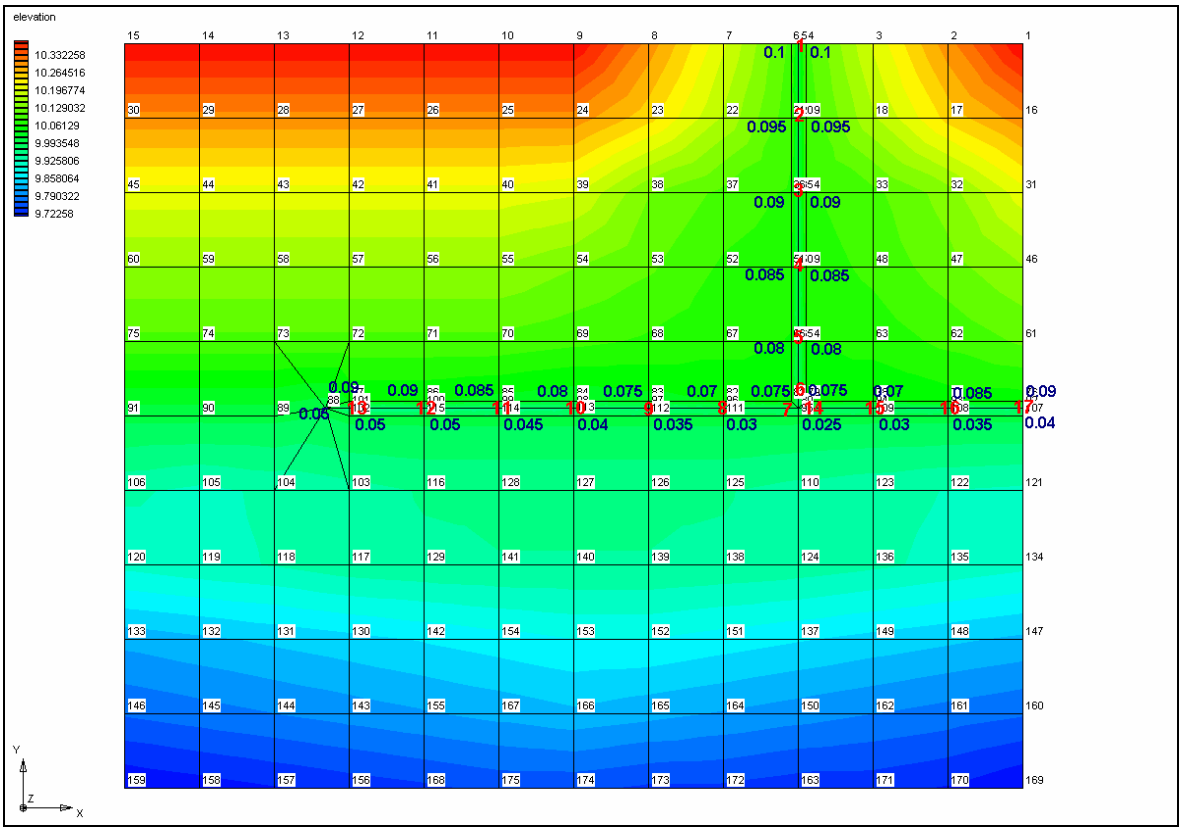

Fig. 4.1.7-1. 1-D/2-D Discretization and Surface Elevation of Example 4.1.7

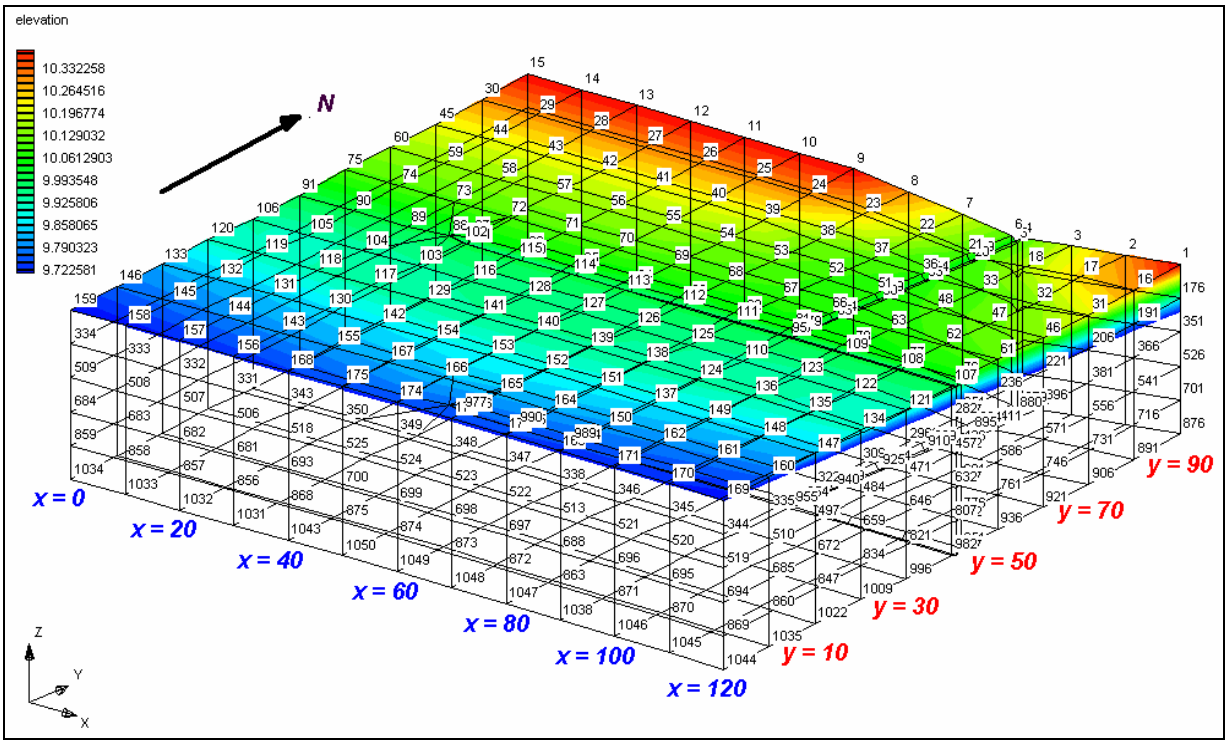

Fig. 4.1.7-2. 3-D Discretization of Example 4.1.7

To compute 3-D subsurface flow, a total head of 10.01 m was specified on the northern boundary and 9.5 m on the southern boundary. The east, west, and bottom boundaries were assumed impermeable. The Manning's roughness was set to 0.01 for both 2-D overland and 1-D canal flow. In computing 2-D overland flow, a Dirichlet boundary condition of zero depth was specified for Nodes 1, 9, 10, 11, 12, 13, 14, and 15, which represented high grounds; a depth-dependent flux boundary condition was given on the low ground (or south) boundary (i.e., the boundary that emprises Nodes 159, 158, 157, …, 169); and a channel-overland interaction boundary condition was specified for the channel-related overland boundary sides, which included a depth-dependent flux when flow was from overland to canal and a canal stage condition when flooding occurred. A time-dependent water depth was controlled at both the upstream and downstream 1-D nodes (i.e., Nodes 1 and 17 in red in Fig. 4.1.7-1), which started at 0.01 m at time = 0 second, then increased linearly to 0.04 m at time = 1,800 seconds, and stayed at 0.04 m for the rest of the simulation (i.e., to time = 14,400 s). A zero-velocity condition was applied at the dead-end node.

The initial subsurface head distribution (Fig. 4.1.7-3) was computed by solving for a steady-state subsurface flow solution, where Dirichlet boundary conditions were applied to the north and the south boundaries as mentioned above, a rainfall rate of 10^{-8} m/s was assumed as the variable boundary flux on the top boundary, and a ponding depth of 0.01m was enforced and applied to those subsurface boundary nodes that were corresponding to 1-D canal nodes. At the beginning of the simulation, the overland domain was completely dry, while a constant depth of 0.01 m was assumed at every node in the 1-D spreader canal. A constant rainfall rate of 10^{-7} m/s was applied throughout the entire simulation period of 14,400 seconds. The time-step size was set to 50 seconds for computing 3-D subsurface flow, 10 seconds for 2-D overland flow, and 2 seconds for 1-D channel

flow. It is noted that after the transient simulation began, the top boundary of 3-D subsurface served as the interface between surface and subsurface domains, and the boundary condition that was applied on it depended on both rainfall and water depth on ground surface.

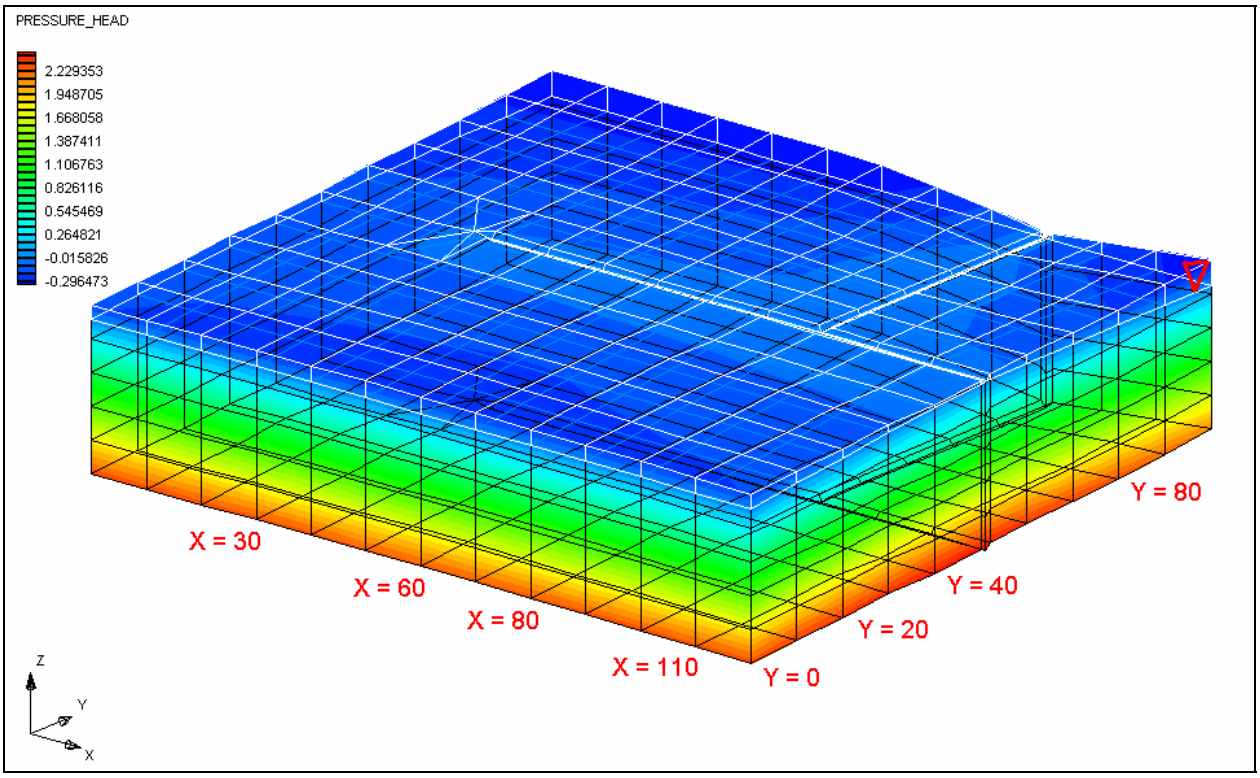

Fig. 4.1.7-3. The Computed Initial Steady-State Pressure Head Distribution of Example 4.1.7

Figure 4.1.7-4 plots the variation of water depth with time at five 1-D canal nodes: 3, 6, 9, 12, and 15. Also, a dash line that represents the bank height over which canal water will overflow to the downstream overland regime is given as reference for Nodes 6, 9, 12, and 15 (marked with respective colors). The bank height was 0.09 m for Node 3, which is out of scale in Figure 4.1.7-4. Figure 4.1.7-5 provides a zoom-in plot of Figure 4.1.7-4 for the period of Time = 0 through 2,000 s, where the four "X" symbols indicate the moments that water started to flow from canal to overland at Nodes 6, 9, 12, and 15.

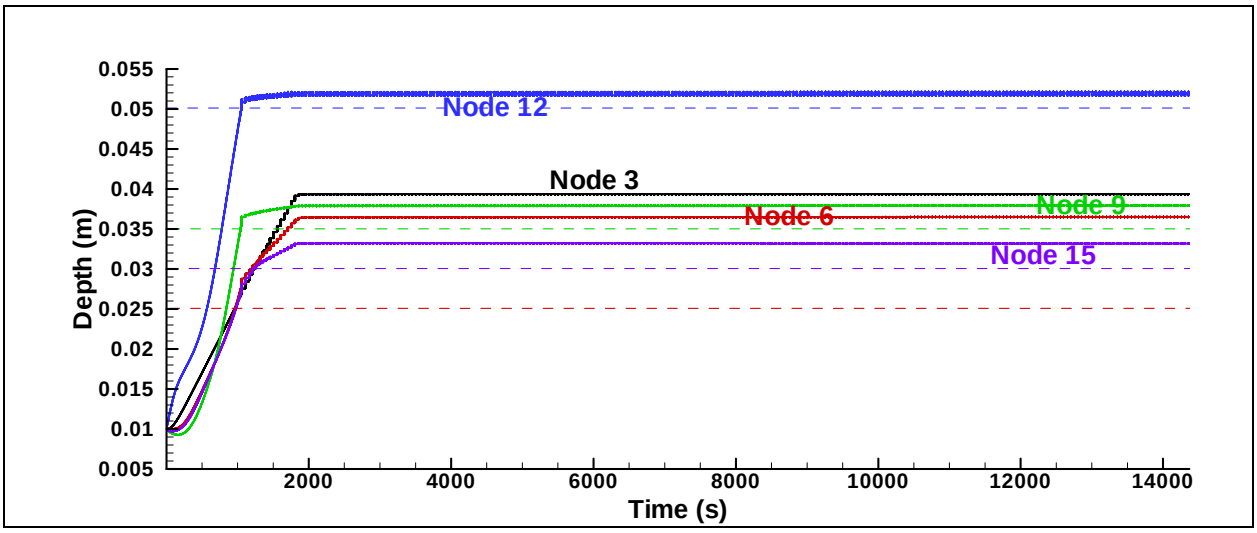

Fig. 4.1.7-4. Computed Water Depth at Various 1-D Canal Locations for Example 4.1.7 (Time = 0 through 14,400 s).

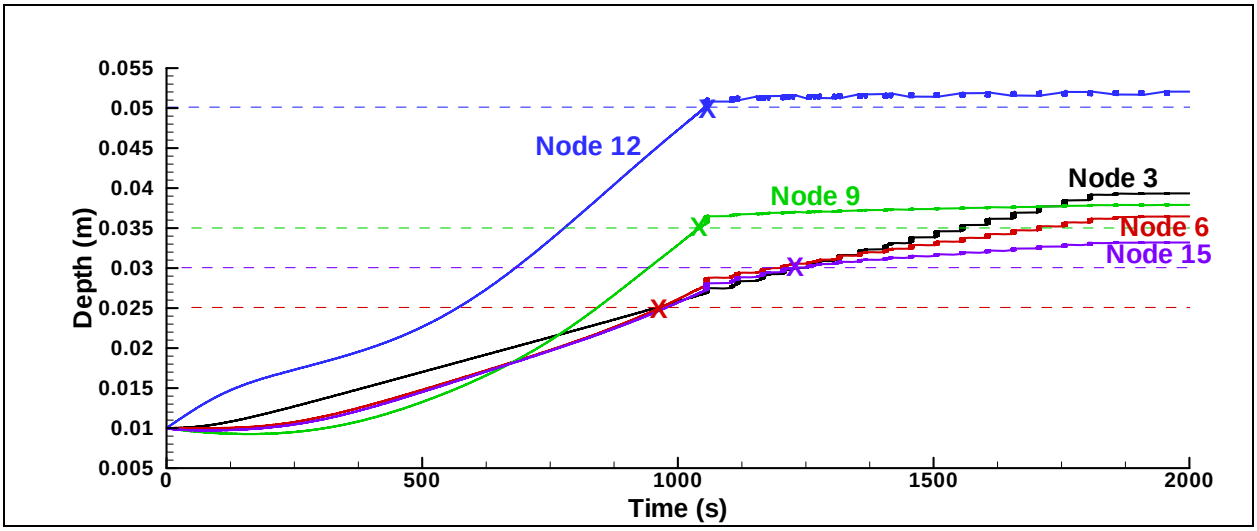

Fig. 4.1.7-5. Computed Water Depth at Various 1-D Canal Locations for Example 4.1.7 (Time = 0 through 750 s)

Figure 4.1.7-6 plots the distribution of water depth in the overland domain at various times. Figures 4.1.7-7 and 4.1.7-8 plot the distribution of subsurface pressure head on several x and y, respectively, cross sections at various times, where the unsaturated zone is highlighted in white and water table is marked in red.

Time = 1,200 s

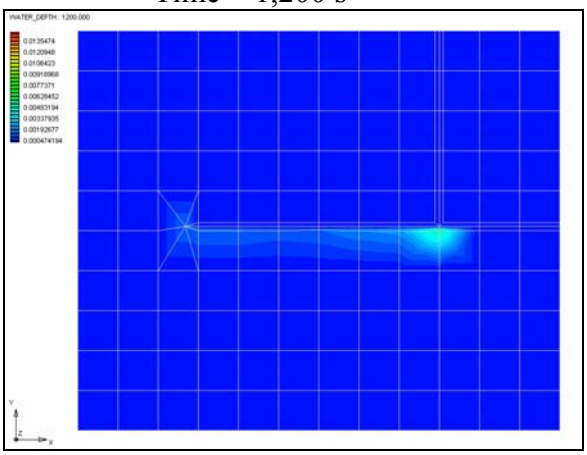

Time = 2,400 s

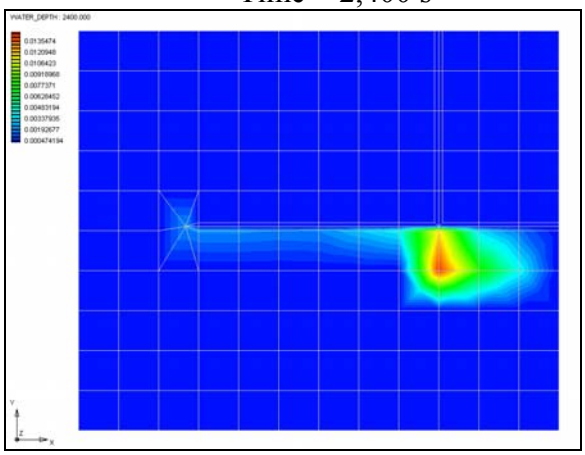

Time = 3,600 s

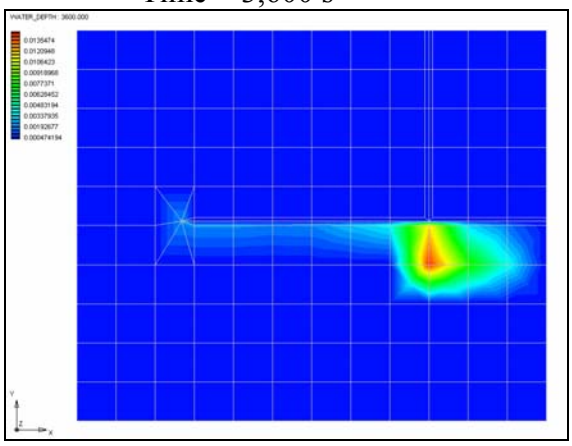

Time = 4,800 s

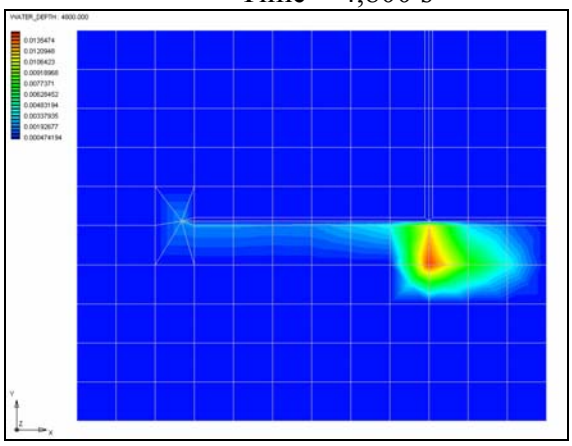

Time = 6,000 s

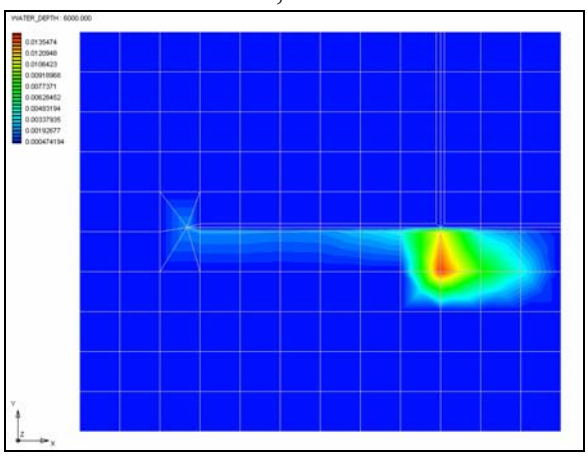

Time = 7,200 s

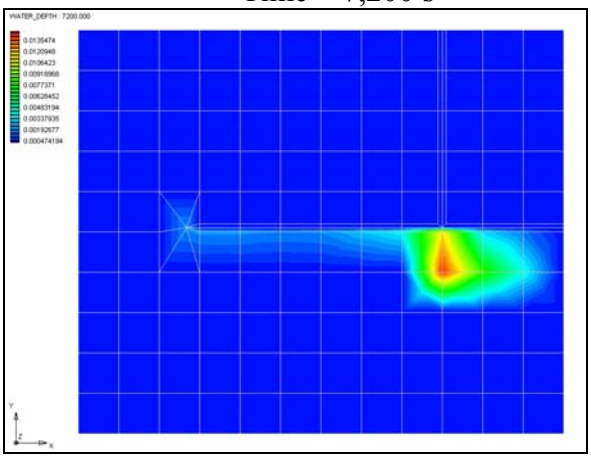

Fig. 4.1.7-6. Computed Distribution of Water Depth of Overland at Various Times (Example 4.1.7, Part 1)

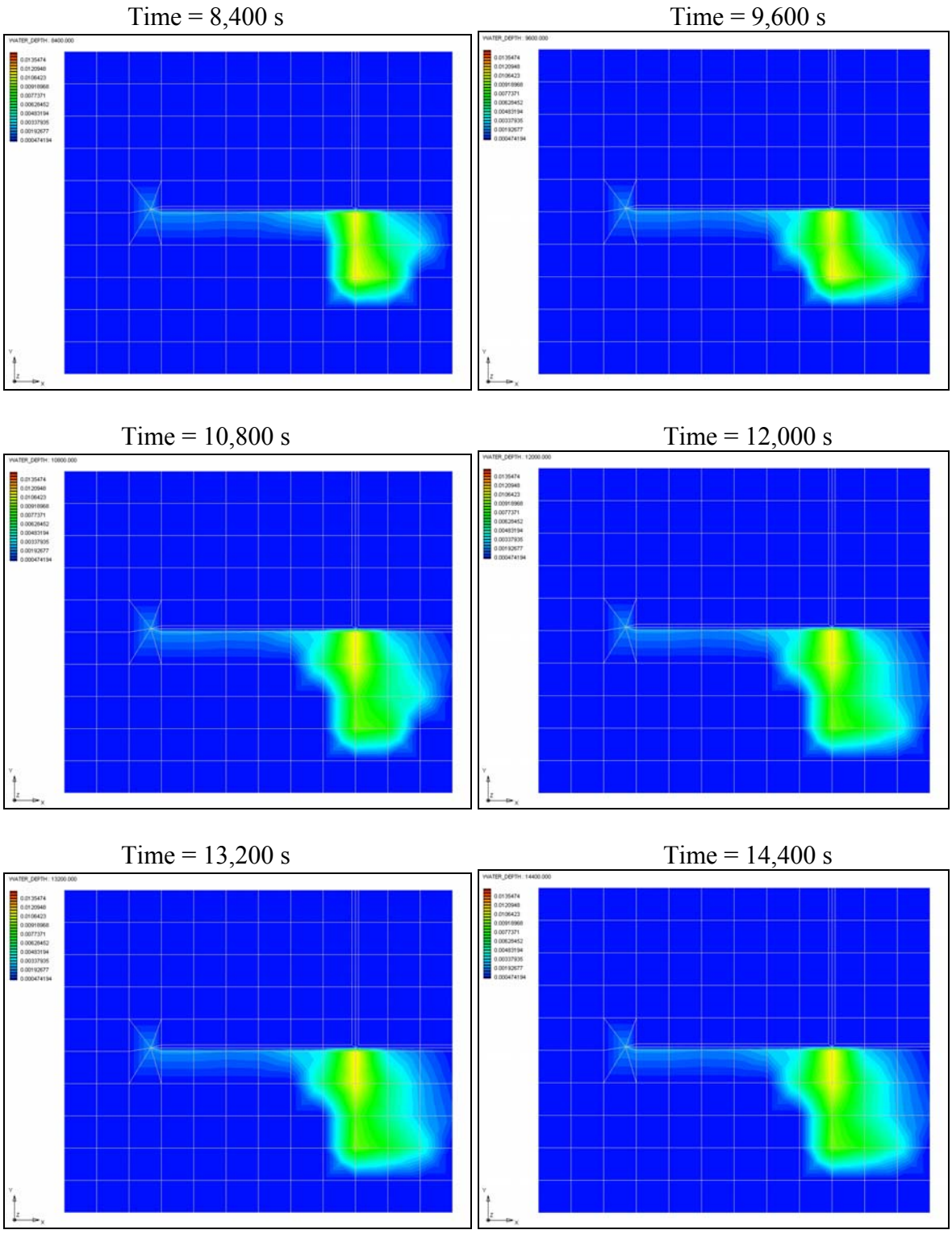

Fig. 4.1.7-6. Computed Distribution of Water Depth of Overland at Various Times (Example 4.1.7, Part 2)

Time = 1,200 s

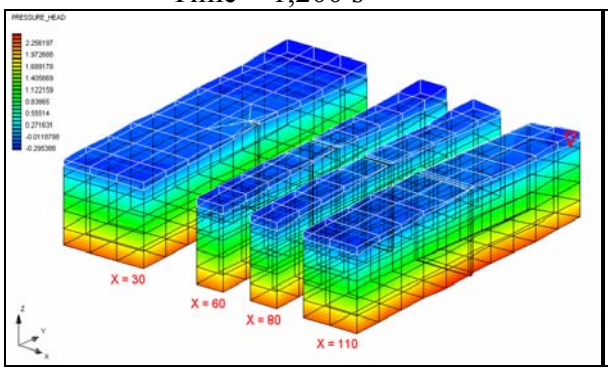

Time = 2,400 s

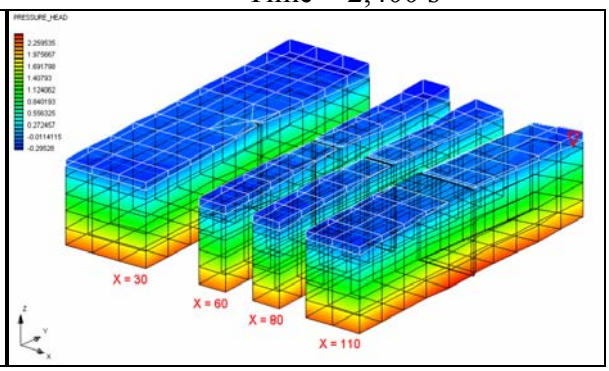

Time = 3,600 s

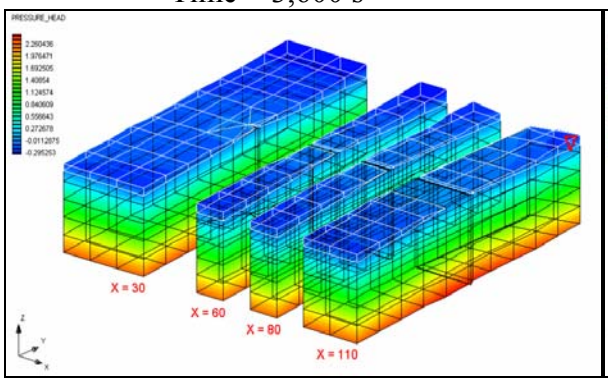

Time = 4,800 s

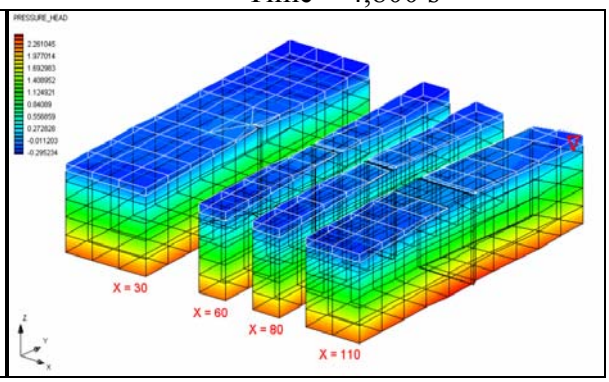

Time = 6,000 s

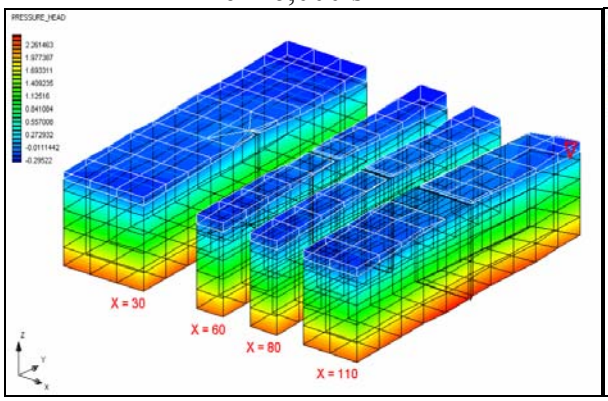

Time = 7,200 s

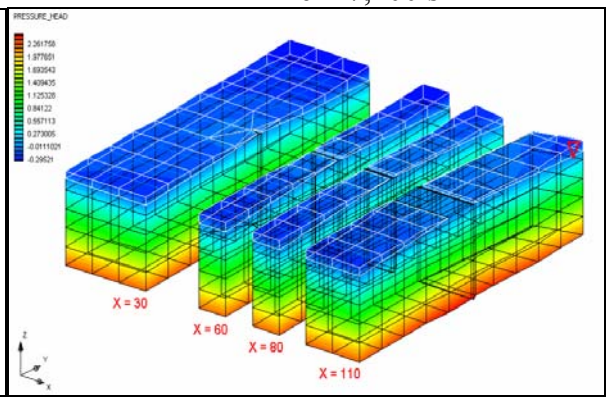

Fig. 4.1.7-7. Computed Pressure Head Distribution on Several X Cross Sections at Various Times (Example 4.1.7, Part 1)

Time = 8,400 s

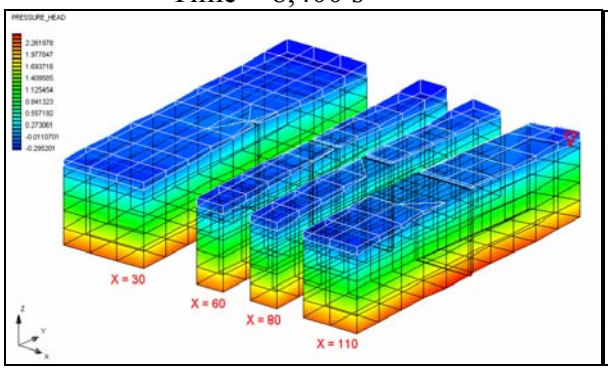

Time = 9,600 s

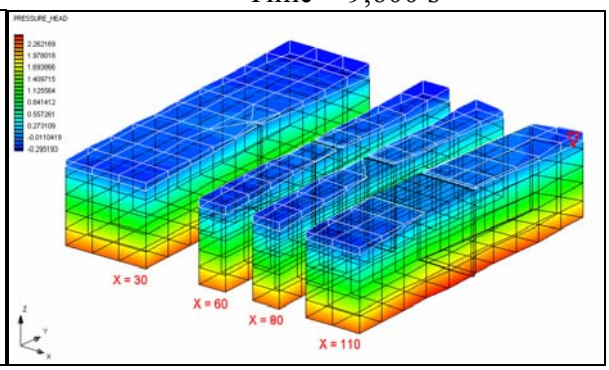

Time = 10,800 s

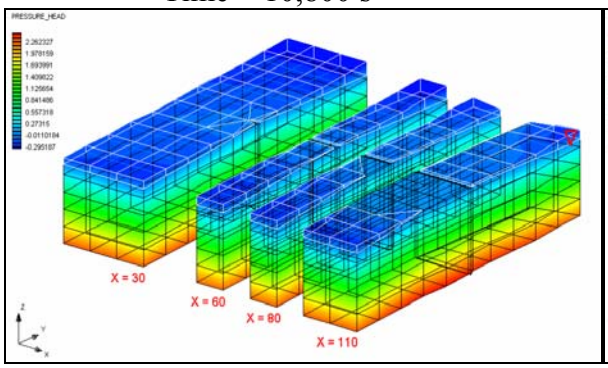

Time = 12,000 s

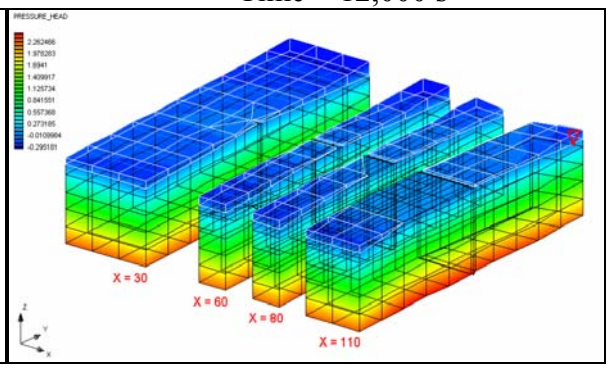

Time = 13,200 s

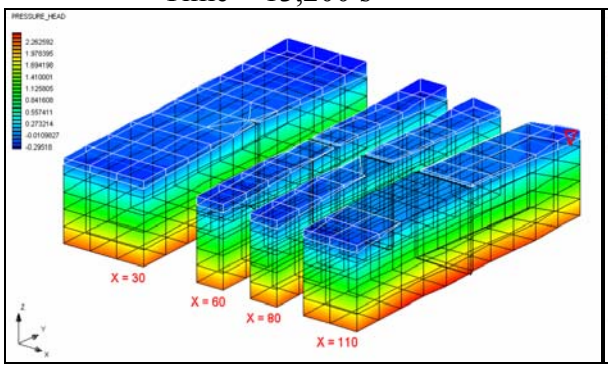

Time = 14,400 s

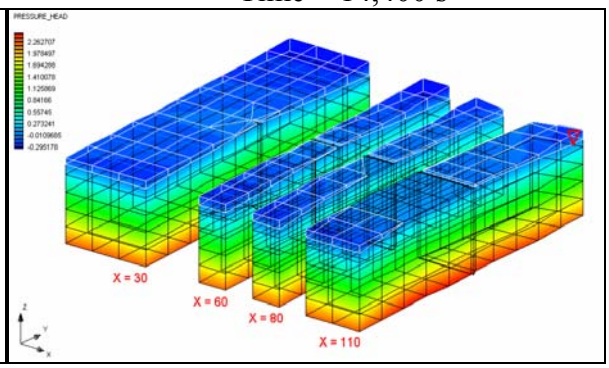

Fig. 4.1.7-7. Computed Pressure Head Distribution on Several X Cross Sections at Various Times (Example 4.1.7, Part 2)

Time = 1,200 s

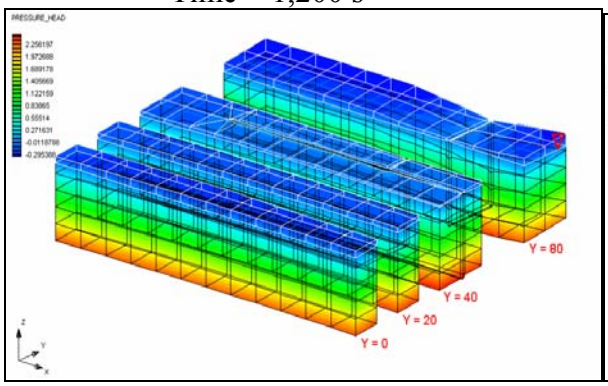

Time = 2,400 s

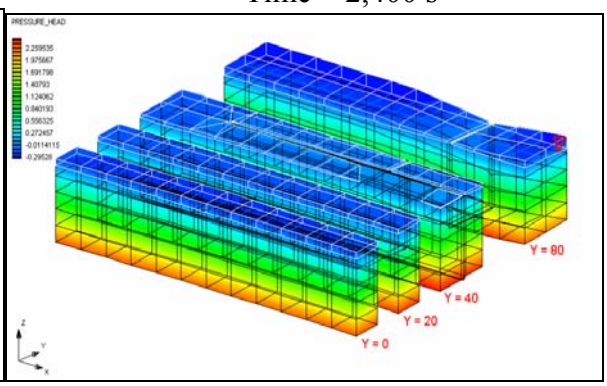

Time = 3,600 s

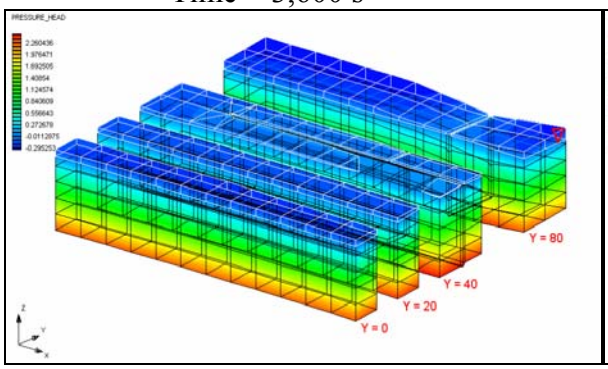

Time = 4,800 s

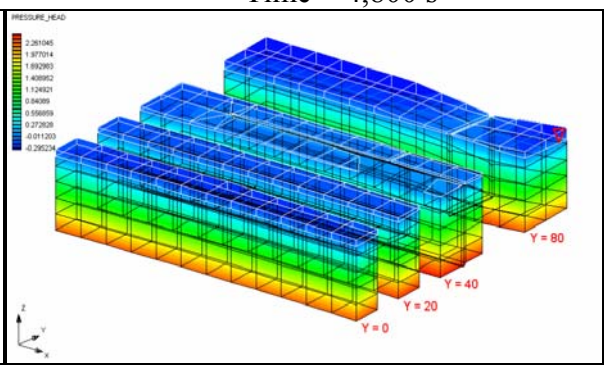

Time = 6,000 s

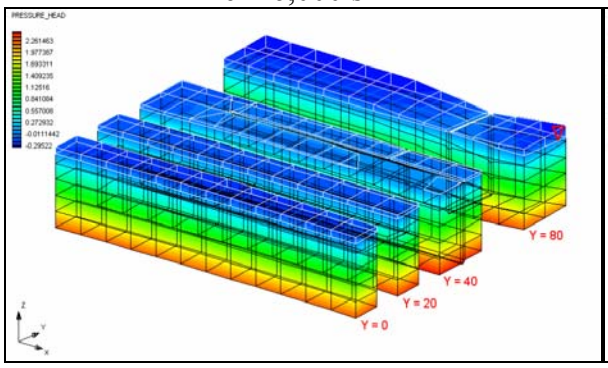

Time = 7,200 s

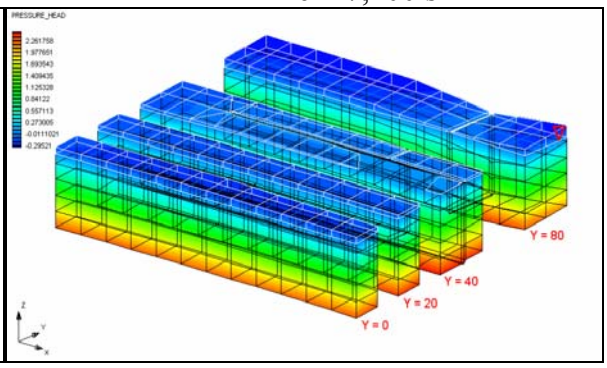

Fig. 4.1.7-8. Computed Pressure Head Distribution on Several Y Cross Sections at Various Times (Example 4.1.7, Part 1)

Time = 8,400 s

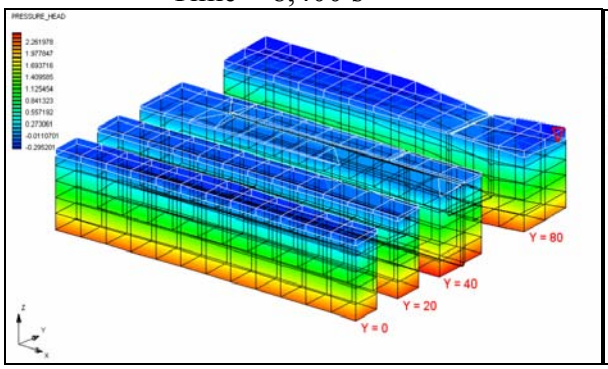

Time = 9,600 s

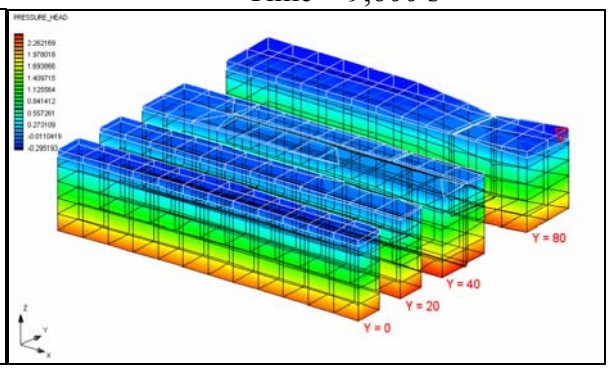

Time = 10,800 s

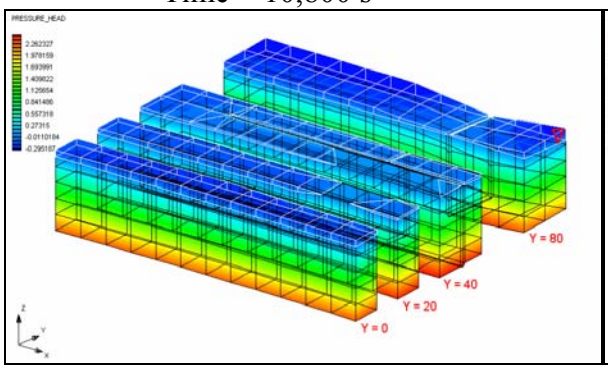

Time = 12,000 s

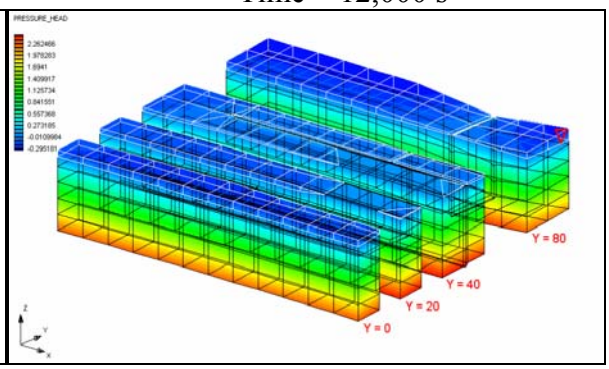

Time = 13,200 s

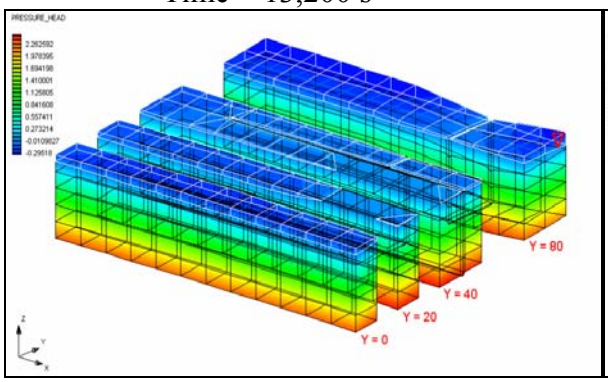

Time = 14,400 s

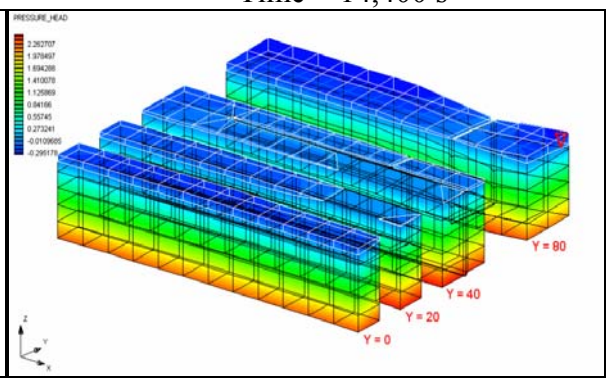

Fig. 4.1.7-8. Computed Pressure Head Distribution on Several Y Cross Sections at Various Times (Example 4.1.7, Part 2)

It is observed from Figure4.1.7-4 that the 1-D canal flow may be considered to be reaching a steady state after time = 3,000 seconds. However, the change of water depth and pressure head with time in Figures 4.1.7-6 and in Figures 4.1.7-7 and 4.1.7-8, respectively, shows that 2-D overland flow and 3-D subsurface flow have not reached a steady state even at the end of the simulation.

From Figure 4.1.7-6, it is observed that the overland water seems to be confined within a certain region during Time = 2,400 s through Time = 7,200 s and during Time = 12,000 s through Time = 14,400 s. After a close examination on the numerical results, we determine that this confinement was caused by infiltration at the respective downstream locations, which was greatly influenced by the Dirichlet boundary condition (total head = 9.5 m) that was specified on the southern boundary. As time passes, infiltration from overland to subsurface raised water table, and the overland water front moved further downstream when water table arose to near ground surface and water coming in from the upstream could overcome infiltration.

Figures 4.1.7-6 through 4.1.7-8 show consistent results between overland water depth and subsurface pressure head. This has verified that we have successfully implemented the coupling of surface and subsurface flow in WASH123D.

4.2 Three Optional Approaches to Modeling Flow in WASH123D

Three approaches are taken to model flow problems in WASH123D: kinematics-wave, diffusive-wave, and fully dynamic-wave models. In this section, four example problems are presented to show possible differences in simulations using these three different approaches and to illustrate that only fully dynamic-wave approaches can be taken to model very rapidly varying transient flow problems.

4.2.1 One-Dimensional River Flows

Three cases are presented for the one-dimensional problems in the river/stream/canal system. Case 1 is a steady-state subcritical flow problem, which shows there are some errors in the diffusive wave approximation even for this simple problem. Case 2 is a steady-state mixed subcritical and supercritical problem, which is designed to demonstrate the magnitude of errors introduced with the diffusive wave approximation. Case 3 is a steady-state, mixed subcritical and supercritical problem with a hydraulic jump. This problem demonstrates that the diffusive wave approximation is not adequate for this complicated problem. In all three cases, steady-state simulations were achieved via transient simulations with constant boundary and source conditions.

1. Subcritical Flow. This is the test problem published by MacDonald et al. (1997), where an analytical solution for the problem is available. The channel is rectangular with a width of 10 m. The total length is 1,000 m. A constant flow of 20 m^3/s passes through. The flow is subcritical over the entire channel. A water depth of 0.748409 m is specified at the downstream outlet. The Manning's n value is 0.03. The bed slope is given by an analytical function of the water depth. Simulated steady-state profiles of water depth with diffusive wave (DIW) and fully dynamic wave

(FDW) approaches are given in Figure 4.2.1-1. It is seen that the FDW approach yields excellently accurate results while the DIW approach produces some errors.

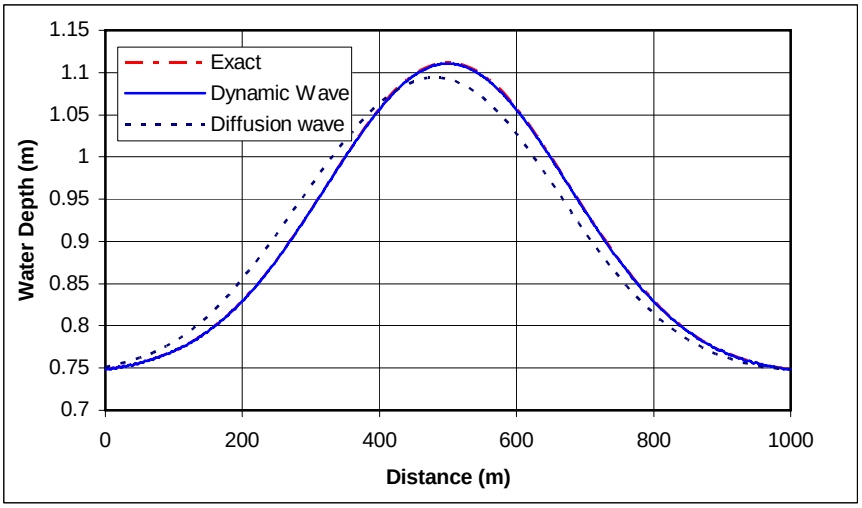

Fig. 4.2.1-1. Comparison of Simulated Water Depth Profile with Exact Solutions

2. Mixed Subcritical and Supercrical Flow. This test case was described in MacDonald et al. (1997). A 1,000 m of rectangular channel with a width of 10 m is given a constant flow rate of 20 m^3/s. The bottom slope is variable such that the flow condition at the inflow is subcritical and is supercritical at the outlet. The Manning's n value is 0.02. For the dynamic wave approach, one inflow boundary condition is specified at the upstream and no boundary condition is needed at the downstream since supercritical flows occur therein. For diffusive wave model, two boundary conditions must be given: one is the upstream boundary condition where the inflow rate is prescribed as in the case of FDW approach and the other is the downstream boundary condition. In this case, the known water depth at outlet is specified as the Dirichlet boundary conditions.

The dynamic wave model is able to solve this mixed flow problem with good accuracy (Fig. 4.2.1-2). No numerical instabilities have been encountered. The diffusive wave model also provides satisfactory results (4% error in water depth). The Froude number profile plot shown in Figure 4.2.1-3 confirms the mixed flow condition. It is interesting to note that the DIW model requires more input data than the FDW model, yet yields poorer simulations.

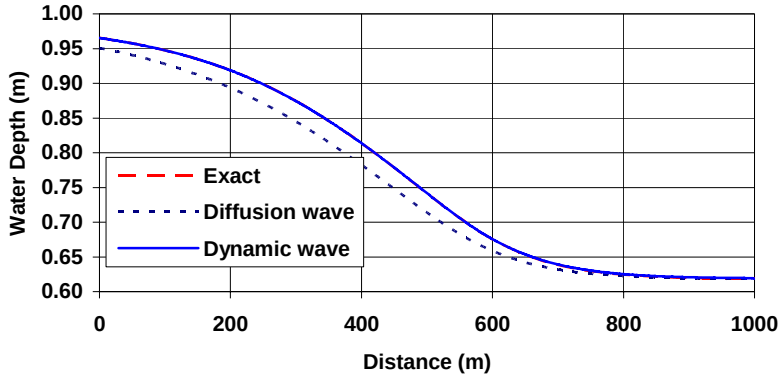

Fig. 4.2.1-2. Comparison of Simulated Water Depth Profile with Exact Solutions

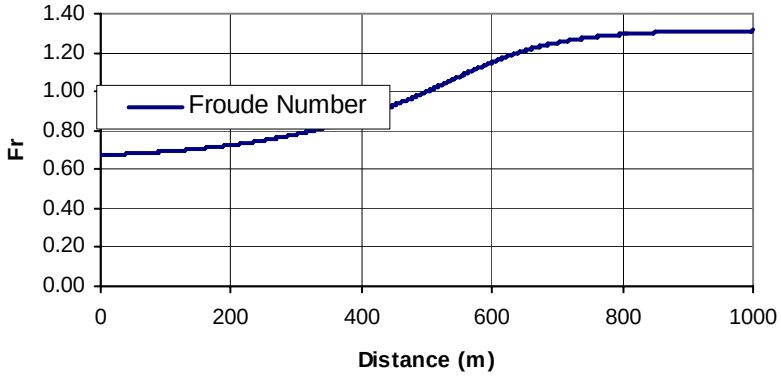

Fig. 4.2.1-3. Froude Number Profile

3. Mixed Subcritical and Supercrical Flow with Hydraulic Jump. This test case was described in MacDonald et al. (1997). The channel is trapezoidal with a total length of 1,000 m. The upstream inflow is a constant discharge 20 m^3/s. At the downstream outlet, a specified water depth of 1.349963 m is applied. The side slope of the trapezoidal cross-section is 1:1. The Manning's n value is 0.02. There is an abrupt change in the bed slope at x = 500 m, causing a hydraulic jump. The bottom elevation and bed slope were given in MacDonald et al. (1997). Both inflow and outflow boundaries are subcritical. The analytical solution of the steady state water depth is provided in MacDonald et al. (1997)

$$h(x)=\begin{cases} 0.723449\left[1-\tanh\left(\dfrac{x}{1,000}-\dfrac{3}{10}\right)\right] & 0\le x\le 300 \\ 0.723449\left\{1-\frac{1}{6}\tanh\left[6\left(\dfrac{x}{1,000}-\dfrac{3}{10}\right)\right]\right\} & 300\le x\le 600 \\ \dfrac{3}{4}+\sum_{k=1}^{3}a_k\exp\left[-20k\left(\dfrac{x}{1,000}-\dfrac{3}{10}\right)\right]+\dfrac{3}{5}\exp\left(\dfrac{x}{1,000}-\dfrac{3}{10}\right) & 600\le x\le 1,000 \end{cases} \quad \textbf{(4.1.3.4)}$$

This is a non-trivial problem with source terms (roughness and bed slope) and is more realistic in testing the performance of the FEM based method of characteristics. As expected, the accuracy of the diffusive wave approximation for this mixed flow case is not satisfactory. The error induced by diffusive wave approximation is high at the supercritical zone (Fig. 4.2.1-4).

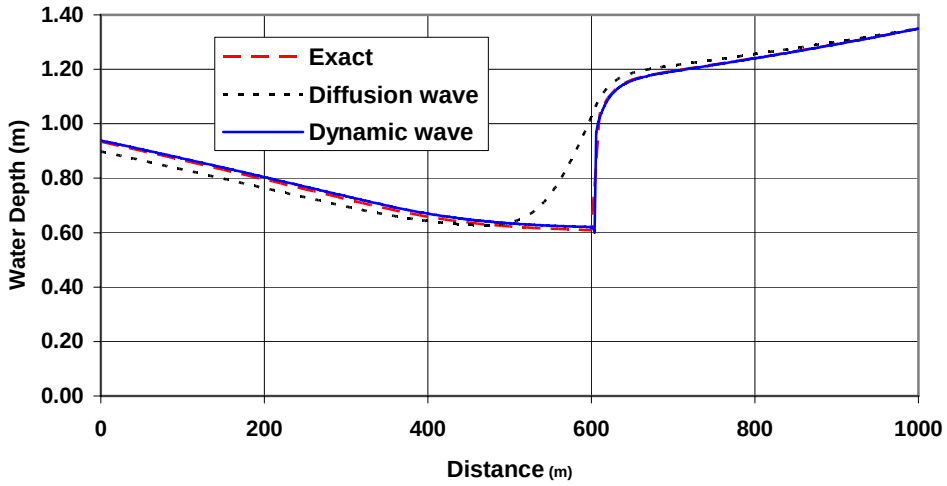

Fig. 4.2.1-4. Comparison of Simulated Water Depth Profile with Exact Solution

4.2.2 Two-Dimensional Overland Flows.

A rainfall-runoff process on an impervious curved surface is simulated (Fig. 4.2.2-1). The domain is 150 m x 40 m. The bottom elevation ranges from 0.11 m to 0.31 m over a horizontal length of 150 m. The overland domain is divided into 80 elements and 105 nodes. A specified water depth of 0.1 m is applied to the downstream end boundary. All other sides are assumed to be no-flow boundaries. A Manning's n value of 0.02 is used. The rainfall intensity is 3.0-5 m/s for 1,800 seconds (30 minutes). The purpose of this numerical experiment is to compare the simulation results obtained with different computational methods for 2-D overland flow and validate the numerical implementation for dynamic, diffusive and kinematic wave models. The average bottom slope is 0.00133.

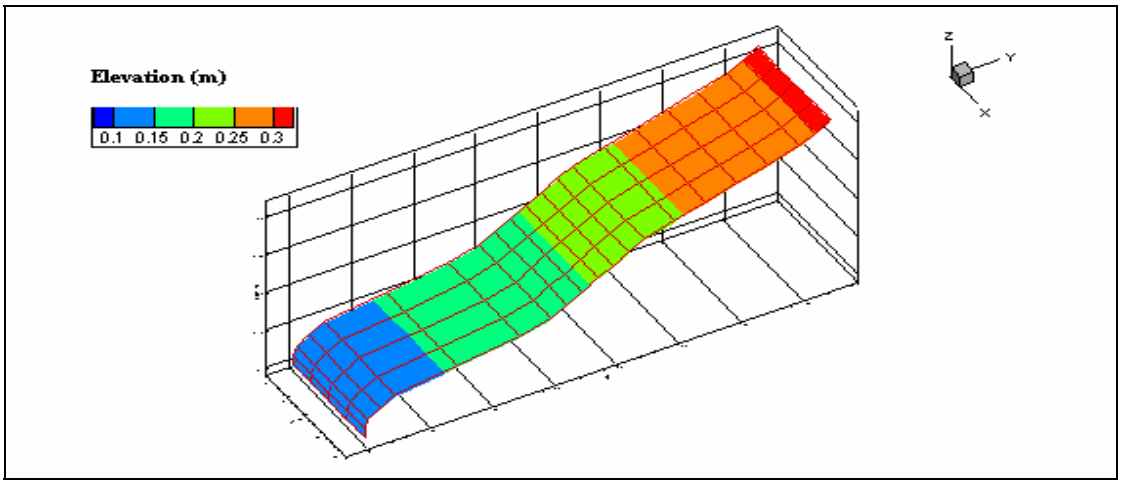

Fig. 4.2.2-1. Topography of the Land Surface

The fully dynamic wave equations and diffusive wave and kinematic wave approximations were applied to this problem. The simulation results were compared. The computed water levels at Node 28 (x = 20 m, y = 30 m, Z_o = 0.152 m) were compared (Fig. 4.4.2-2). This location is close to the downstream end. The maximum value of water level, found to be 0.173 m, 0.180 m and 0.181 m, was obtained with fully dynamic wave (MOC), diffusive wave (SL), and kinematic wave (SL) approaches. The difference between the dynamic wave and diffusive wave models is about 6%. This may indicate the diffusive wave approximation is not accurate for this problem. Similar conclusions can be made for the kinematic wave model. Water levels at Node 88 (x = 20 m, y = 130 m and Z_o = 0.278 m), which represent the flow at upper part of the surface, were compared (Fig. 4.2.2-3). The maximum water depth at this site is 0.01124 m, 0.0094 m and 0.00776 m for FDW (MOC), DIW (SL), and KIW (SL), respectively. The differences between the fully dynamic wave and diffusive/kinematic wave models at the upstream nodes are smaller than those at the downstream nodes as expected.

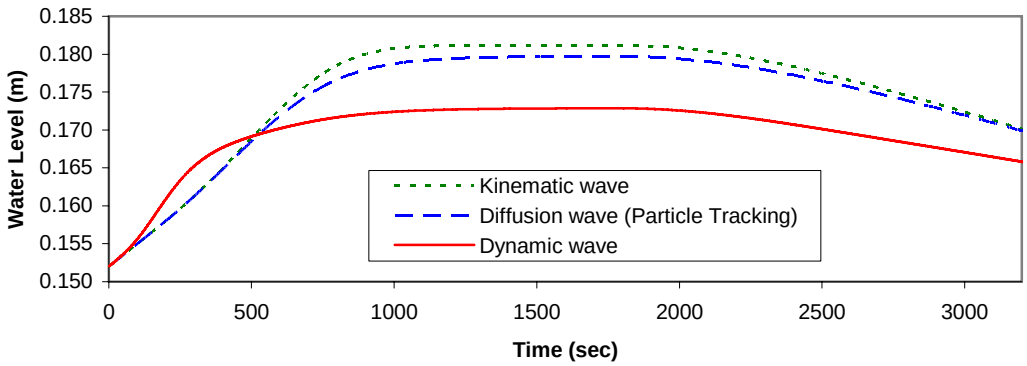

Fig. 4.2.2-2. Comparison of Simulated Water Levels at a Node Closed to Downstream

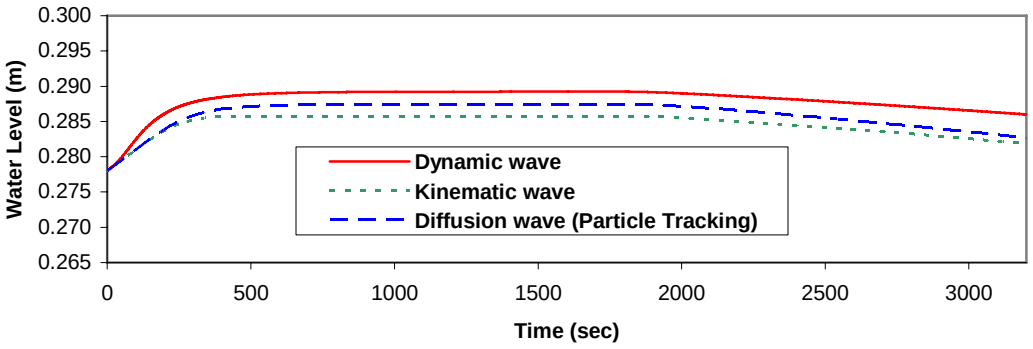

Fig. 4.2.2-3. Comparison of Simulated Water Levels at a Node Closed to Upstream

4.2.3 Circular Dam Break Problems.

This is a typically idealized dam break problem designed to test the performance of the two-dimensional method of characteristics (2-D MOC) in solving two-dimensional fully dynamic wave problems. This example has been extensively applied in the hydraulic literature to test performance of new numerical schemes for two-dimensional shallow water equations.

An idealized circular dam is located on a frictionless horizontal bottom (40 m x 40 m). A nominal circular thin wall is located at the circle from the center with a radius of 2.5 m. At the beginning of the simulation, the circular wall has collapsed instantly. At time t = 0, the water depth in the dam is 2.5 m, and a water depth of 0.5 m is presented elsewhere (Fig. 4.2.3-1).

This is a symmetrical wave propagation problem. The radial direction is the wave direction. Isotropic nature of the solution may be destroyed in some grid orientation dependent numerical schemes such as a finite volume method.

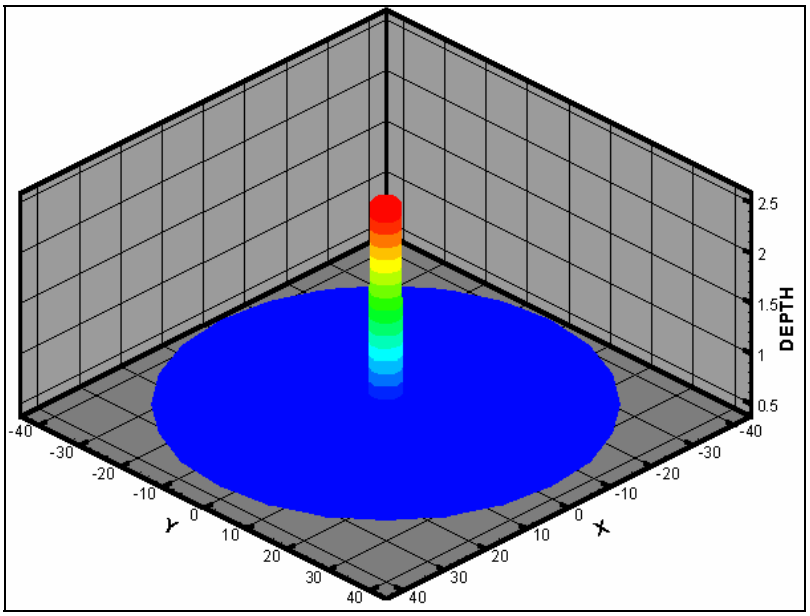

Fig. 4.2.3-1. Three-Dimensional Plot of Initial Water Depth

The most important and difficult aspect of the 2-D MOC method is the selection of the characteristic directions for the three characteristics. In this case, the wave directions are known *a priori* from the physical nature of the flow. It was found that if the characteristic directions were chosen along the radial direction at each node, the computation was very stable. When the selection of the characteristic directions is updated through the solution process, the convergence rate and the isotropic nature of the solution were very sensitive to time step and mesh size.

The computational mesh comprises 2,854 linear triangular elements and 1,440 nodes. Starting from the center of the circular dam, nodes are located evenly on circles with increasing radius. This is designed to follow the physical nature by taking advantage of finite element method (Fig. 4.2.3-2).

The time step size is 0.01 second and the total simulation time is 3.0 seconds. The following plots of water surface elevations (Fig. 4.2.3-3, 4.2.3-4 and 4.2.3-5) demonstrate the development of water wave movement. It can be seen that water depth has dropped below the initial water depth of 0.5 m outside of the dam. These numerical results are consistent with those presented in the hydraulic literatures.

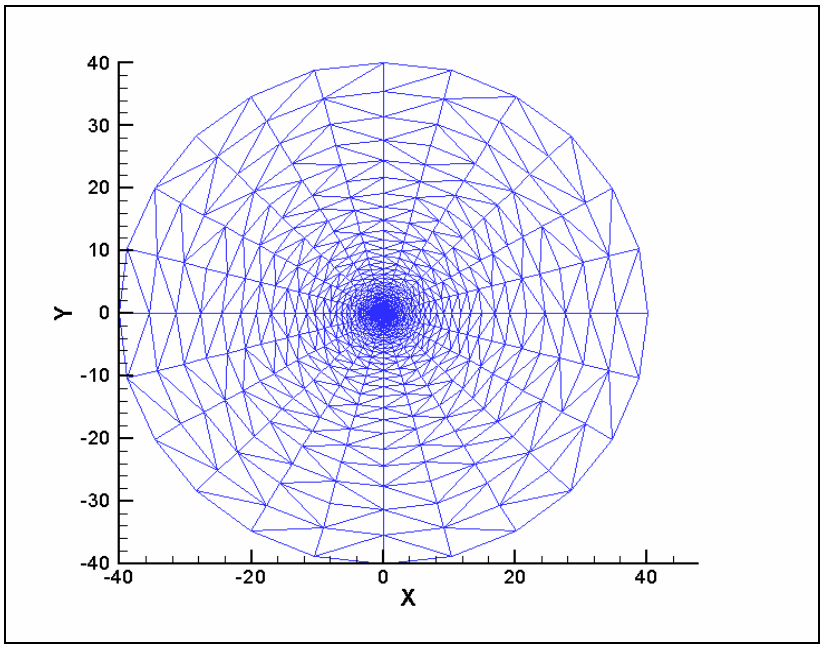

Fig. 4.2.3-2. Two-Dimensional Finite Element Mesh of Example 4.2.3

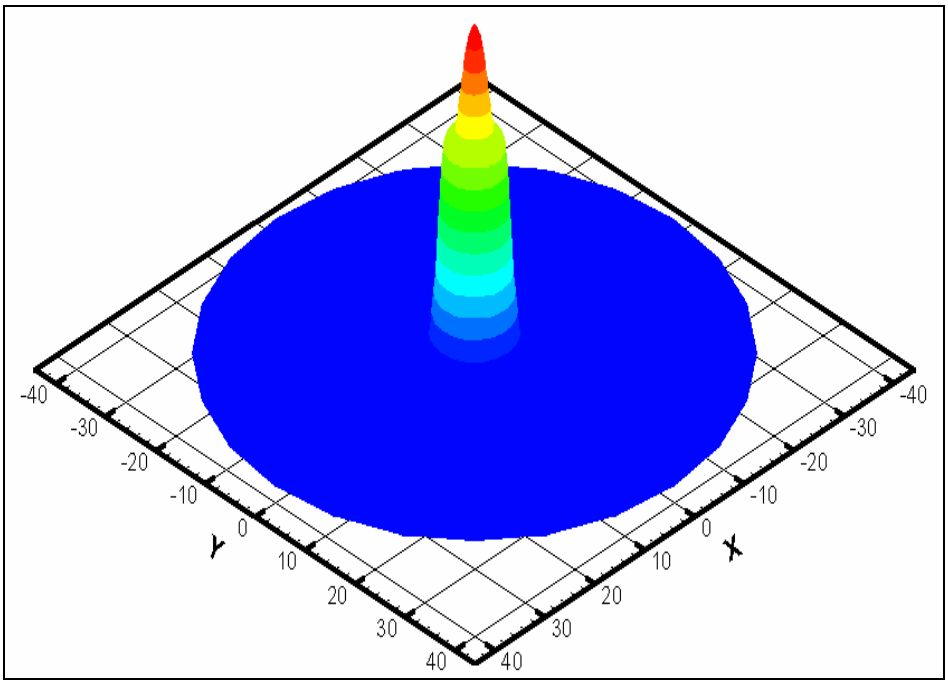

Fig. 4.2.3-3. Water Surface Elevation at Time = 0.7 s for Example 4.2.3

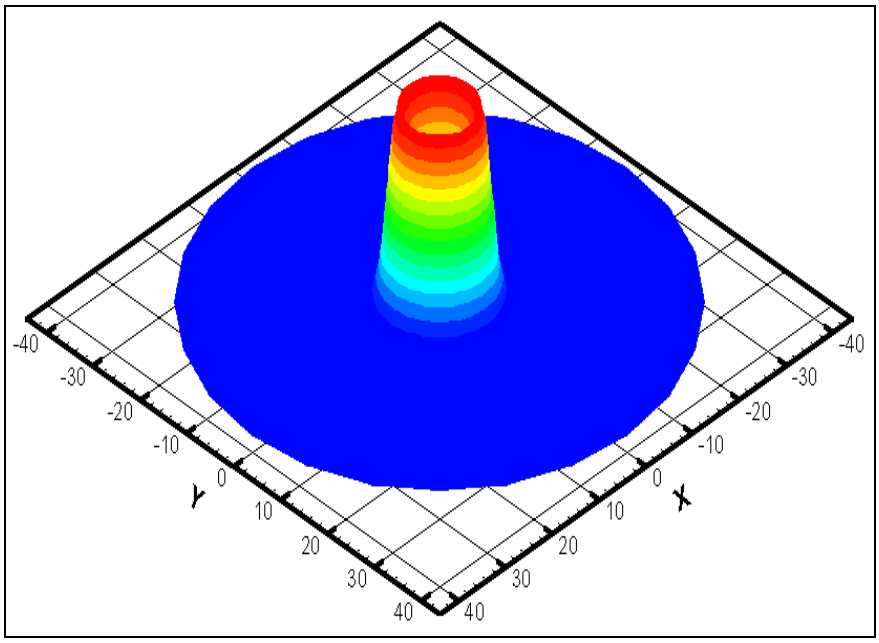

Fig. 4.2.3-4. Water Surface Elevation at Time = 1.4 s for Example 4.2.3

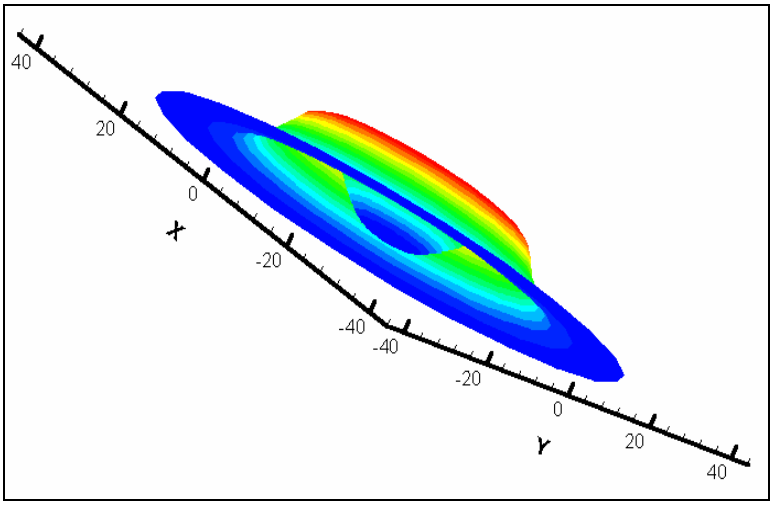

Fig. 4.2.3-5. Bottom View of Water Surface Elevation at Time = 2.8 s for Example 4.2.3

The symmetrical nature of the solution was preserved quite well. This is demonstrated in the stage hydrograph at nodes at the center of the circular domain (Fig. 4.2.3-6).

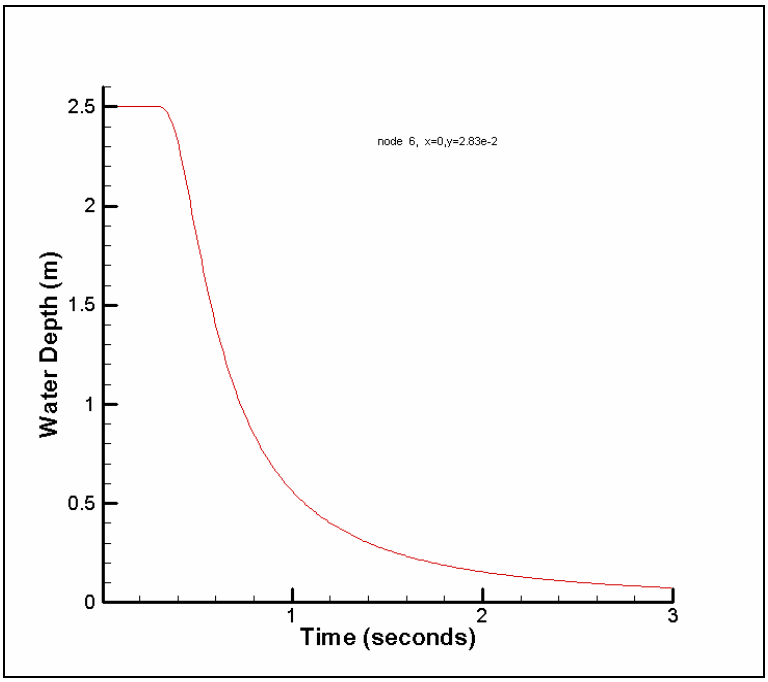

Fig. 4.2.3-6. Water Depth Hydrograph for a Location near the Center of the Circular Dam

The depth hydrograph in Figure 4.2.3-6 confirms that there is a depression in water surface after the dam break. The water depth decreases from 2.5 m to below 0.5 m.

An animation showing the circular dam break over the entire simulation period is attached in Appendix A (File Name: dambkcir(4-2-3).avi).

4.2.4 Two-Dimensional Dam Break Problems.

This a two-dimensional frictionless partial dam break problem that has been extensively used in hydraulic literature for testing numerical performance. The water depth behind the dam is assumed to 10 m. The downstream water depth was set to 0.05 m, so it is a nearly dry-bed simulation. This problem is very difficult to solve numerically with conventional finite difference or finite element methods.

The rectangular channel is horizontal with a dimension of 200 x 200 m in length and width, respectively. The initial water depth is 10 m in the reservoir and 0.05 m in the downstream. The breach or opening of sluice gates is 75 m, between x = 95-170 m. The domain was divided into 40 x 40 rectangular elements and the elements at the location of the dam are excluded (Fig. 4.2.4-1).

The two-dimensional fully dynamic wave model was applied to this problem and solved with the Method of Characteristics (MOC). A time step of 0.15 second was used. Figures 4.2.4-2 through 4.2.4-4 depict the water stages at various time = 2.0 s, 5.0 s, 7.0 s, respectively. This demonstrates that the 2-D MOC can solve this kind of sharp front problem without having to use higher order numerical schemes, all of which produce wiggles and peak clipping. Diffusive or kinematic wave approaches cannot adequately simulate this type of problems.

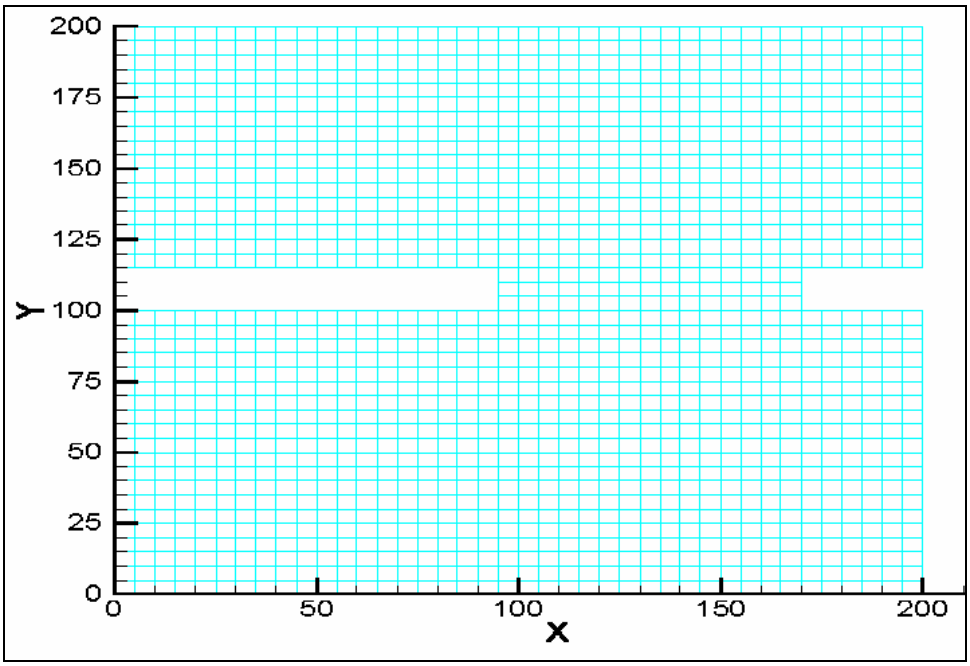

Fig. 4.2.4-1. Problem Description and Finite Element Discretization for Problem 4.2.4

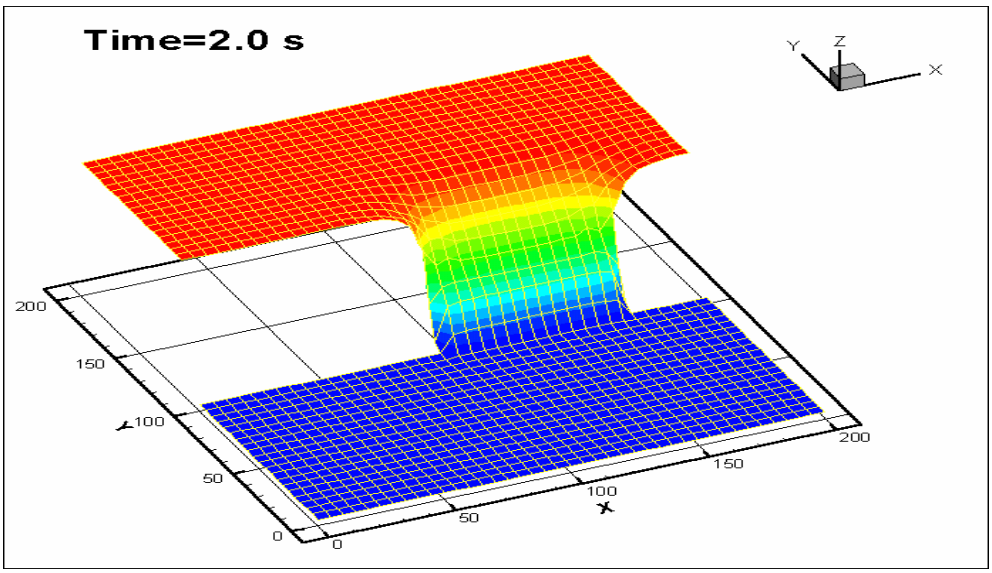

Fig. 4.2.4-2. 3-Dimensonal Perspective View of Water Surface at time = 2 s for Problem 4.2.4

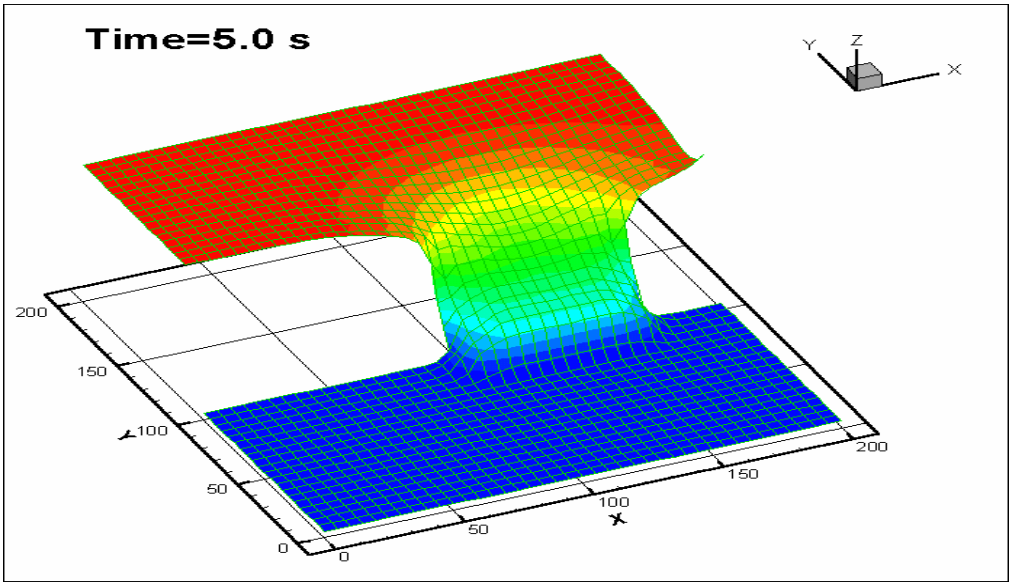

Fig. 4.2.4-3. 3-Dimensonal Perspective View of Water Surface at time = 5 s for Problem 4.2.4

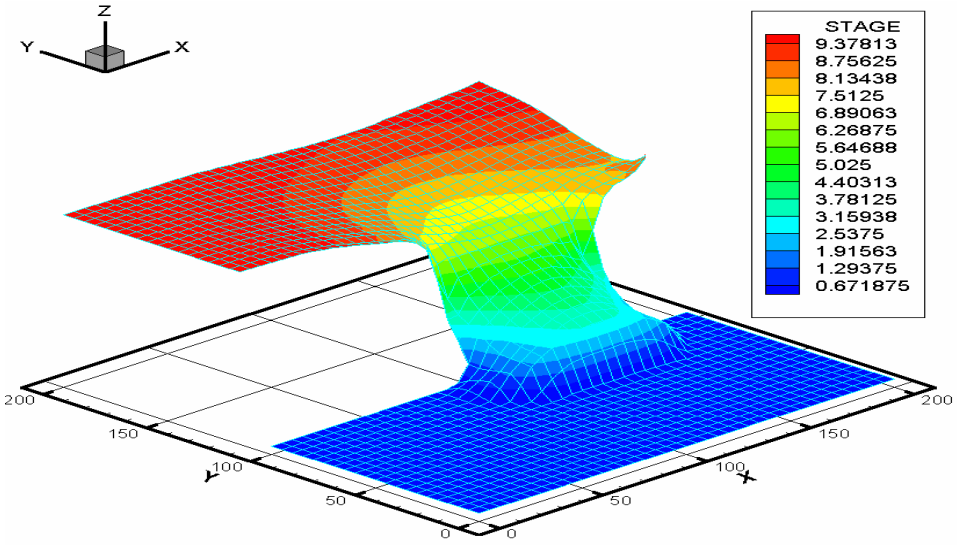

Fig. 4.2.4-4. 3-Dimensonal Perspective View of Water Surface at time = 7 s for Problem 4.2.4

An animation showing the two-dimensional dam break over the entire simulation period is attached in Appendix A (File Name: dambk2d_dry(4-2-4).avi).

4.3 Preliminary Field Applications Using WASH123D

WASH123D is developed to be a primary, first-principle, physics-based tool to simulate realistic, real-world, field problems. In this section, six example problems are presented to illustrate the types of problems that WASH123D can be used for field applications. No attempt is made to conduct thorough calibration and verification studies because this is not the purposes of this report. Preliminary calibrations have been made for some of the examples though. The first example involves the modeling of aquifer storage recovers. The second example is to design a spreader canal. The third example is the application of WASH123D to Biscayne Bay Coastal Wetland (BBCW) watershed to investigate the redistribution of overland flows and the overland fluxes to Biscayne Bay. The fourth example involves the modeling of stormwater treatment area (STA). The fifth example is the employment of WASH123D to model reservoirs and canal networks in Northern Beach County in Florida. The sixth example is the employment of WASH123D to model interactions among canal networks, overland flow, and subsurface flow in Dade County in South Florida.

4.3.1 Aquifer Storage Recover (ASR)

Aquifer Storage and Recovery (ASR) is means to store fresh water deep underground in brackish water aquifers. This stored water can be recovered at a later date during emergencies or times of water shortage. ASR is expected to provide a cost-effective solution to many of the world's water management needs. However, the quality of the stored water may degrade over time due to mixing and buoyancy stratification. Water quality may further be reduced during extraction due to upcoming of saline water underlying the ASR well. This water quality degradation may reduce the volume of the available fresh water during recovery to the point that the ASR well is no longer cost effective.

A simple case of a single ASR well is simulated. Some data is referred to the 1989 ASR pilot project at Lake Okeechobee, Florida (CH_2M Hill, 1989). But overall it is for demonstration purpose only. Three-dimensional density driven flow and transport is simulated. The injected freshwater is stored and mixed with the brackish water in the aquifer. The diameter of the ASR well is 24 inches. The screened area is located at 1,300 ft to 1,600 ft below land surface. So the storage zone is in the artesian aquifers with a confining layer of 400 ft overlying it. The saturated hydraulic conductivity is 177.6 ft/day. The effective porosity is 0.25. Only the storage zone will be simulated. The thickness of the aquifer is 300 ft. A rectangular area, with a scale of 1,600 x 1,600 ft is chosen for the modeling domain. The boundary is set far away from the ASR well, so that injected water is stored within the domain.

Specified head boundary conditions are assigned in the direction of natural groundwater flow to represent the background groundwater flow. Variable boundary conditions are specified at the perimeter of the ASR well. The boundary condition at the screen of the ASR well can be specified head or flux depending on the injection pumping pressure. During the recover period, the head condition is specified on the boundary.

The three-dimensional finite element mesh contains three layers. The total number of subsurface nodes is 3,280 and the total number of elements is 4,674. The size of the elements is designed to be finest within the vicinity of the well (Fig. 4.3.1-1).

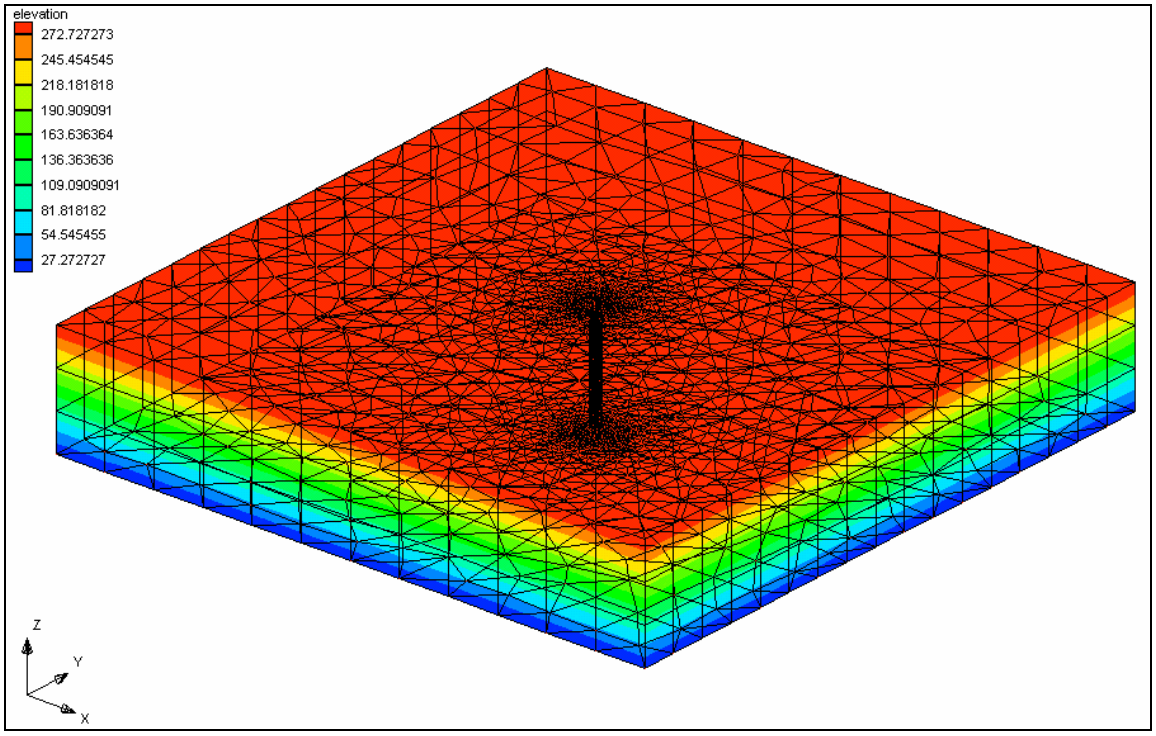

Fig. 4.3.1-1. Three-Dimensional Finite Element Mesh for ASR

The injection/recovery processes were simulated for 720 hours. The injection stopped at time = 360 hours and then recovery started till the end of the simulation. The total head distributions and saline concentrations at different times were plotted in Figures 4.3.1-2 to 4.3.1-5 and Figures 4.3.1-6 to 4.3.1.9, respectively, in the following. The spatial distributions of the total head and concentration presented these figures demonstrated the impact of the background flow and density effect.

From the animations (Files totalhead_inject(4-3-1).avi and totalhead_recov(4-3-1).avi in Appendix A), it is seen that the steady-state simulations were achieved in one–time step. This is so because the compressibility of the water and media were assumed zero which makes the aquifer specific storativity zero. On the other hand, from the animation (File concentration(4-3-1).avi in Appendix A), one can see that the concentration distribution is highly transient. This is so because the storage coefficient for salt transport is the porosity of the aquifer.

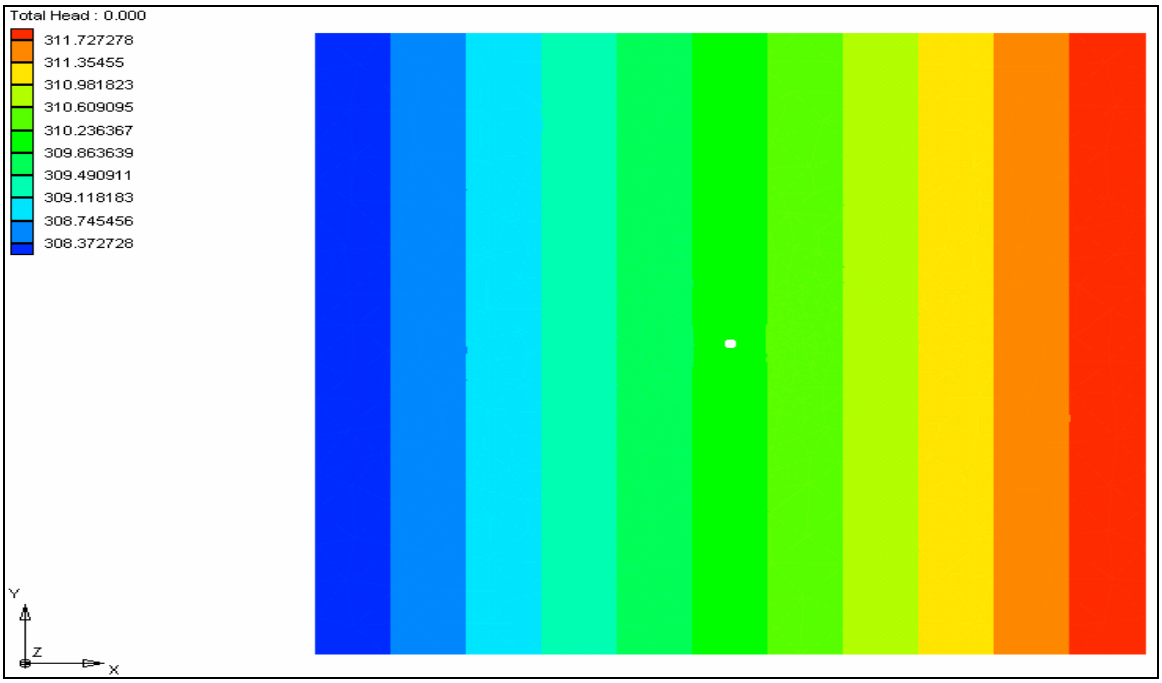

Fig. 4.3.1-2. Total Head Distribution (Time = 0 hour)

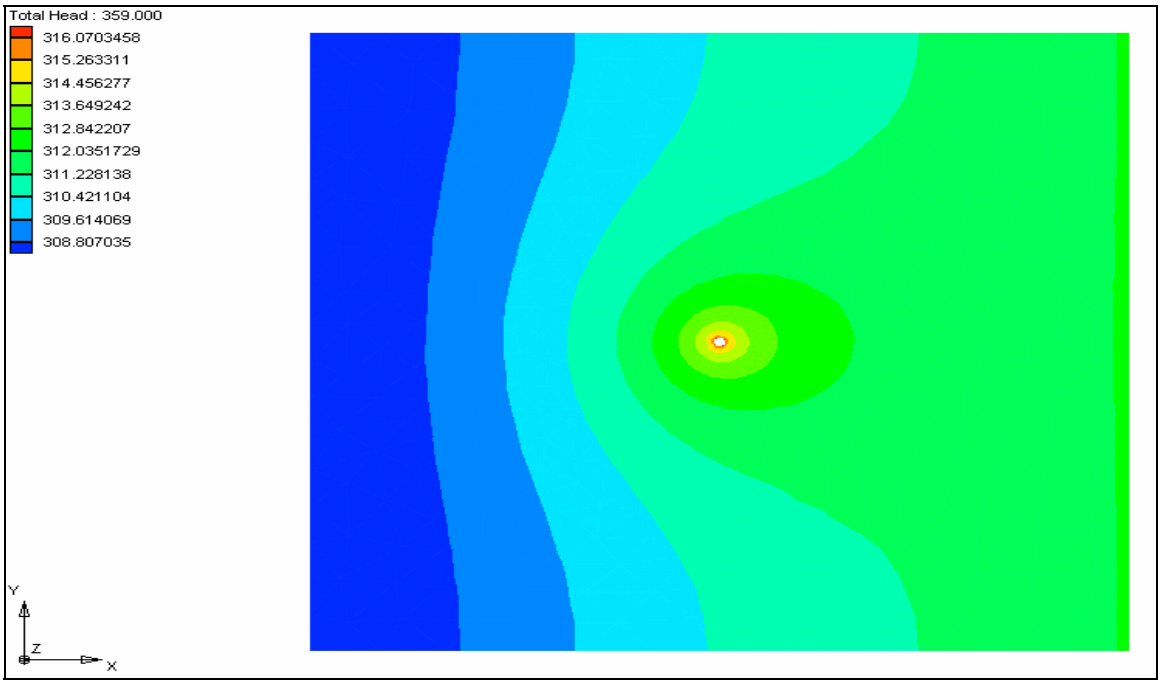

Fig. 4.3.1-3. Total Head Distribution (Time = 359 hours)

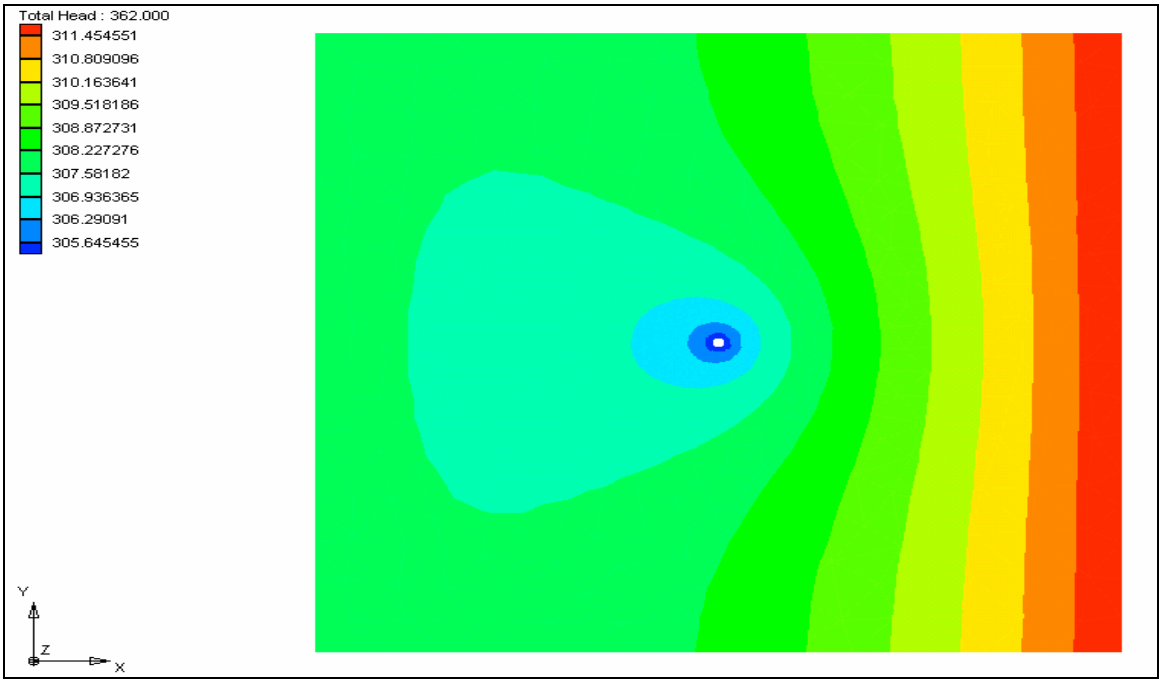

Fig. 4.3.1-4. Total Head Distribution (Time = 362 hours)

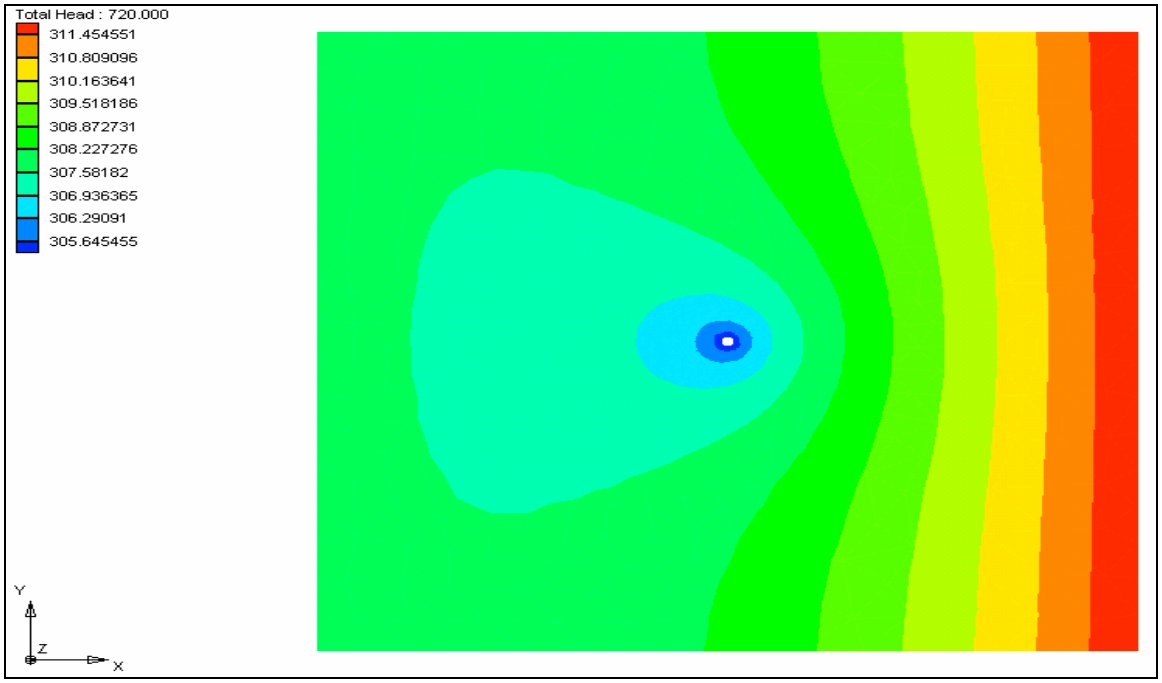

Fig. 4.3.1-5. Total Head Distribution (Time = 720 hours)

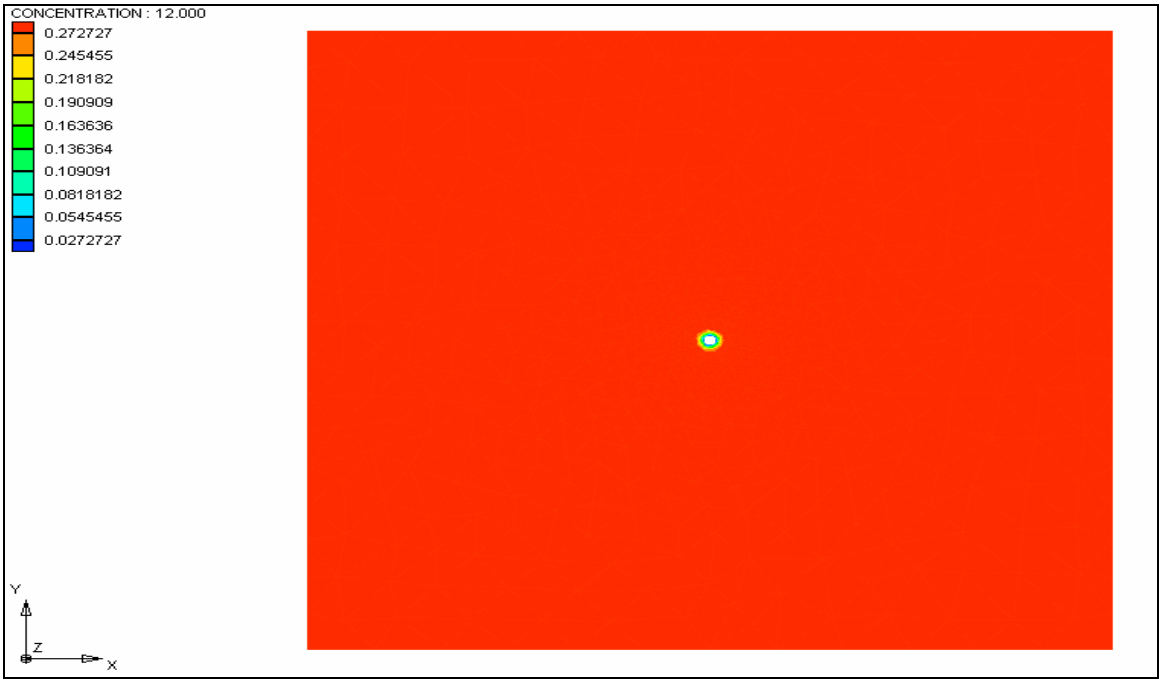

Fig. 4.3.1-6. Saline Concentration at Time = 12 hours

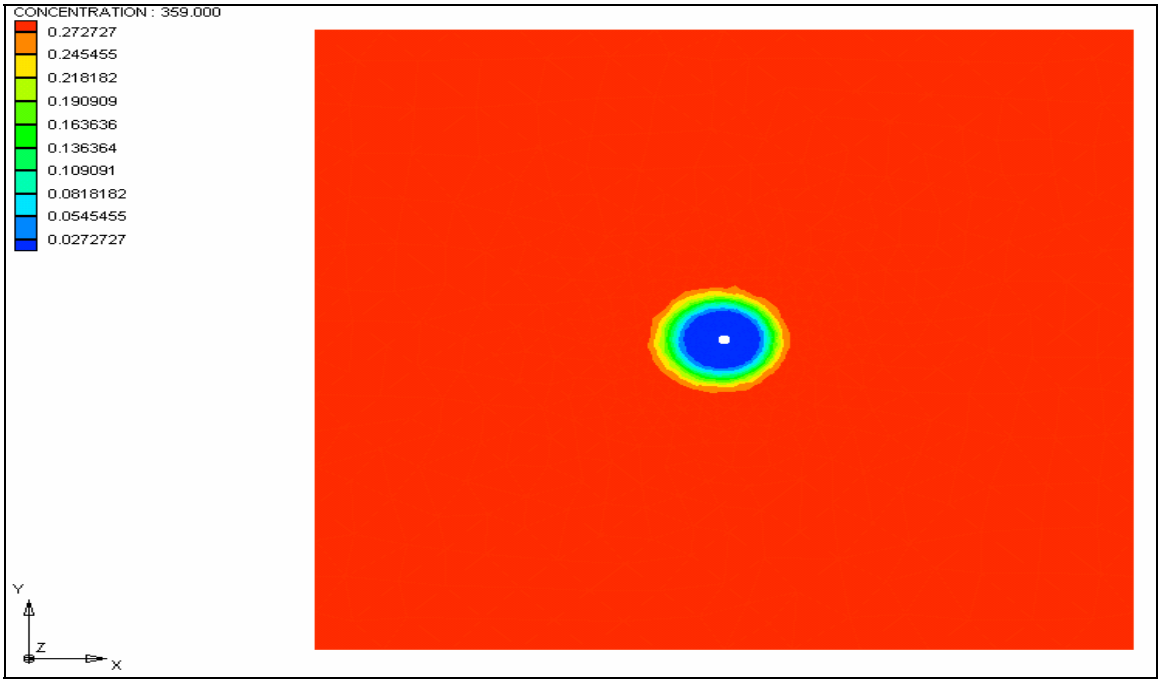

Fig. 4.3.1-7. Saline Concentration at Time = 359 hours

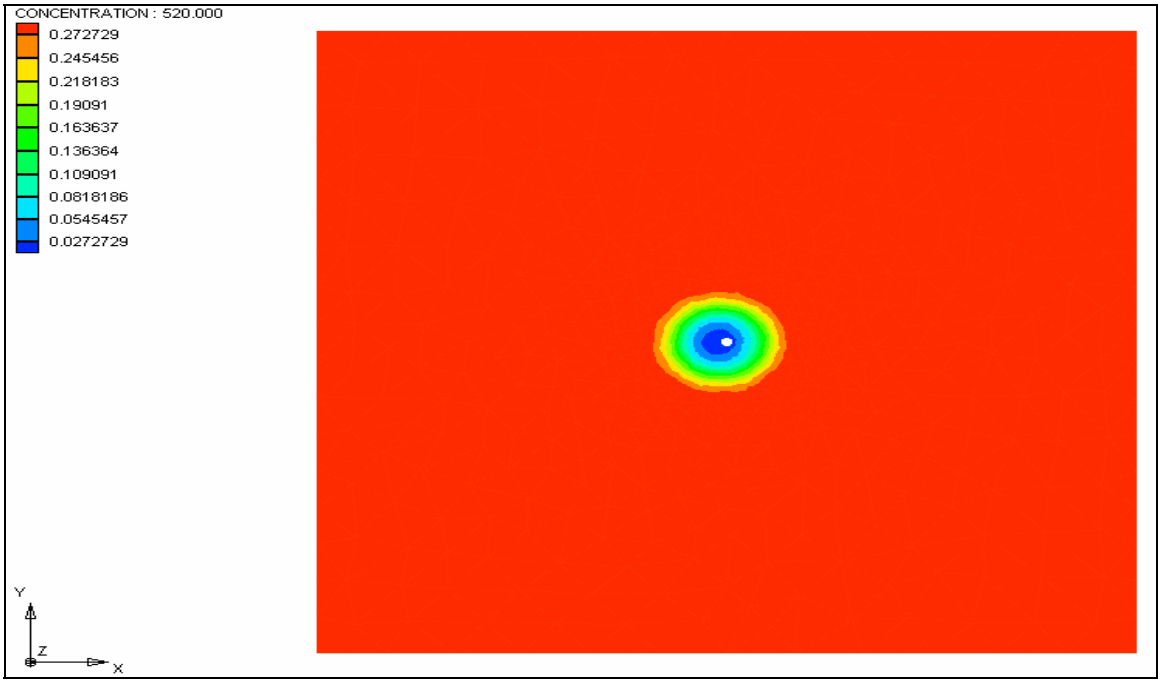

Fig. 4.3.1-8. Saline Concentration at Time = 520 hours

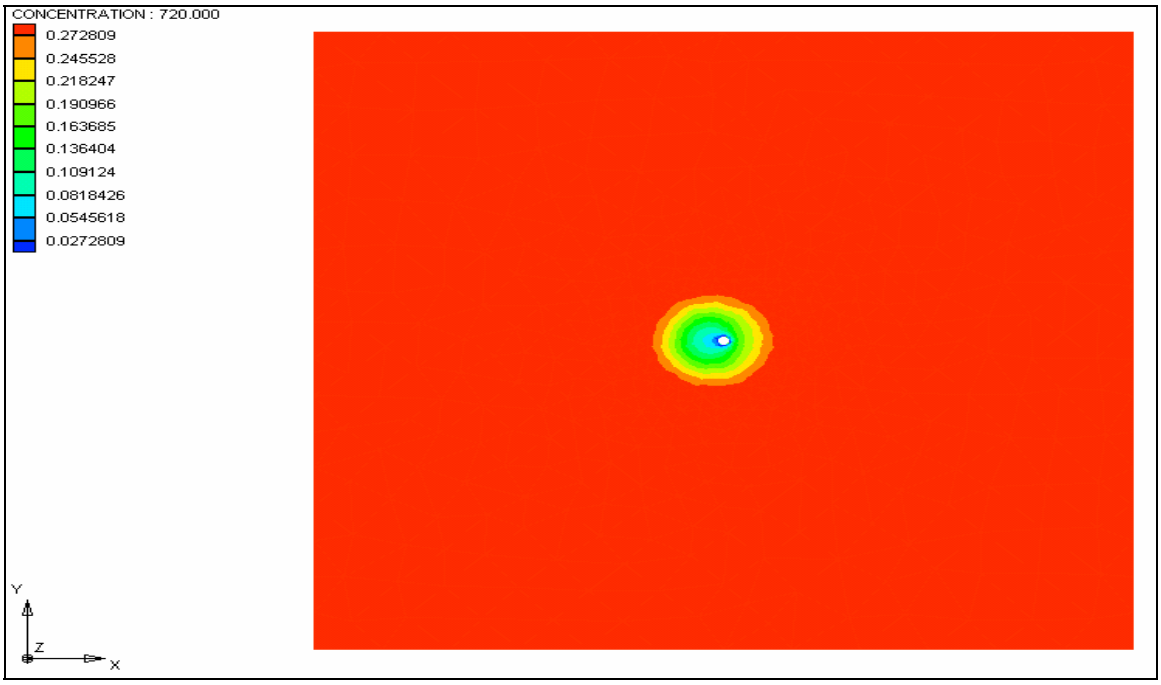

Fig. 4.3.1-9. Saline Concentration at Time = 720 hours

4.3.2 Design of a Spread Canal

The Biscayne Bay Coastal Wetlands (BBCW) Project is one component of the more than 60 restoration plans and has a goal to restore the coastal wetlands area in Central and South Biscayne Bay along its western shoreline. In the existing condition, fresh water plumes emanating from the mouths of canals and well-defined ditches can create local freshening of Biscayne Bay that can be harmful to sea grasses and the ecology of Biscayne Bay. Current restoration efforts in southern Florida are examining alternative water management plans that could change the quantity and the timing (Q & T) of freshwater delivery to the bay by restoring coastal wetlands along its western shoreline of the Biscayne Bay. In contrast to these well-defined surface features, shallow water wetlands can diffuse the introduction of fresh water into Biscayne Bay. Using wetlands to recharge fresh water into the groundwater system can be useful to minimize fresh water plumes extending into Biscayne Bay and to help minimize and/or impede saltwater intrusion. One scenario to address this effort is to create a spreader canal system to redistribute available surface water entering the area from the regional canal system (Cheng, et al., 2004). The spreader canal system would consist of a delivery canal and shallow swales (i.e., spreader canals) where water flows across the swale banks and becomes a more natural overland flow through existing coastal wetlands. Studying such a scenario on a design level involves the modeling of a coupled flow system of 1D canal network, 2D overland, and 3D subsurface.

The top of Figure 4.3.2-1 depicts a conceptual model of a spreader canal system. As water is introduced from a delivery canal, the spreader canal is designed to distribute water to its downstream wetland area in order to reduce the impact to the ecological system of the bay that is further downstream. The bottom of Figure 4.3.2-1 presents two scenarios that are associated with the spreader canal and need to be accounted for by the computational model: the left one shows a scene in which canal water is kept in canal, while the right one has canal water stage high enough to contribute to the downstream overland area. In the left case, the canal collects water from its upland surface (overland and canal waters are separate here) but has no contribution to its downland surface area. In the right case, the canal receives water from its upland surface on one hand and gives out water to its downland surface (canal and overland waters are connected here) on the other hand. When the subsurface is also taken into account, surface-subsurface interactions through infiltration and seepage (red arrows in Figure 4.3.2-1) may play crucial roles in determining subsurface water table, overland water depth, and canal water stage. In WASH123D, flux continuity is ensured on the medium interfaces, while state variable continuity is imposed when waters between two media are connected.

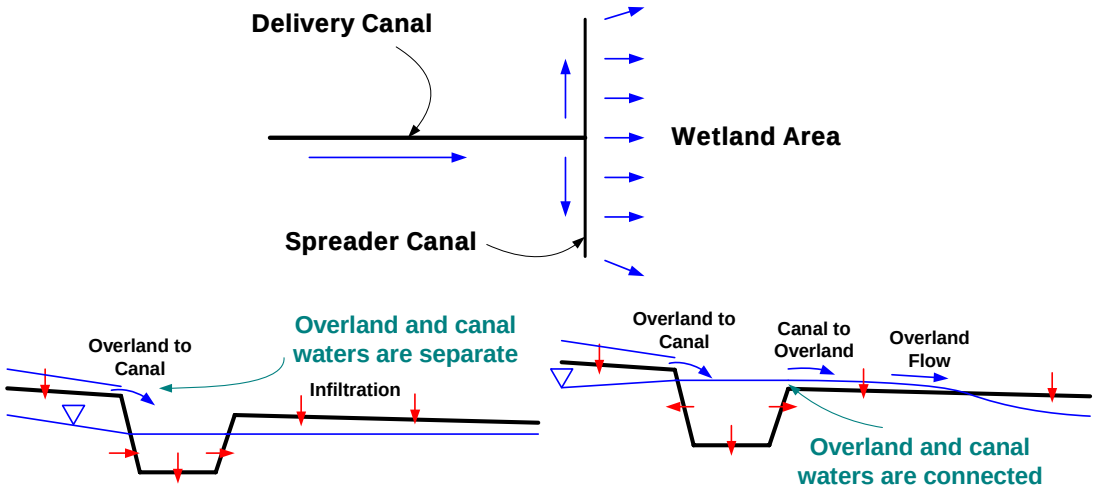

Fig. 4.3.2-1. A Conceptual Model (top) and Two Scenarios (bottom) of the Spreader Canal

This hypothetical example demonstrates how WASH123D may help model and design a spreader canal system that includes one-dimensional canal, two-dimensional overland, and three-dimensional subsurface flow. It used the topographic data in the BBCW project area (Fig. 4.3.2-2) to construct the discretized domain of interest. The study area of this example is marked in Figure 4.3.2-2. A spreader canal was placed in the domain to distribute water that came in from the west boundary (marked with a red A in Figure 4.3.2-3). The two-dimensional overland domain, which covered an area of approximately 1.1 square miles, was discretized with 28,340 elements and 14,390 nodes, where the mesh size was about 50 ft. The one-dimensional canal embraced 91 elements, 94 nodes, one upstream boundary node (A in Figure 4.4.2-3), two dead ends (DE1 and DE2 in Figure 4.3.2-3), and one junction (J in Figure 4.3.2-3) to connect the three canal reaches. The underlying three-dimensional domain contained 113,360 elements and 71,950 nodes. The width of the assumed rectangular canal was set 90 ft for Reach 1, 20 ft for Reach 2, and 60 ft for Reach 3 (Figure 4.3.2-3). The cross-sectional area was proportional to the depth, where the depth of the spreader canal was computed by solving one-dimensional diffusive wave equations.

The Manning's roughness was set to 0.015 for two-dimensional overland flow and 0.008 for one-dimensional canal flow. The subsurface medium was sandy loam and was assumed homogeneous through the entire domain, where the saturated hydraulic conductivity was 1,000 ft/day. The soil retention curves for the unsaturated zone were generated with the van Genuchten functions.

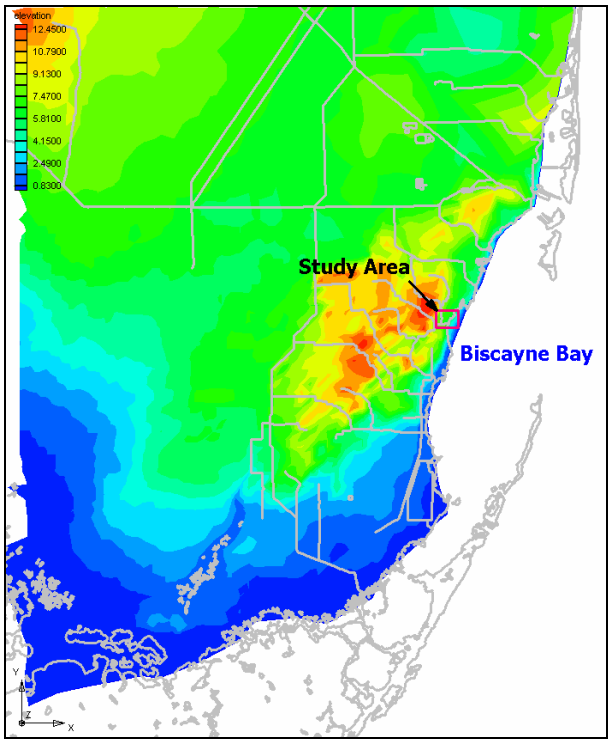

Fig. 4.3.2-2. Location of the Simulated Area of the Demonstration Example

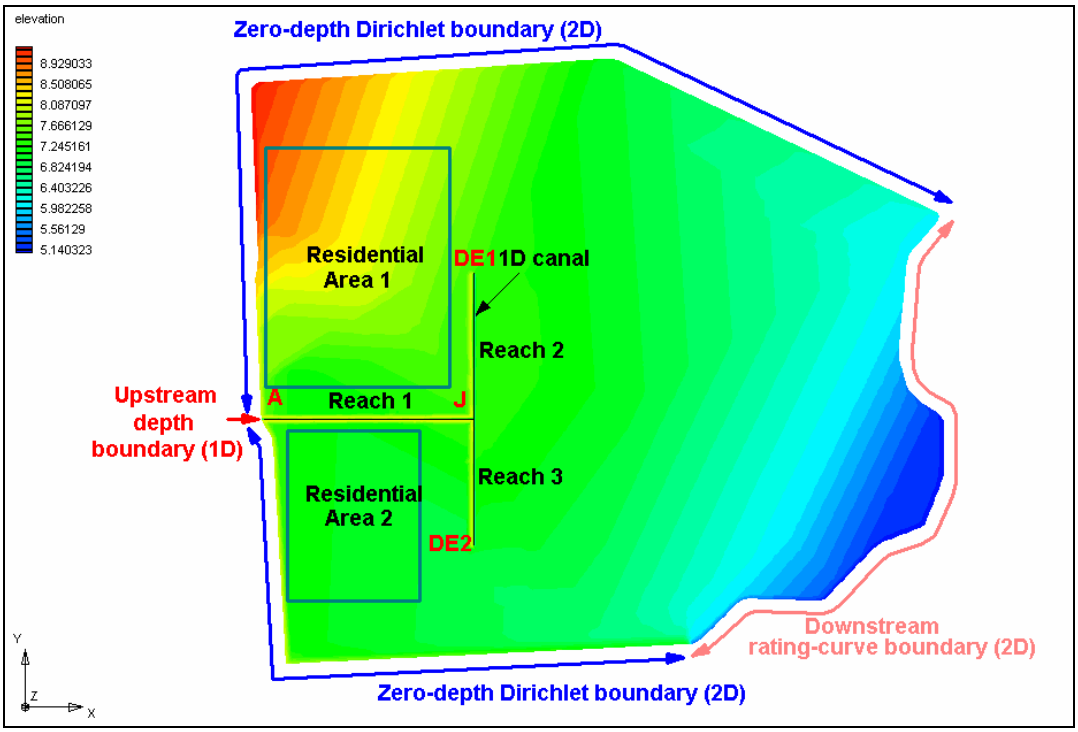

Fig. 4.3.2-3. 1D canal and 2D Overland Boundary Conditions Used for the Demonstration Example

In computing one-dimensional canal flow, a time-dependent water depth was given in Table 4.3.2-1 as the upstream boundary condition for the incoming water as indicated in Figure 4.3.2-3; a zero-velocity condition was applied at the two downstream dead-end nodes; and the continuity of both flow rate and water stage was enforced at the canal junction. In computing two-dimensional overland flow, its north, west, and south boundaries were imposed the zero-depth boundary condition throughout the simulation; a depth-dependent flux (i.e., rating curve) was given on the downstream depth-dependent (rating curve) boundary (Fig. 4.3.2-4); and a canal-overland interaction boundary condition was specified for the canal-related overland boundary sides, which includes (1) a depth-dependent flux when water flowed from overland to canal and overland water and canal water were separated and (2) a canal stage condition when flooding occurred (i.e., when overland water and canal water were connected). In computing three-dimensional subsurface flow, an interface boundary condition that accounted for the interaction between surface and subsurface waters was applied to the top boundary face of the three-dimensional domain; three total head boundary conditions were employed for (1) the subsurface boundary nodes associated with the one-dimensional canal upstream boundary node on the west vertical boundary face (time-dependent head that matches one-dimensional upstream boundary condition at the inlet (i.e., A in Fig. 4.3.2-3), (2) all the subsurface nodes, except those mentioned in (1), on the west boundary (a constant head of 7.12 ft), and all the subsurface nodes on the east boundary face (a constant head of 4.95 ft) as shown in Figure 4.3.2-4; and an impermeable boundary condition for the rest of the vertical boundary face and the bottom boundary. It is noted that for the vertical boundary face with total head specified, the Dirichlet boundary condition applied only to the boundary nodes below water table (i.e., in the saturated zone). For the vertical boundary face that was above water table, an impermeable boundary condition was assumed.

Table 4.3.2-1 Upstream Water Depth Boundary Condition used for the 1D Canal Flow

Time (seconds)	0	600	3600	7200
Depth (ft)	0.5	0.58	0.88	1.28

The initial pressure head in the subsurface was computed by solving the steady-state version of Richards' equation with a constant rainfall rate of 1.0×10^{-9} ft/s, while a constant water depth of 0.5 ft was enforced at the three-dimensional boundary nodes that were corresponding to one-dimensional spreader canal nodes and zero water depth was assumed at those corresponding to two-dimensional overland nodes. For a demonstration purpose, such setup allowed us to expect water flow from the spreader canal to its neighboring overland regime within a short period of time after the transient simulation began. As the transient simulation began, the rainfall rate of 1.0×10^{-9} ft/s was applied throughout the entire simulation period of 2 hours. The time-step size was 60 seconds for computing three-dimensional subsurface flow, 2 seconds for computing two-dimensional overland flow, and 0.01 second for computed one-dimensional canal flow. The absolute error tolerance was 1.0×10^{-5} ft for determining nonlinear convergence in computing one-dimensional, two-dimensional, and three-dimensional flow, respectively.

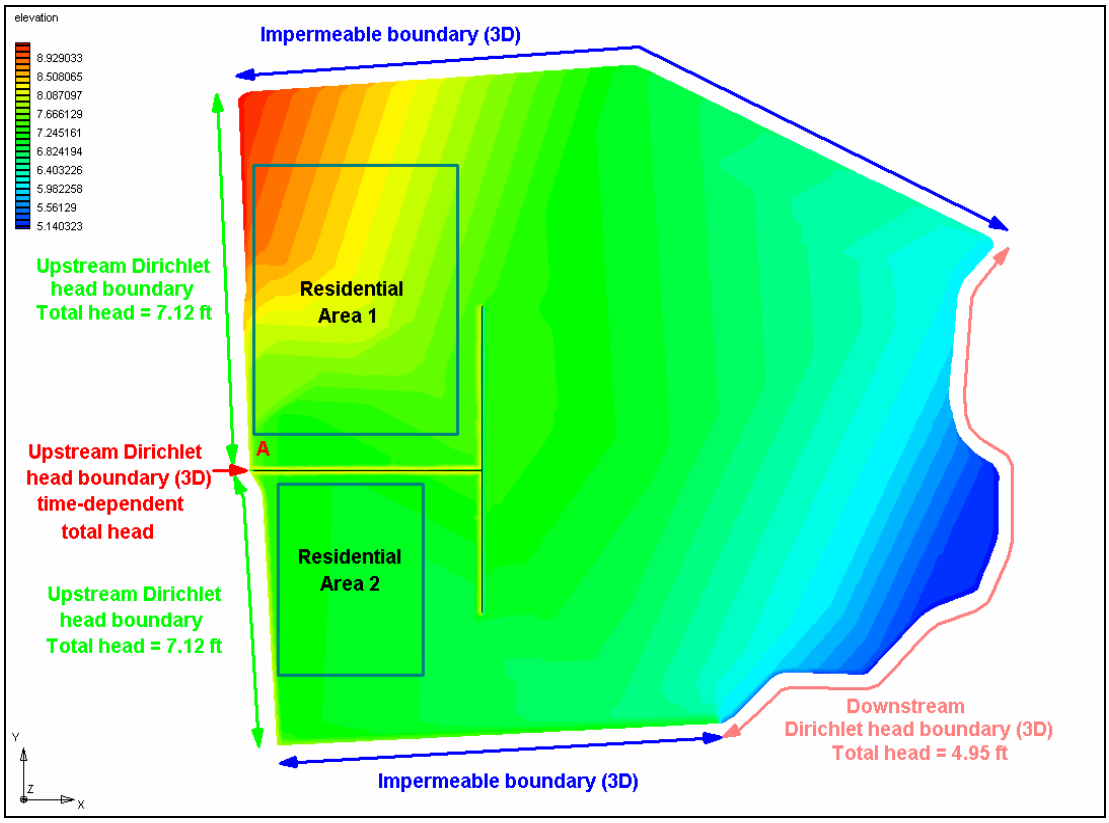

Fig. 4.3.2-4. 3D Subsurface Boundary Conditions used for the Demonstration Example

Figure 4.3.2-5 shows the distribution of water depth on the 2D overland (left) and 3D subsurface pressure head on ground surface (right) at time = 2 hours. On the right half of the figure, the portion shaded with blue color has groundwater below ground surface, while the portion without shade has water table reach ground surface. It is seen that most water coming out from Reach 3 of the spreader canal to overland is due to natural terrain (the north ground was higher than the south ground). And because the ground south to the second dead end (i.e., DE2) was so flat, water coming out of spreader canal near DE2 could flow westward and affect the southeast corner of Residential Area 2. Moreover, as water stage increased with time in Reach 1 (not shown), which was subject to the increasing upstream water depth over time (Table 1), seepage through levee was observed around the upstream section of Reach 1 even though there was no water flow over the bank of Reach 1 throughout the simulation. This, as a result, would cause problems for people living in the north part of Residential Area 2 based on the topography around this area (Fig. 4.3.2-6).

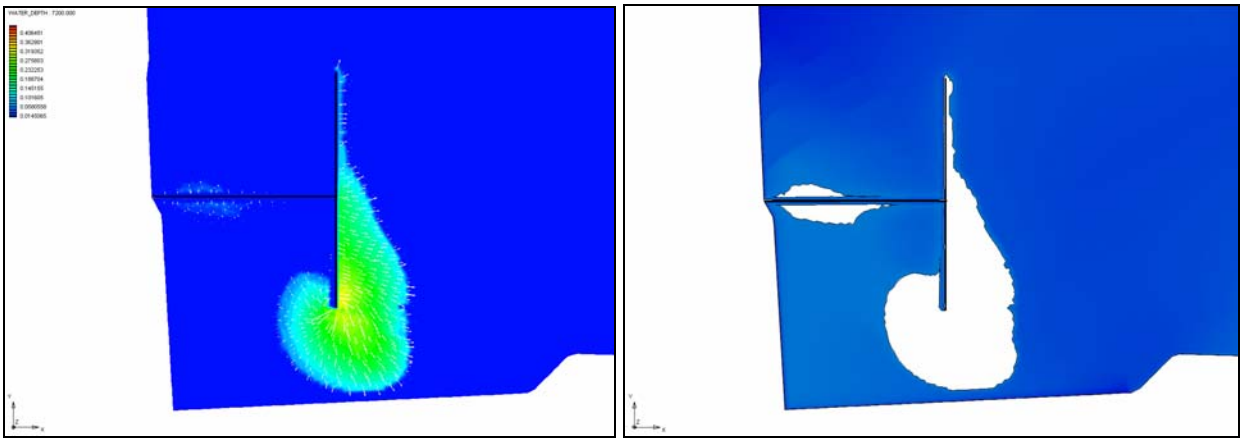

Fig. 4.3.2-5. 2D Overland (left) and 3D Subsurface (right) Flow results of Case 1 at Time = 2 hr

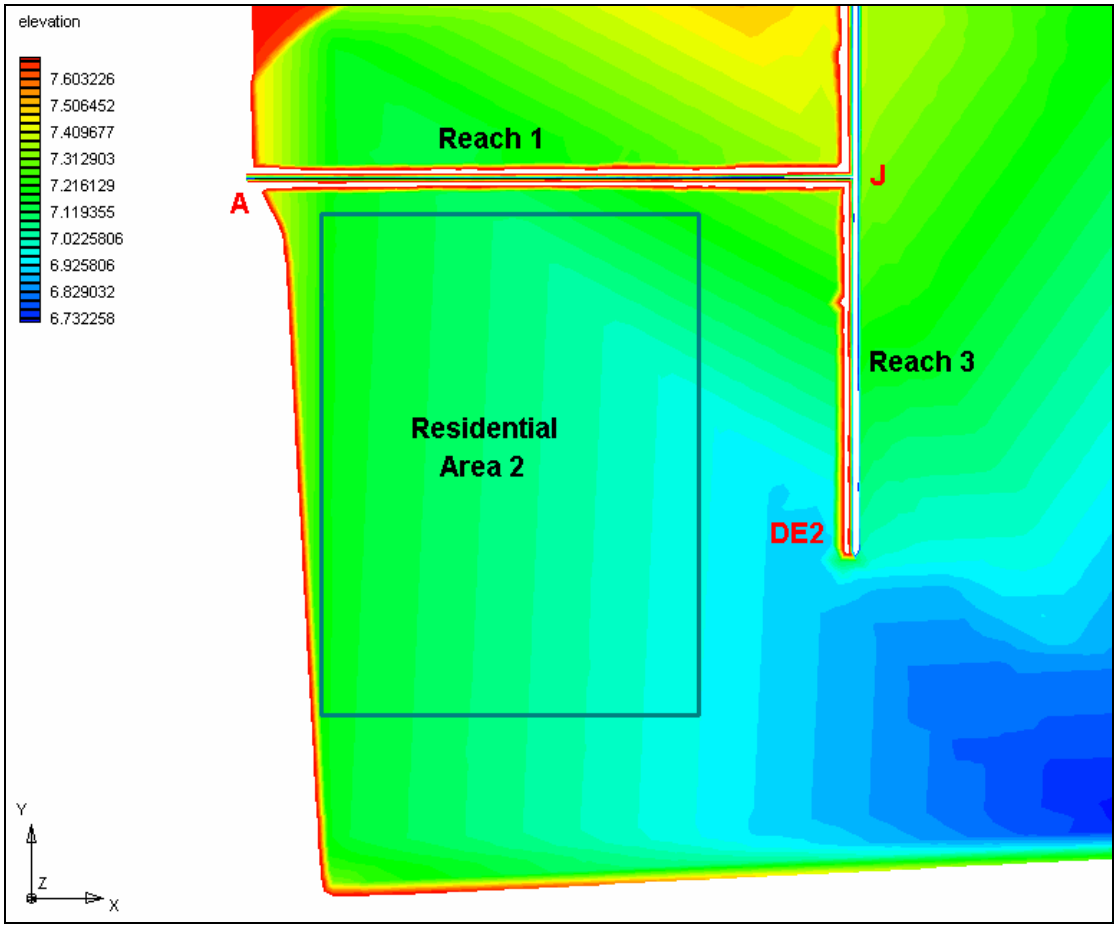

Fig. 4.3.2-6. Topo of Residential Area 2 and its Neighborhood Before an Extended Levee Was Applied

To protect Residential Area 2 from getting flooded, a waterproof liner was installed in Reach 1 and an additional levee from DE2 to the south overland boundary (Fig. 4.3.2-7) was considered in this study. Table 4.3.2-2 lists the three cases included in this study: Case 1 serves as the base case where neither a liner nor an additional levee is adopted; Case 2 has the liner; and Case 3 has both. Figure 4.3.2-7 shows the topography around Residential Area 2 after an additional levee was applied. Figures 4.3.2-8 and 4.3.2-9 show the computational results of Cases 2 and 3, respectively, which are corresponding to Figure 4.3.5 for comparison. It is obvious from Figure 4.3.2-8 that the waterproof liner has prevented seepage from occurring. From Figure 4.3.2-9, the extended levee has successfully stopped overland water from entering Residential Area 2.

Table 4.3.2-2 Three Cases in the Demonstration Example

Case 1 (base case)	Case 2	Case 3
No liner in Reach 1	Liner in Reach 1	Liner in Reach 1
No extended levee	No extended levee	Extended levee applied

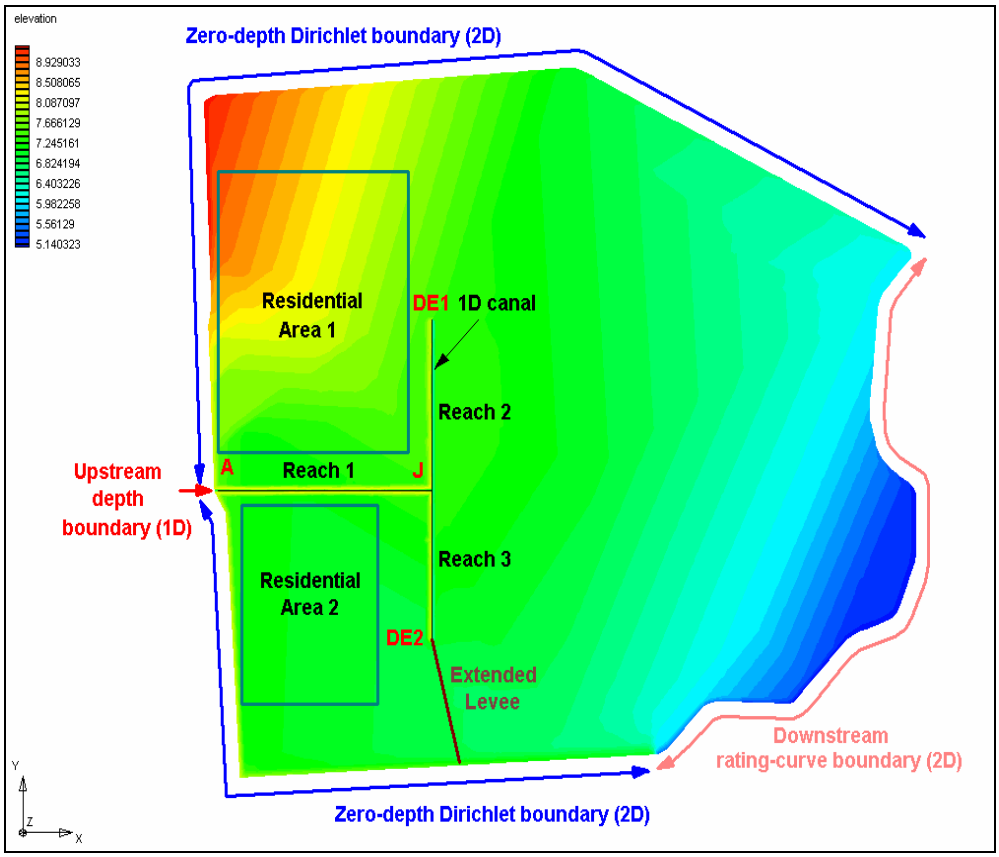

Fig. 4.3.2-7. With an Extended Levee to Prevent Flooding in Residential Area 2 (left) and the Topography of Residential Area 2 and its Neighborhood after an Extended Levee Was Applied.

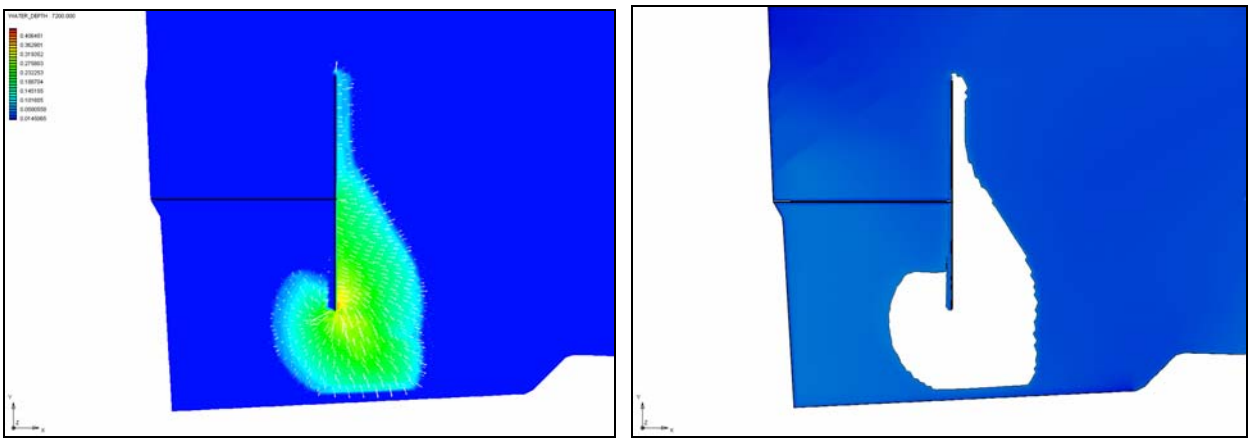

Fig. 4.3.2-8. 2D Overland (left) and 3D Subsurface (right) Flow Results of Case 2 at Time = 2 hr

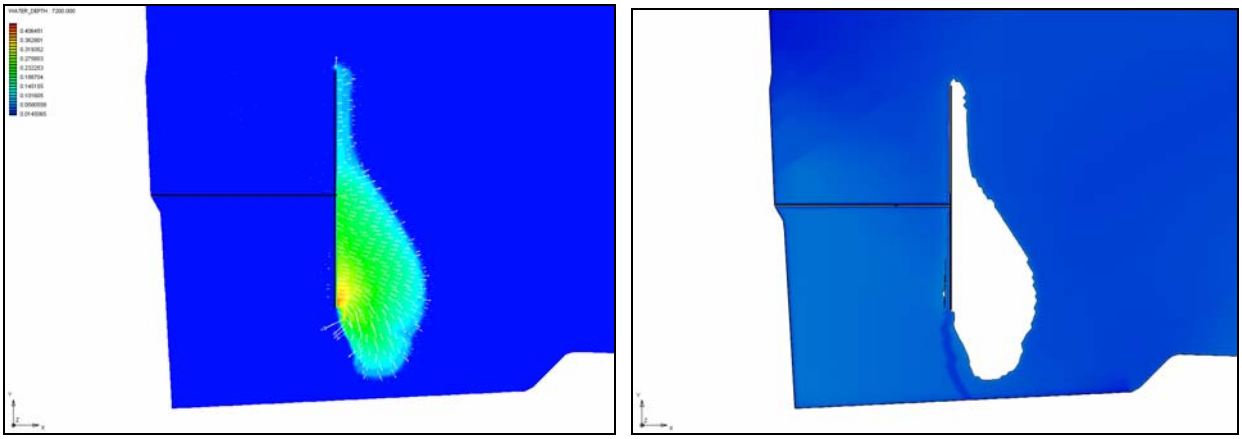

Fig. 4.3.2-9. 2D Overland (left) and 3D Subsurface (right) Flow Results of Case 3 at Time = 2 hr

In studying a spreader canal system on the design level, such as the demonstration example above, a couple of important issues were revealed. First, a high-resolution mesh is needed to achieve desired goals on the design level. In the demonstration example, for instance, canal water was successfully directed to the downstream overland without impacting Residential Area 2 after a liner and an additional levee were installed. However, canal water was not evenly distributed to overland (Fig. 4.3.2-9) as desired. To accurately determine what alternatives may help evenly distribute water, a high-resolution mesh that allows modelers to adequately catch most important physical processes and necessary details is a MUST.

Animations showing the spatial-temporal distribution of water depths and groundwater tables for Cases 1 (DE_1_wd.avi and DE_1_wt.avi), Case 2 (DE_2_wd.avi and DE_2_wt.avi), and Case 3 (DE_3_wd.avi and DE_3_wt.avi), respectively, are attached in Appendix A. Readers can visualize these moves by clicking the file contained in the attached CD.

4.3.3 Biscayne Bay Coastal Wetland (BBCW) Watershed Modeling.

The Biscayne Bay Coastal Wetland (BBCW) Project is one of more than 60 projects included in the federally approved Comprehensive Everglades Restoration Plan and has a ultimate goal to restore or enhance freshwater wetland, tidal wetland, and near shore bay habitat. The primary purpose of the BBCW project is to redistribute runoff form the watershed into the Biscayne Bay, away from the canal discharge that exists today and provide a more natural and historical overland flow through the existing and or improved coastal wetlands. This example presents the modeling effort to restore the wetlands including modeling approaches, building hydro-geologic conceptual model, selecting model domain and boundaries and calibrating model parameters. Discussions of calibration and preliminary results were given elsewhere (Lin et al., 2004).

WASH123D (Yeh et al., 2003) was used to develop the BBCW flow model. This flow model conceptualizes the BBCW watershed as a combination of 1D canal network, 2D overland flow regime, and 3D subsurface media. The graphical user interface GMS5.1 was used to construct the hydro-geologic conceptual model for the BBCW project area. Figure 4.3.3-1 shows the BBCW project area. Figure 4.3.3-2 shows the solids model generated from borehole data. Figure 4.3.3-3 shows the computational mesh for the BBCW flow model.

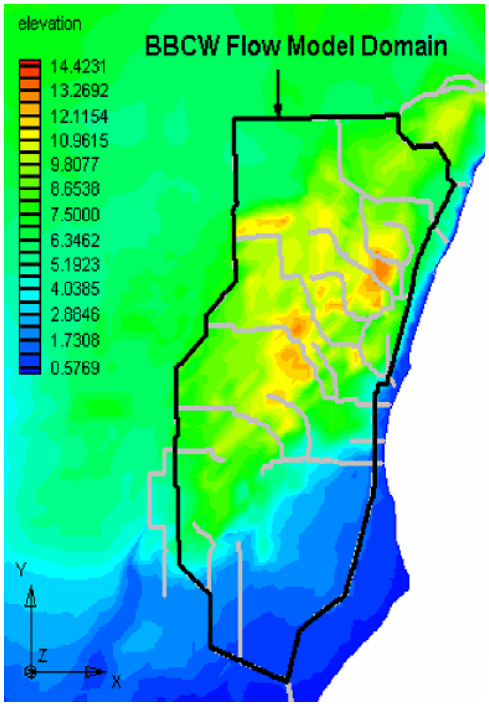

Fig. 4.3.3-1. BBCW Project Area

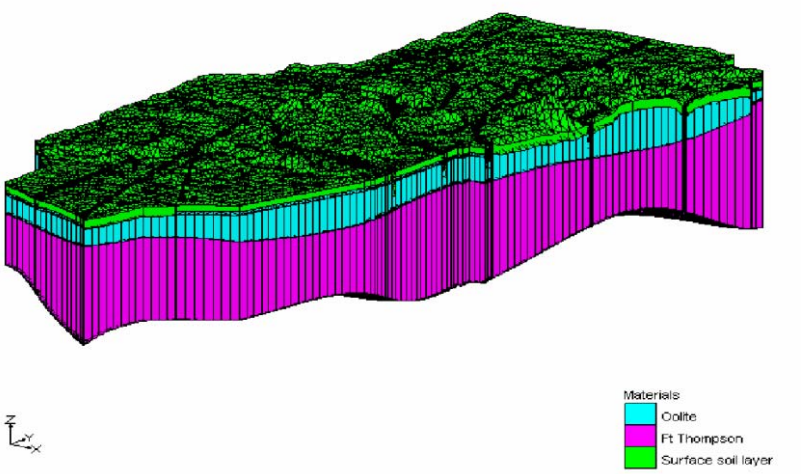

Fig. 4.3.3-2. Solid Model for the BBCW Project Area

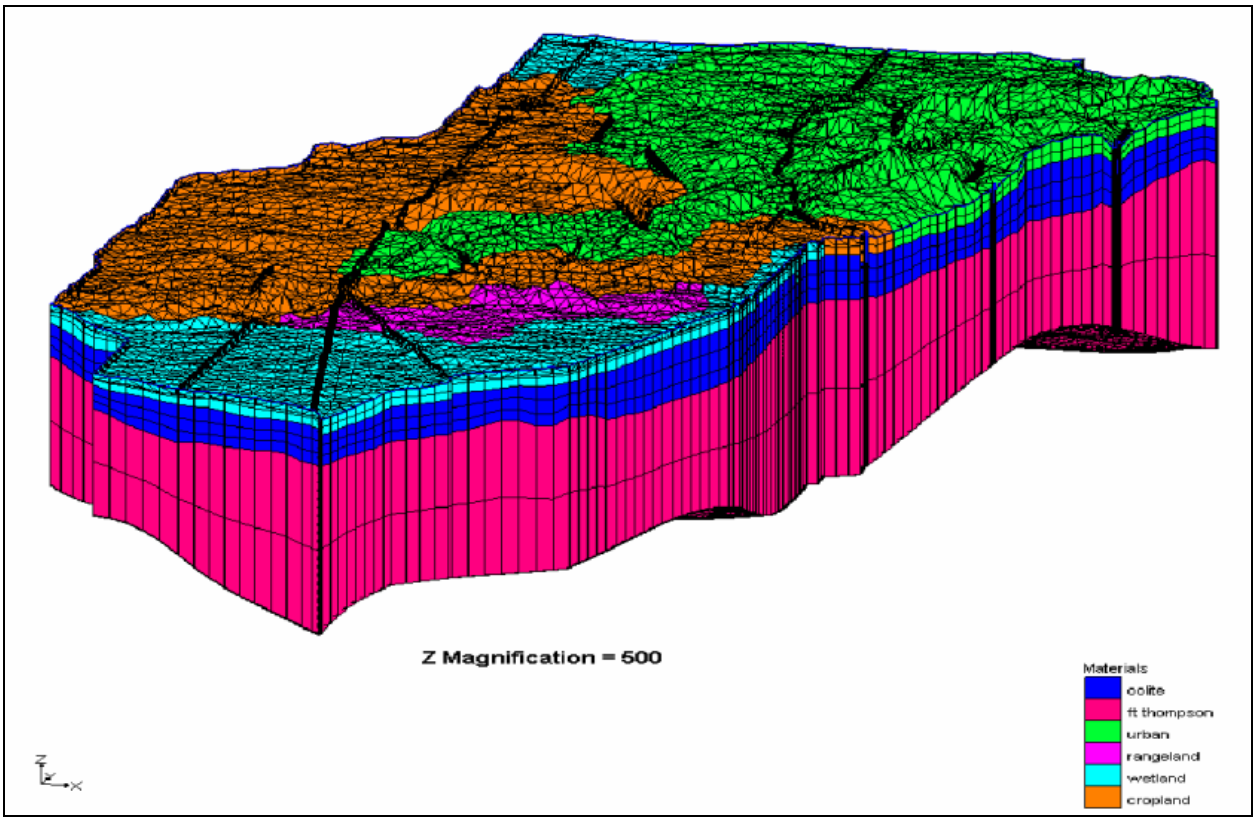

Fig. 4.3.3-3. Computational Mesh
(2D Nodes = 8,339; 2D Elements = 16,388; 3D Nodes = 66,712; 3D Elements = 114,716)

Figure 4.3.3-4 shows the 2D boundary conditions assigned to the model. Flux boundary was specified at the east side of model boundary. Observed stages were prescribed at the internal canals. Time-dependent rainfall and evapotranspiration (ET) were obtained from field measurements. Figure 4.3.3-5 shows the locations of rain gages and Figure 4.3.3-6 depicts the locations of ET gates.

Figure 4.3.3-7 shows the 3D boundary conditions assigned to the model. Continuity of flux and/or heads were imposed on the surface-subsurface interface. Observed heads and stages were specified on the 3D vertical side boundary. Impermeable condition was assumed on the bottom boundary. Internal head boundary conditions were prescribed along the canals. Time-dependent pumping rates and water levels in observation wells were obtained from field measurements. Figure 4.3.3-8 shows the locations of pumping wells and Figure 4.3.3-9 depicts the locations of observation wells.

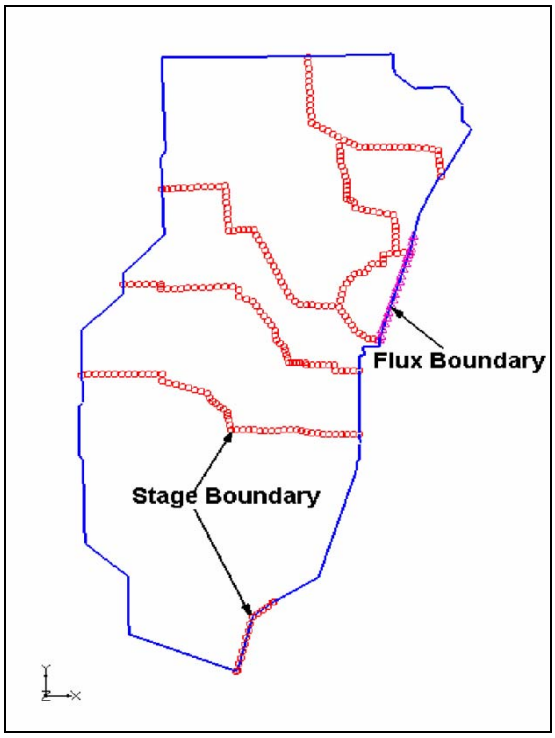

Fig. 4.3.3-4. 2D Boundary Conditions

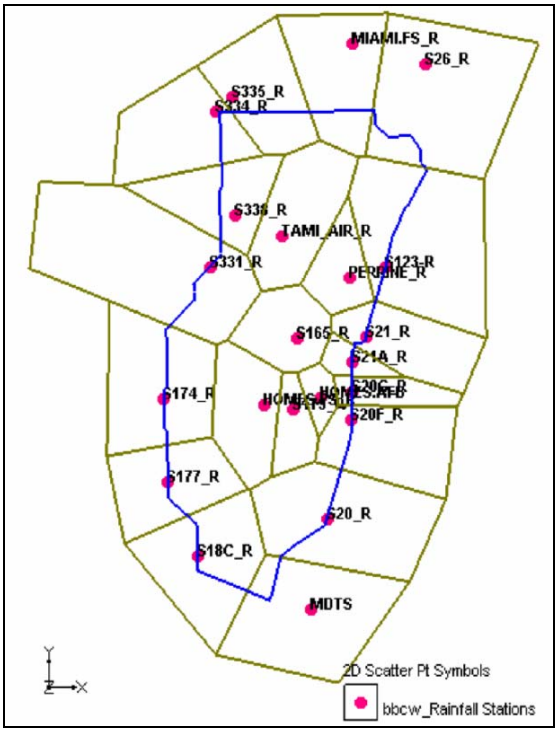

Fig. 4.3.3-5. Locations of Rain Gages

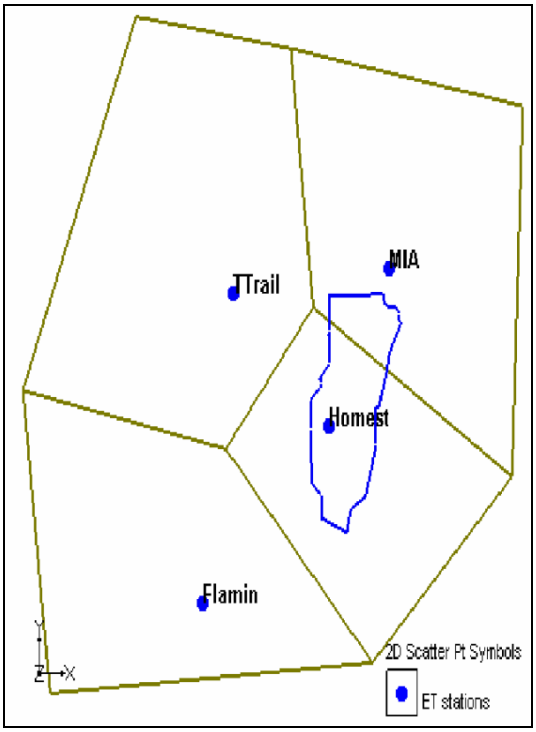

Fig. 4.3.3-6. Locations of ET Gages

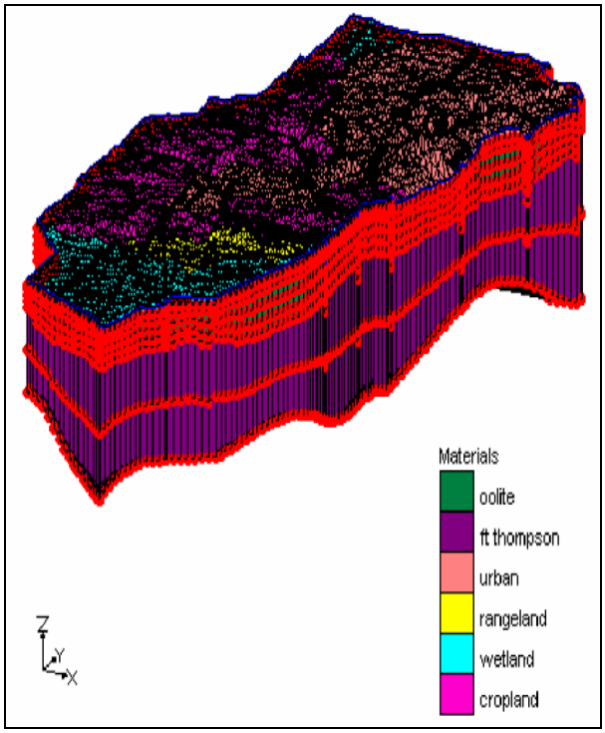

Fig. 4.3.3-7. 3D Boundary Conditions

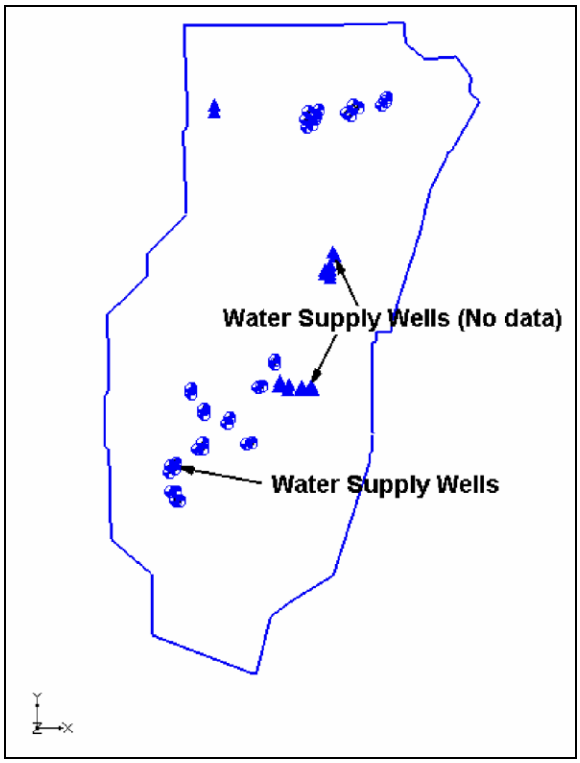

Fig. 4.3.3-8. Locations of Pumping Wells

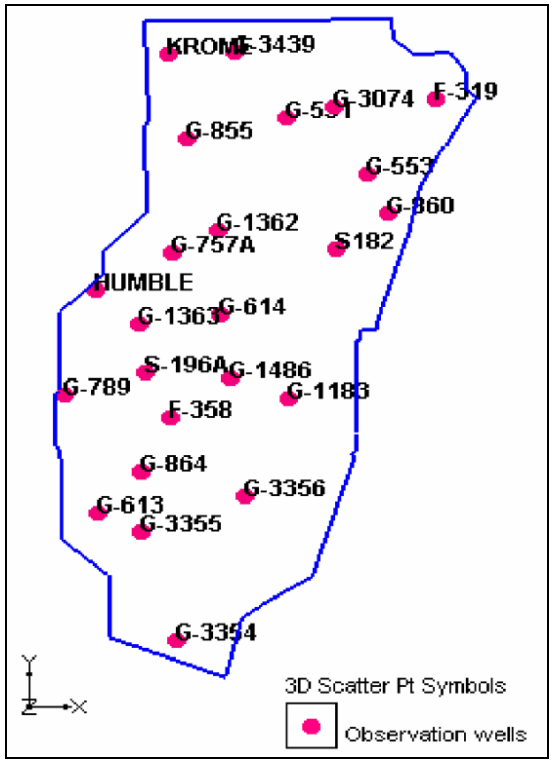

Fig. 4.3.3-9. Locations of Observation Wells

In model calibration with WASH123D, an approach of four steps is employed so that the more model runs can be performed and run time can be saved. Step 1: Calibrating coupled 2D/3D flow model. Step 2: Calibrating the 1D flow model. Step 3: Verifying the calibrated model obtained from Step 1 and Step 2. Step 4: Validating the coupled 1D/2D/3D model. This report presents primary results of Step 1. The complete modeling activity of the BBCW project is still undergoing and should be referred elsewhere (Cheng et al., 2006).

Table 4.3.3-1 lists the estimated range of hydraulic conductivities used in the beginning of the calibration processes.

Table 4.3.3-1 Estimated Hydraulic Conductivity for Initial Guesses in Calibration

Geologic Unit	Hydraulic Conductivity range (ft/day)
Top surface soil layers	0.01 to 10
Miami Oolite	10,000 to 40,000
Ft Thompson Formation	1000 to 20,000

The observed stages of overland flow and groundwater wells from May 1, 1999 through April 30, 2000 are used for the model calibration. Four samples of plotting the computed and the observed values at four represented locations are shown. Figure 4.3.3-10 shows the plotting results in east coastal ridge area (S-182). Figure 4.3.3-11 shows the plotting results in the water supply wells area

(G-551). Figure 4.3.3-12 shows the plotting results in the east of Homestead airport (G-1363). Figure 4.3.3-13 shows the plotting results of Model Land area (G_3354)

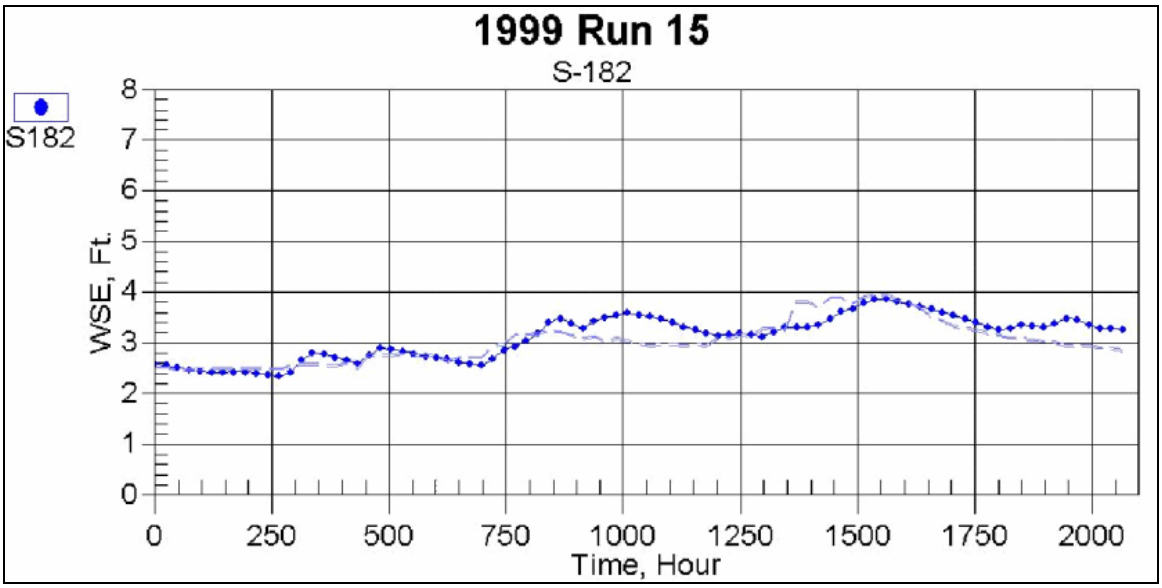

Fig. 4.3.3-10. Results in the East Coastal Ridge Area (S-182)

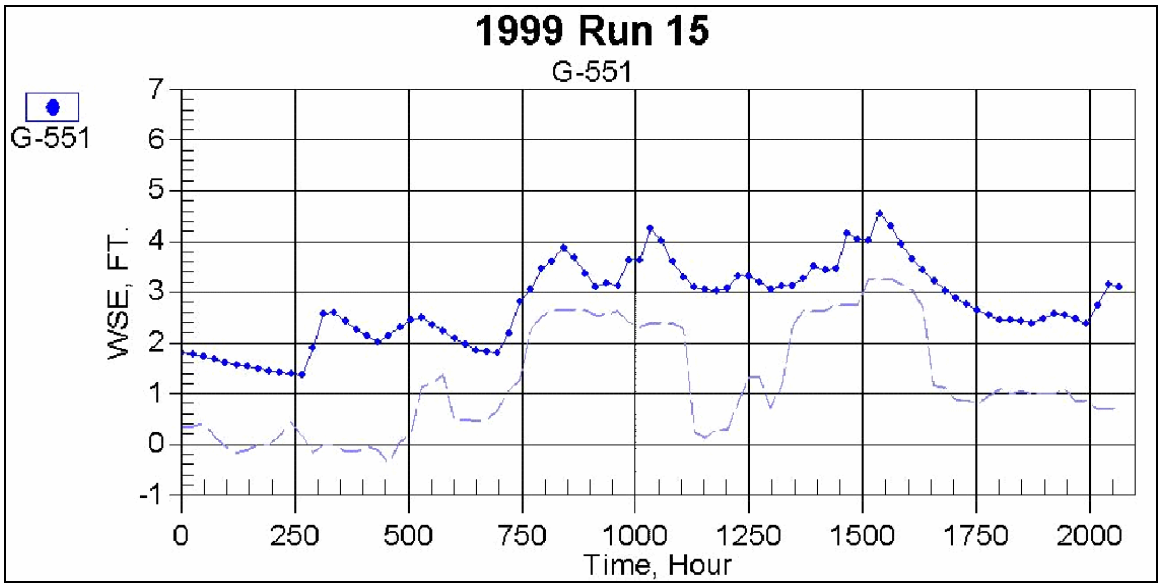

Fig. 4.3.3-11. Results in the Water Supply Area (G-551)

Fig. 4.3.3-12. Results in the East of Homestead Airport (G-1363)

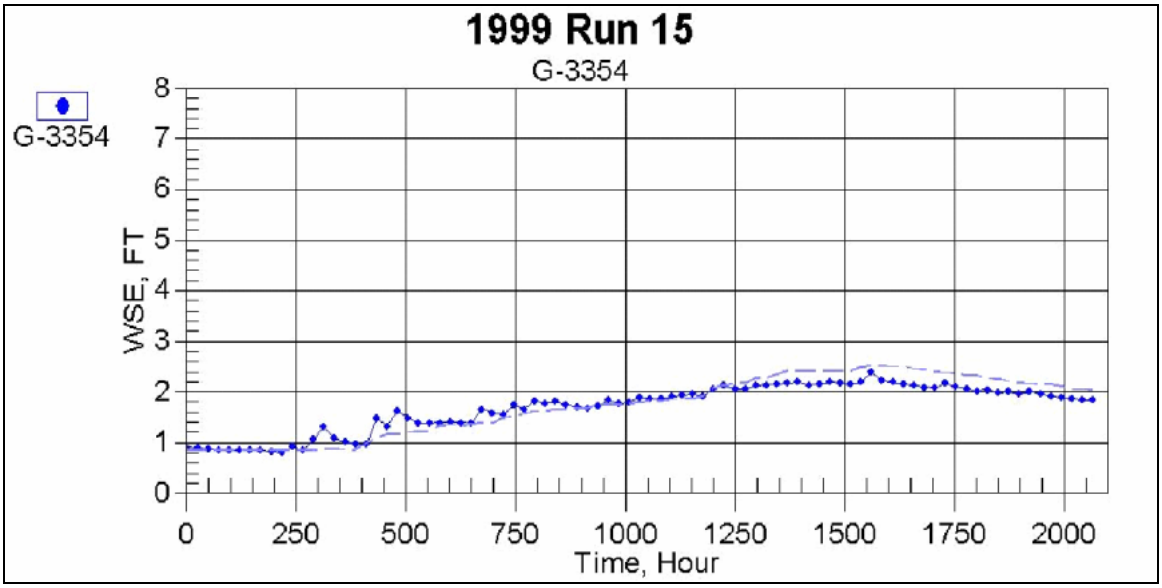

Fig. 4.3.3-13. Results in the Model Land Area (G-3354)

Figures 4.3.3-10 through 4.3.3-13 indicate that the model responds well to the observed stage fluctuations except for the case near the water supply wells and the computed stages are sensitive to the rainfall events as comparison to observed stages. Further investigation is needed to find out the discrepancies between simulations and measurements near the supply wells.

4.3.4 Stormwater Treatment Area.

Artificial treatment wetlands have been extensively used for wastewater treatment or stormwater nutrient removal in the United States of America. Typically, these surface water impoundments are built for flow-through treatment of stormwater by plant intakes of nutrients or pollutants.

In south Florida, the Everglades restoration effort has led to the design and construction of a series of constructed wetlands called Stormwater Treatment Areas (STAs) to reduce phosphorus level from stormwater runoff before they can enter the Everglades protection areas (SFWMD, 2004a). These constructed wetlands were located on former natural wetlands or farmlands that have strong hydraulic connection with the underlying highly conductive surficial aquifers.

Until recently, the hydraulic models applied for the design and management of these STAs are quite limited in scope and details. Most built models are two-dimensional model for steady state flow (for example, Burns & Mcdonell, 2000, 2003 and SFWMD, 2001). They are good for design purpose or as a screening tool but lack some important details. More detailed two-dimensional hydraulic models of existing STAs are being built for management and operation needs. They are calibrated and validated with historic time series data, considering only the two-dimensional surface flow (Sutron Corporation, 2004).

RMA2 (Norton, et al., 1973) and FEMWMS-FLO2DH (Froehlich, 2002) are the two popular two-dimensional surface water flow model codes for modeling wetland hydraulics. They were originally developed for coastal hydrodynamic modeling. Some limitations need to be addressed before they can be applied for wetland simulations. The incorporation of hydraulic structures, explicit representation of rainfall and evaporation, and treatment of wetting and drying are some examples. Swain et al. (2004) has described their experience in adapting and modifying the USGS SWIFT2D (Leendertse, 1987) originally developed for coastal tidal flow, to simulate the southern Everglades wetland hydrology. WASH123D does not have these limitations (Yeh et al., 2005).

This WASH123D application is an example of coupled surface/subsurface water flows in a constructed wetland for stormwater treatment in south Florida. Stormwater generated from farmlands is flown through the wetland for nutrient removal by wetland plants. The inflow and outflow rates are controlled by hydraulic structures. A significant portion of the inflow volume can be infiltrated into the highly conductive surficial aquifer.

Current two-dimensional hydraulic models cannot handle seepage losses properly. An integrated surface/groundwater model is needed to study the losses through bottom and perimeter levees due to dynamic interactions of surface flow within and groundwater flow underneath the treatment area. One-dimensional canal flow is also needed to simulate inflow/outflow and seepage collection. The impact of neglecting seepage loss is a likely distorted hydraulic model.

The purpose of a hydraulic model of a constructed wetland is to evaluate the hydraulic performance under different flow conditions. The hydrodynamic component is also a pre-requisition of the reactive transport computation because the transport and fate of nutrients including phosphorus and nitrogen are described with biogeochemical reactive transport equations. All these modeling

objectives can be effectively acheved using WASH123D.

The study area selected for this demonstrative modeling study is a typically constructed wetland in south Florida. The background information is excerpted from the STA-6 data (SFWMD, 2004b). The total area of the treatment cells is about 870 acres. There is a supply canal along the western boundary and a discharge canal located at the eastern boundary. Stormwater runoff is pumped into the north end of the supply canal and enters the marsh area through three inflow weirs. Eventually, treated stormwater is collected by outflow structures and flows into the discharge canal (Figure 4.3.4-1). In Figure 4.3.4-1, the supply canal is adjacent to and in parallel to L-3 borrow canal. The three inflow weirs are labeled as G-601, G-602 and G-603. Stormwater runoff enters the supply canal via the G-600 pump station. The outflow structures are G-354A through G-354C and G-393A through G-393C. They connect the treatment cells 3 and 5 with the discharge canal.

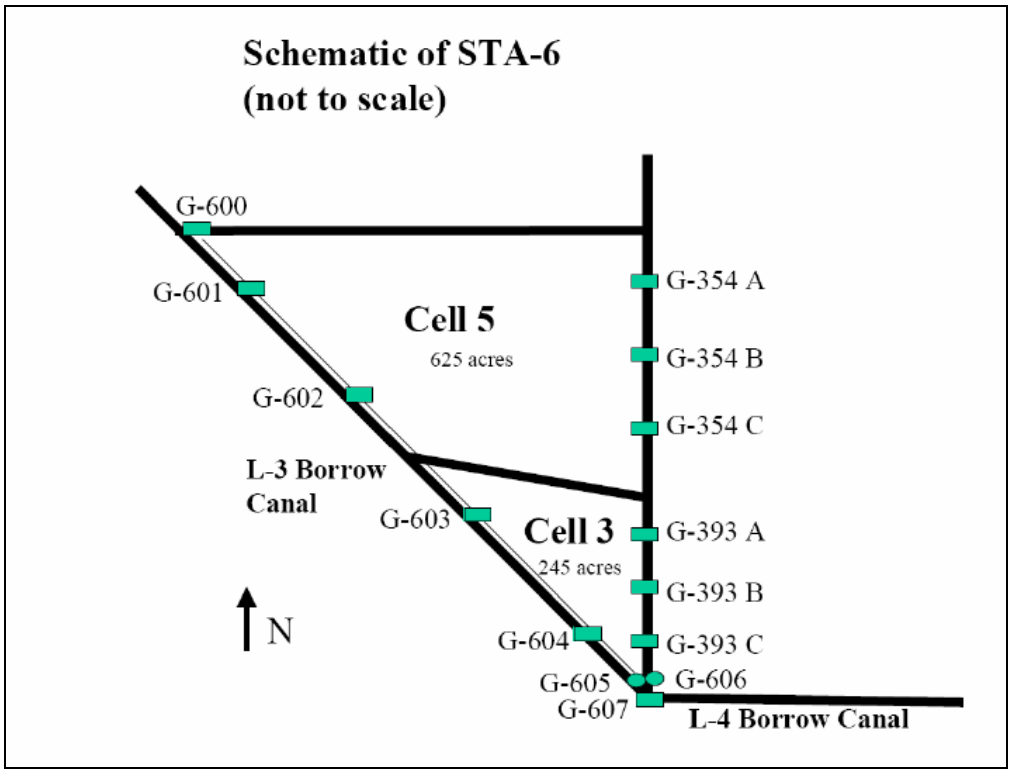

Fig. 4.3.4-1. Schematic Map of STA-6 Layout (SFWMD, 2004b)

The conceptualization of the study area leads to a relatively closed flow system. Stormwater runoff is pumped into the supply canal and flow into the treatment cells through control structures. The treated water is discharged at the downstream into the discharge canal and eventually enters the Everglades protection areas.

The surface water flows can be simulated by two-dimensional surface flow only or by coupled one-dimensional canal flow and two-dimensional flows. Vegetations were built into the treatment cells. They are categorized as emergent cattails and submerged aquatic vegetation (SAV). Previous studies have demonstrated that a water depth-dependent friction coefficient is appropriate for vegetation (Yen, 1992 and Wu et al., 1999). The base value of Manning's n used ranges from 0.095 to 0.95 for the above mentioned vegetation types.

For numerical simulations, the underlying surficial aquifer was vertically divided into several layers, the top two layers, extending from land surface to a few ft in thickness, are the poorly permeable peat and the lower layers are composed of sand or lime rock. Figure 4.3.4-2 shows the three-dimensional finite element mesh, which is made of 8,602 triangular elements with 5,302 nodes, for modeling subsurface flow. For this preliminary simulation, the model domain was selected up to the location of the supply canal and discharge canal. These canals are hydraulic divides for subsurface flow.

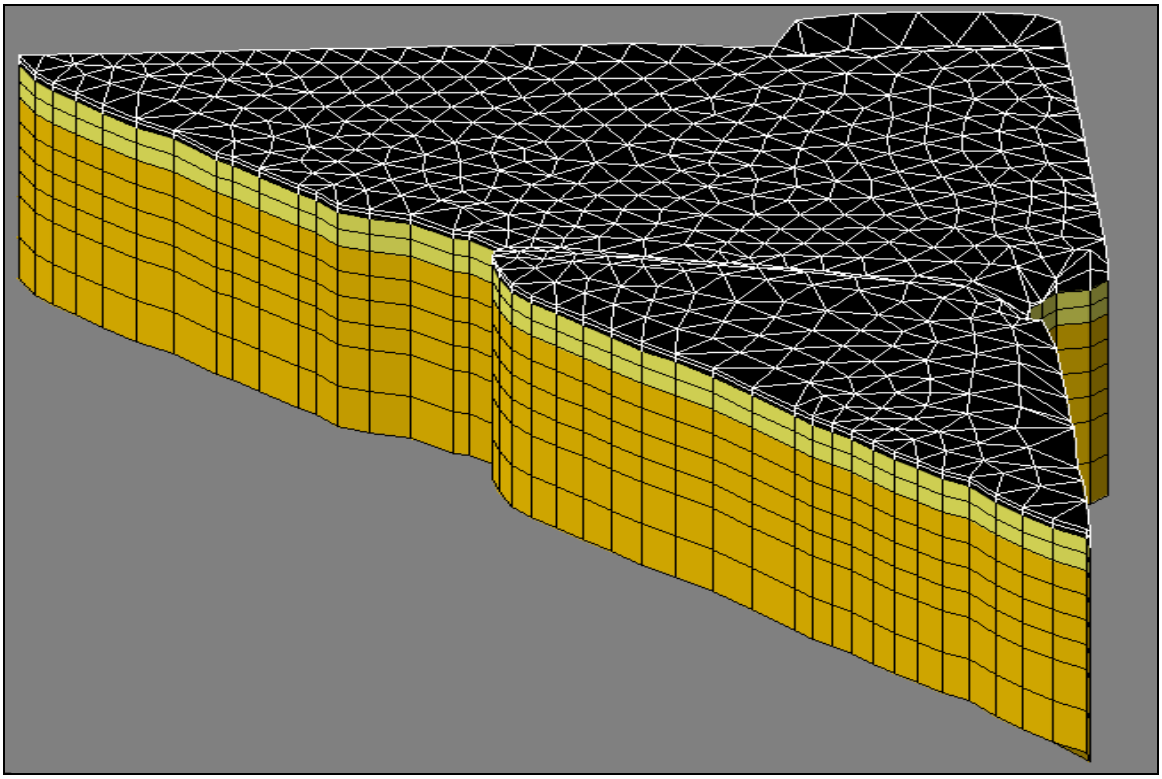

Fig. 4.3.4-2. Three-Dimensional Subsurface Finite Element Mesh

The hydrogeology was obtained from some relevant reference sources (Fish, 1988 and Harvey et al., 2002). Detailed local hydro-geological data was not available and an average value of hydraulic conductivity was applied. The initial value of saturated hydraulic conductivity used in the model runs is listed in Table 4.3.4-1.

Table 4.3.4-1 Value of Hydraulic Conductivity Used in the Simulation

Model Layer	horizontal	vertical	horizontal	Vertical
	Ft/hr	ft/hr	ft/day	ft/day
Layer 1	35	0.35	840	8.4
Layer 2-3	350	3.5	8400	84
Other layers	3500	35	84000	840

A 10-day simulation was carried out with historic flow and stage data. The total simulation time is 240 hours (10 days). A time step of 15 minutes was applied for one-dimensional canal and two-dimensional overland flows and a time step of 12.0 hours was used for three-dimensional subsurface flow. Three cases were simulated.

Firstly, two-dimensional surface flow only was modeled with the diffusive wave approximation. This was compared with model results from solving for the full shallow water equations by other two-dimensional surface water flow codes. Since the diffusive wave approach is applied in simulating the coupled surface and groundwater flows, for consistent, the diffusive wave option rather than the fully dynamic wave option is used in simulating two-dimensional surface water flow only. A by-product of this approximation is to assess the validity of the diffusive assumptions.

A different two-dimensional mesh from that shown in Figure 4.3.4-2 was designed for this case, in which the canals were included as a part of the two-dimensional finite element mesh rather than as an one-dimensional mesh. Simulation results show that the diffusive wave approximation can be applied to such a two-dimensional sheet flow and with the same Manning' n value; the diffusion wave model yields only a slightly higher water level than the full shallow water equations. The water surface elevation at time = 84.0 hours was plotted in Figure 4.3.4-3. Specified stage boundary conditions were applied to the northern end of the supply canal (upper left corner) and the downstream end of the discharge canal (lower right corner), respectively. An animation showing the spatial-temporal distribution of stages is attached in Appendix A (File Name: 2D_only(4-3-4).avi). Readers can visualize this move by clicking the file contained in the attached CD.

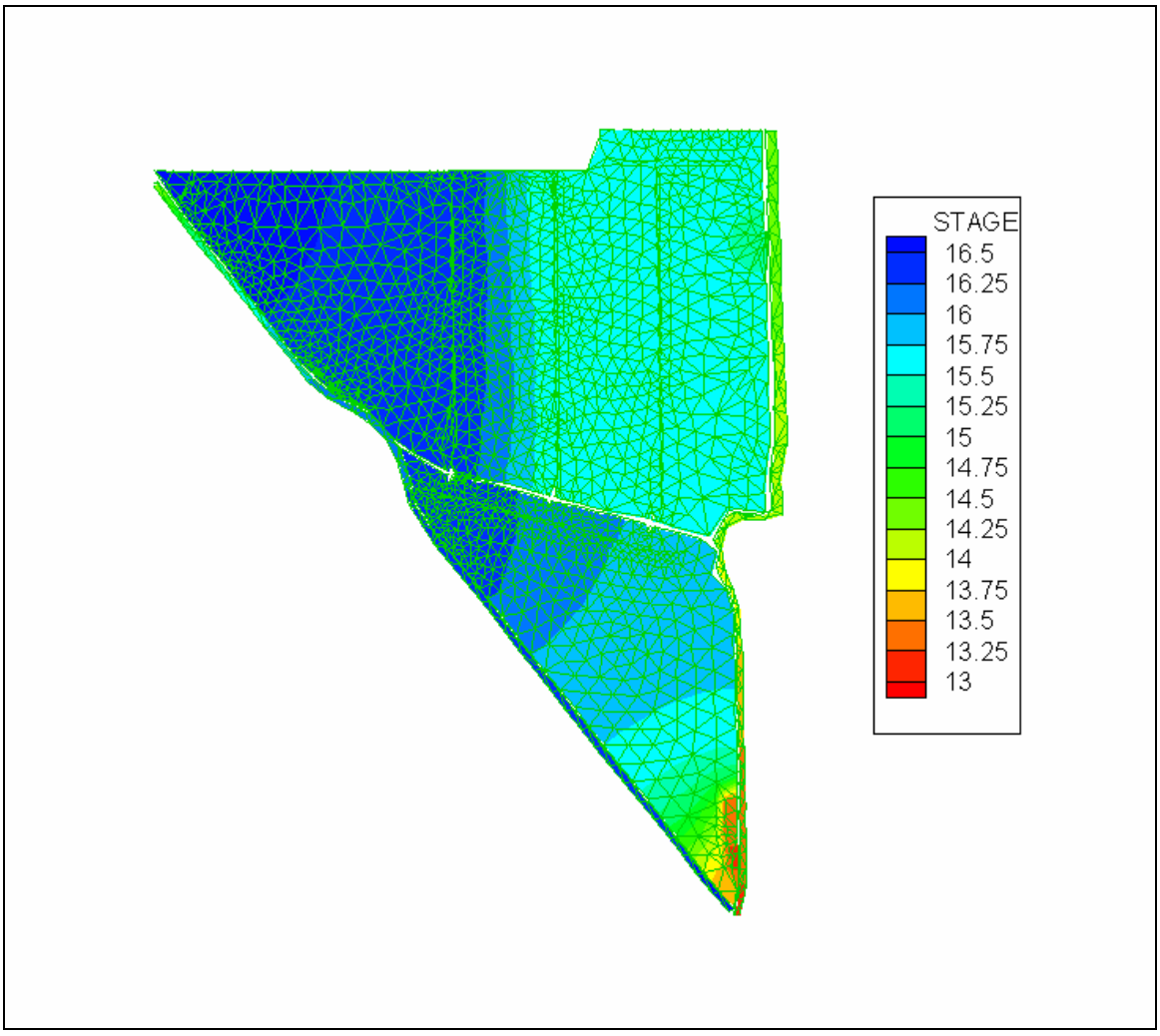

Fig. 4.3.4-3. Simulated Water Surface Elevation at Time = 84.0 hours (ft NGVD)

Secondly, two-dimensional surface flow was coupled with three-dimensional subsurface flow by using the finite element mesh in Figure 4.3.4-2. For this case, the top surface, consisting of 862 triangular elements with 482 nodes, is considered an internal boundary between the two-dimensional overland flow and three-dimensional subsurface flow on which the continuities of volumetric fluxes and pressure head/water depth are imposed. For subsurface flow, a constant specified total head of 10.5 ft NGVD was applied to the boundary nodes of the lower layers to represent the background groundwater flow in the region that is controlled by the maintained canal water level in the surrounding area. Only the vertical seepage through the bottom of the wetland is considered and the detailed geometry of the perimeter levee is not included.

The simulation results demonstrated the impact of seepage on water level in the marsh area (Fig. 4.3.4-4). The water depth at the interior marsh area (for example at node 103 in the overland regime) shows that the consideration of seepage losses has an obvious impact on water level. This indicates that without considering seepage losses, the calibration of two-dimensional hydraulic model may over-estimate model parameters (for example, Manning' n value). The magnitude of this

difference also depends on the hydraulic conductivity value.

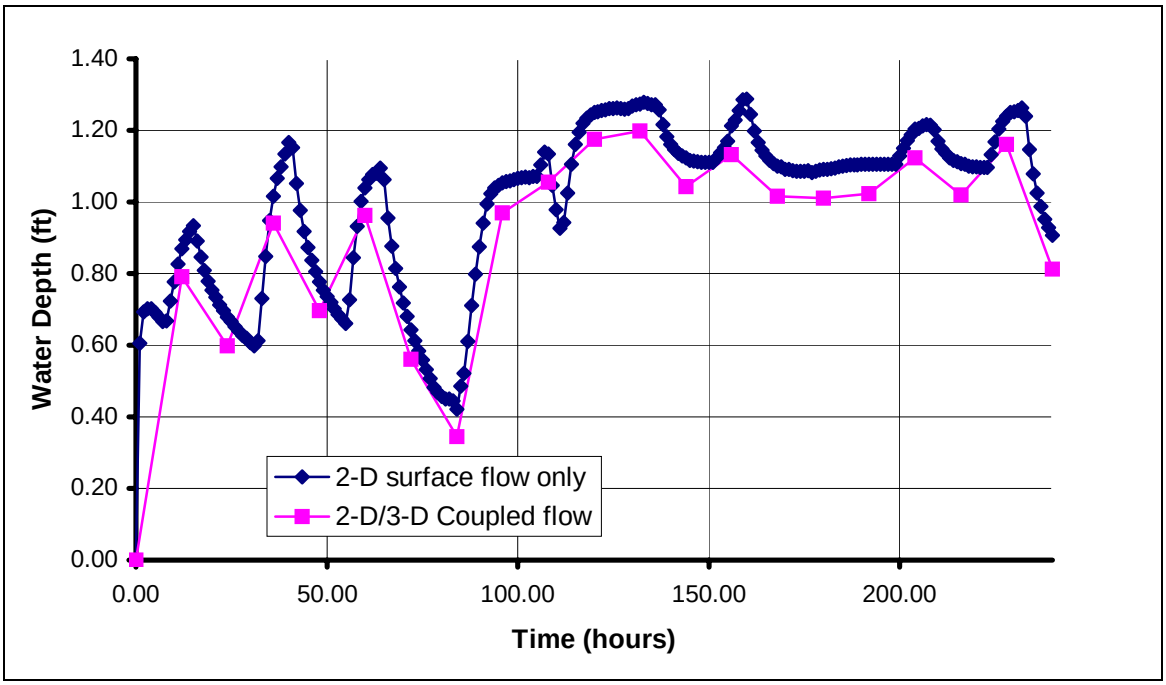

Fig. 4.3.4-4. Water Depth at 2-D Overland Node 103

Thirdly, the flow in supply canals was simulated as one-dimensional channel flow, not included as partial domains of two-dimensional overland flow. It is coupled with overland flow and groundwater flow. The one-dimensional canal flow interacts with two-dimensional overland flow and three-dimensional subsurface flow through their corresponding boundary nodes. In a test model run, the supply canal was simulated with 43 nodes and stormwater enters from the first node and the 43rd node is a dead end. Water was transferred from the supply canal to the treatment cells by two simplistic side weirs. However the discharge canal is considered as a part of the two-dimensional domain. Figure 4.3.4-5 is a contour plot of the vertical component of the subsurface Darcian velocity (ft/hr). It can be seen that the greater magnitude occurs at the vicinity of the supply canal and discharge canal.

The seepage rate depends on the hydraulic gradient and the hydraulic conductivity of the underlying porous media (peat, sand, and limerock). The canals are acting as hydraulic divides for the subsurface flow. The supply canal is a losing stream while the discharge canal is a gaining stream.

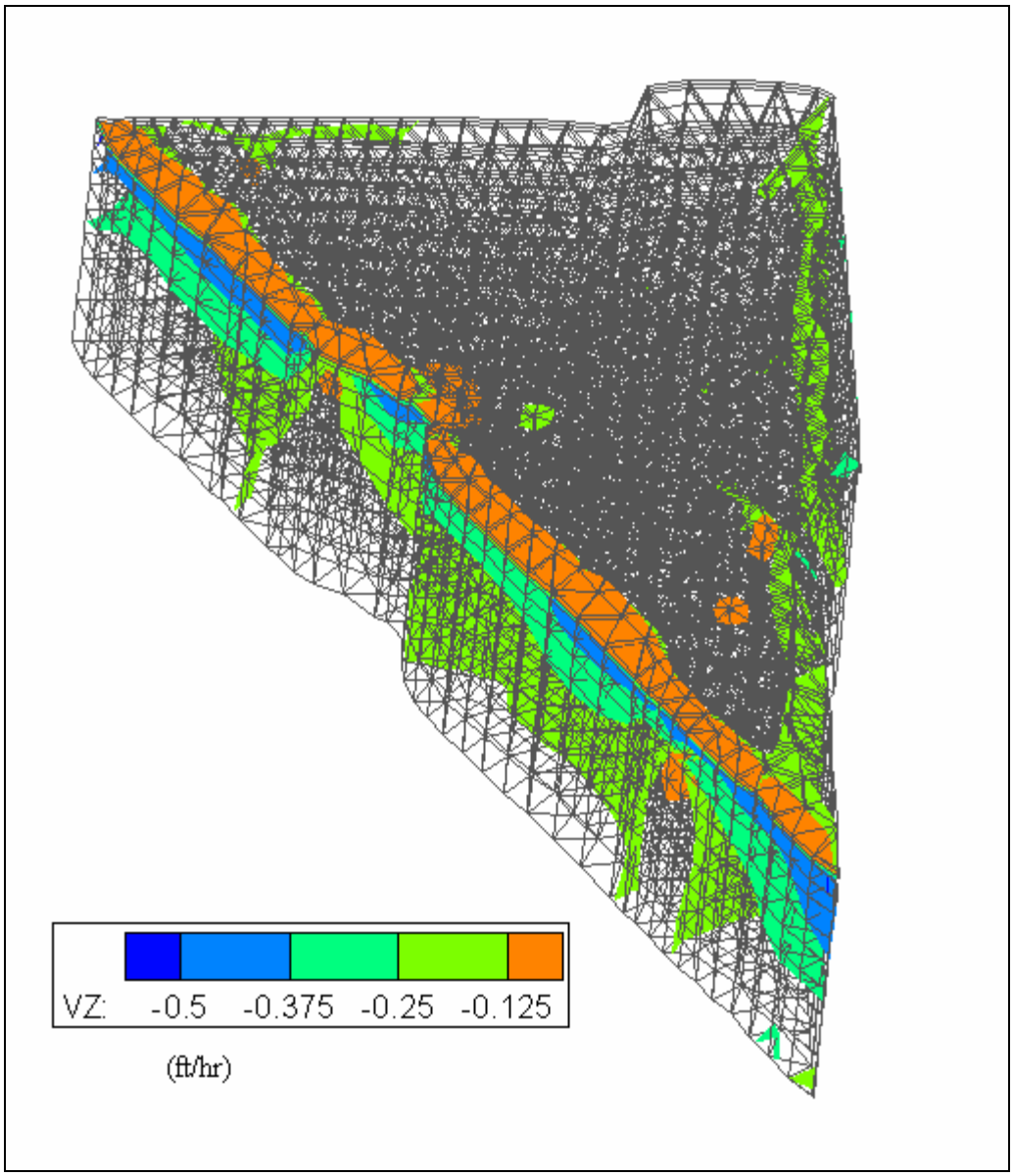

Fig. 4.3.4-5. Contour Map of Vertical Component of Subsurface Darcian Velocity (ft/hr) (Time = 228.0 hours)

4.3.5 Reservoir and Canal Networks Modeling for Evaluations of Storage Values in Northern Beach County in Florida.

The Reservoir Model and the River Model are two major components of WASH123D. The reservoir module takes an approach of water and energy budget, in which evaporation and transpiration modeled, not inputted. The Reservoir Model and the River Model were used for hydraulic modeling of surface water storage areas and canal networks in the study area of northern Palm Beach County (Fig. 4.3.5-1). The canal system is composed of the L-8 Canal, the M-Canal, and the East and West Branches of C-18 Canal. The surface water storage areas include a number of reservoirs within the study area. Details of this example can be found elsewhere (Wanielista et al., 2004).

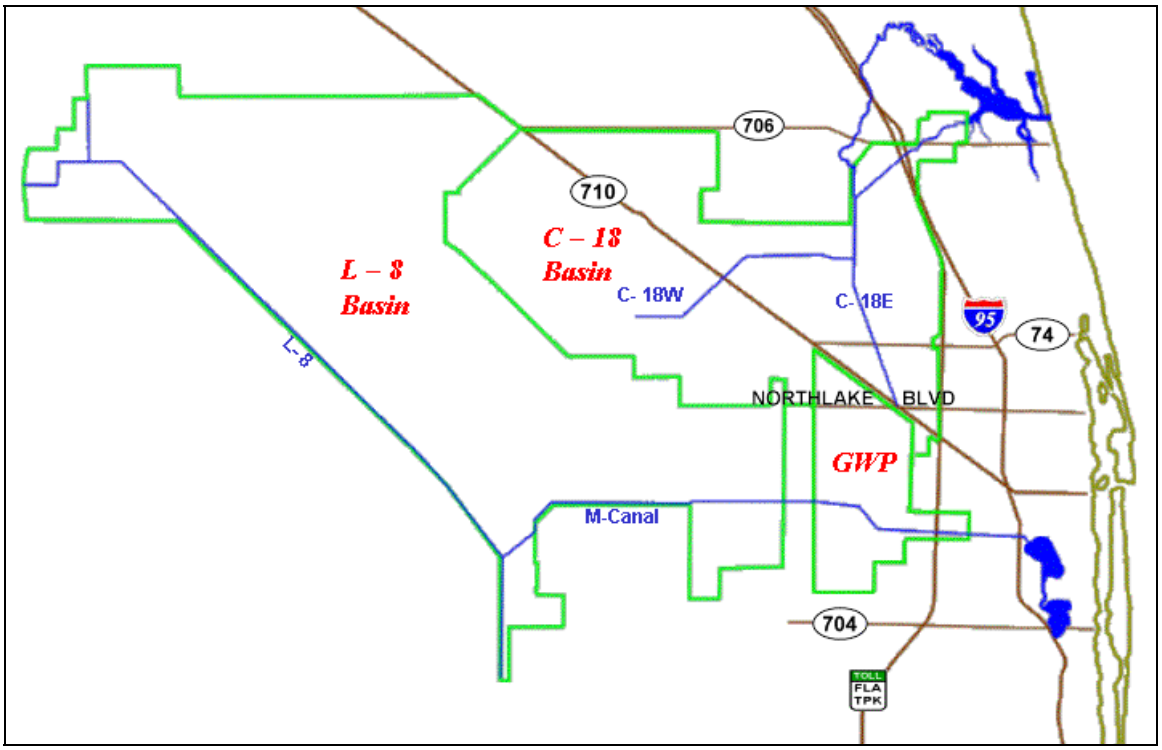

Fig. 4.3.5-1. Study Area Boundary and Local Roads and Landmarks in Northern Beach County

Many internal and external boundary conditions and pumping operations are included as shown Tables 4.3.5-1 and 4.3.5-2. In the River Model, the one-dimensional river channel is divided into reaches. A reach is a river channel segment bounded by hydraulic structures, river junctions, pump stations, or external boundaries of the modeling area. If the end node of a reach is an internal hydraulic structure or a river junction, the internal boundary conditions summarized in Table 4.3.5-1 are imposed. For internal hydraulic structures, the discharge is obtained from analytic formula or rating curve of the structure. Two types of river junctions are listed in Table 4.3.5-1. For a junction without storage capacity, the sum of discharge from all reaches connected at the junction should be zero. For a junction with storage capacity, such as a lake or a reservoir, the end node of the reach

will be treated as an external boundary node.

Table 4.3.5-1 Internal Boundary Conditions

Internal Boundary	Description	Boundary Conditions
Weir	Represents one-dimensional flow transfer by weirs.	Discharge is determined by weir formula or rating curve of the weir.
Gate	Represents one-dimensional flow transfer by gates	Discharge is determined by gate formula or rating curve of the gate.
Culvert	Represents one-dimensional flow transfer by culverts	Discharge is determined by culvert formula or rating curve of the culvert.
Non-Storage Junction	Represents non-storage junctions of one-dimensional river branches.	Sum of discharge from all reaches at the junction equals to zero.

If the end node of a reach is an external boundary, an external boundary condition is applied. There are six types of external boundary conditions showing in Table 4.3.5-2. The Dirichlet boundary condition gives the water depth or stage as a function of time in the simulation. The discharge at the external boundary can be given as a function of time or in the form of a general rating curve. Two special external boundary conditions are designed to simulate the elevation controlled gate and the demand controlled gate, where the gate openings and the rate at which the gate opens and closes are determine by water elevation and demanding discharge, respectively. On a river node where the river is connected directly to a reservoir or lake, the reservoir/lake boundary condition is imposed. Under this circumstance, the River Model is solved in coupling to the Reservoir Model.

The water transferred between these modules is modeled by coupling of the 1-D model and the 0-D model. Two types of coupling between the River Model (1-D model) and the Reservoir Model (0-D model), the on-line coupling and the off-line coupling, are identified. An on-line reservoir is defined as a reservoir that directly connects to river reaches as shown in Figure 4.3.5-2. In the River Model, the coupling is through the external boundary conditions for river nodes at the connection location, where water stage obtained from the Reservoir Model is imposed. In the Reservoir Model, the discharges obtained from the River Model at the connection location are used as inflow and outflow to update the water stage of reservoir. The coupling between the river and the on-line reservoir is modeled in the river-lake module.

Table 4.3.5-2 External Boundary Conditions

Boundary Type	Description	Boundary Conditions
Dirichlet	Water depth or stage is given at all time.	$h = h_B(t)$
Normal Flux	The volumetric flow rate is given at all time.	$Q = Q_B(t)$
General Rating Curve	The volumetric flow rate is given as a function of water depth or stage.	$Q = Q_B(h)$
Rating Curve of Elevation Controlled Gate	The volumetric flow rate is given as a function of water elevation and elevation controlled gate opening.	$Q = Q_B(h, Go(h))$
Rating Curve of Demand Controlled Gate	The volumetric flow rate depends on water elevation and demand controlled gate opening. The gate opening is given as a function water demanding discharge through the gate.	$Q = Q_B(h, Go(Q_D))$
Reservoir/ Lake	The river is connected to a lake/reservoir. It is used to couple the river flow with on-line reservoirs.	$H = H_R$

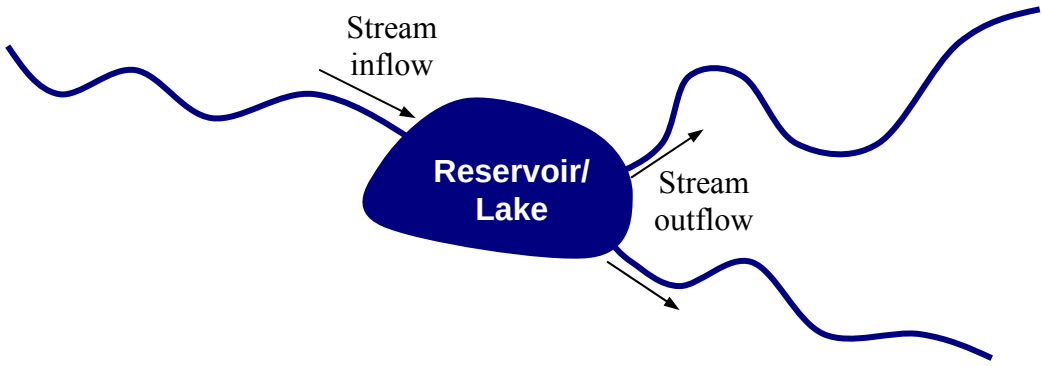

Fig. 4.3.5-2. Schematic Diagram of an On-line Reservoir/Lake

An off-line reservoir is defined as a reservoir that does not directly connect to rivers. A simple illustration of the off-line reservoir is shown in Figure 4.3.5-3. For an off-line reservoir, the water transfer between the reservoir and the river is accomplished through pump stations and/or hydraulic structures, which are implemented through two auxiliary modules: the pump module, and the

gravity-driven hydraulic structure module. A description of these modules can be found elsewhere (Wanielista, et al., 2004).

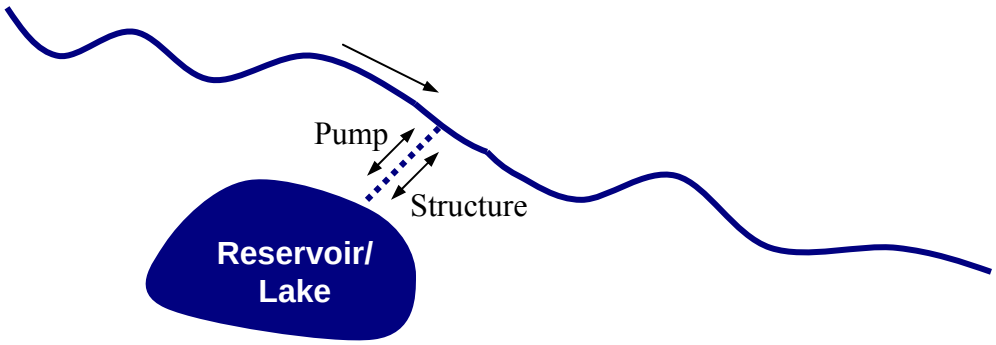

Fig. 4.3.5-3. Schematic Diagram of an Off-line Reservoir/Lake

Figure 4.3.5-4 provides a schematic representation of the model's layout. The primary canal network system consists of eight canals: the L-8 Canal, L-8 North Tieback Canal, L-8 South Tieback Canal, L-8 Outfall Canal, M-Canal, C-18 Canal West Branch, C-18 Canal East Branch, and SIRWCD C-14 Canal. There are four water storage areas: Indian Trail Improvement District (ITID) impoundment area, Grassy Waters Preserve (GWP), Southern L-8 Reservoir (Rock Pits), and C-18 Reservoir.

The L-8 Canal connects Lake Okeechobee to Water Conservation Area 1 (WCA 1). It starts at Culvert 10A at the north end. At the south end, the connection to WCA 1 is by way of S-5A structures.

The L-8 North Tieback Canal drains a small portion of the L-8 basin. It connected with L-8 Canal just east of structure S-76.

The L-8 Outfall Canal connects the ITID impoundment area and the L-8 Canal. On its east end, it makes connections with the impoundment through a culvert structure with riser. On its west end, the connection is also in the form of culvert with riser.

The L-8 South Tieback Canal connects the L-8 Canal and the M-Canal. The northeast end of the canal is a pump station PS-1 (Control #2) owned and operated by the City of West Palm Beach.

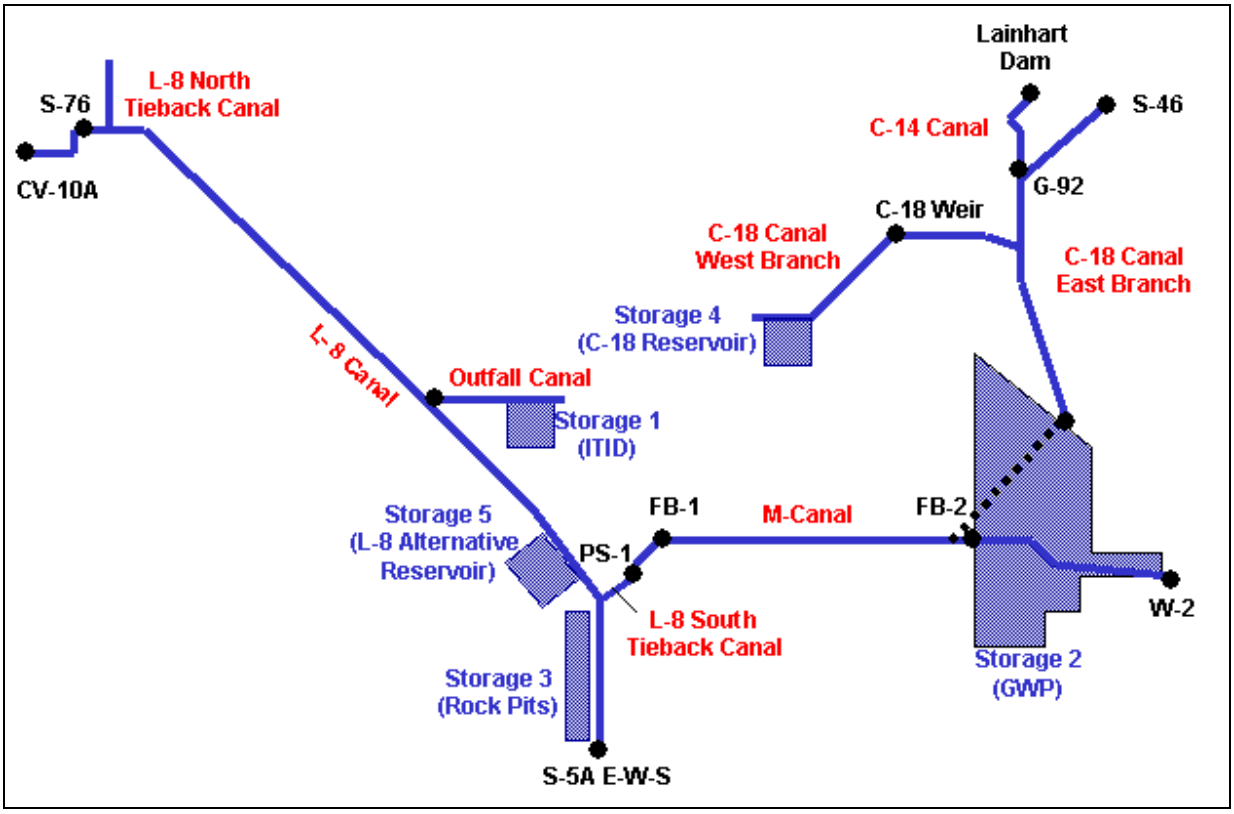

Fig. 4.3.5-4. Model layout of Northern Palm Beach County: Storage Values

The M-Canal starts at PS-1 and extends eastward. In the scope of this model, the east boundary of the M-Canal is a weir structure W-2 located west of the Haverhill Road.

The East Branch of C-18 Canal starts at GWP and extends northward. In the scope of current model, the C-18 Canal ends at structure S-46 which supplies water to the Southwest Fork of the Loxahatchee River.

The West Branch of C-18 Canal begins at the northeast corner of section of Range 40E-Township 42S. It extends eastward and confluences with the East Branch.

The SIRWCD C-14 Canal originates at the G-92 Structure and ends at Lainhart dam – a small weir structure (with a small culvert) located upstream of the Northwest Fork of the Loxahatchee River.

Fifteen canal reaches were created for modeling purpose as shown in Figure 4.3.5-5. Each reach is delimited either by structure, junction, dead end, or external boundary. The length and description of each reach are given elsewhere (Wanielista, et al., 2004).

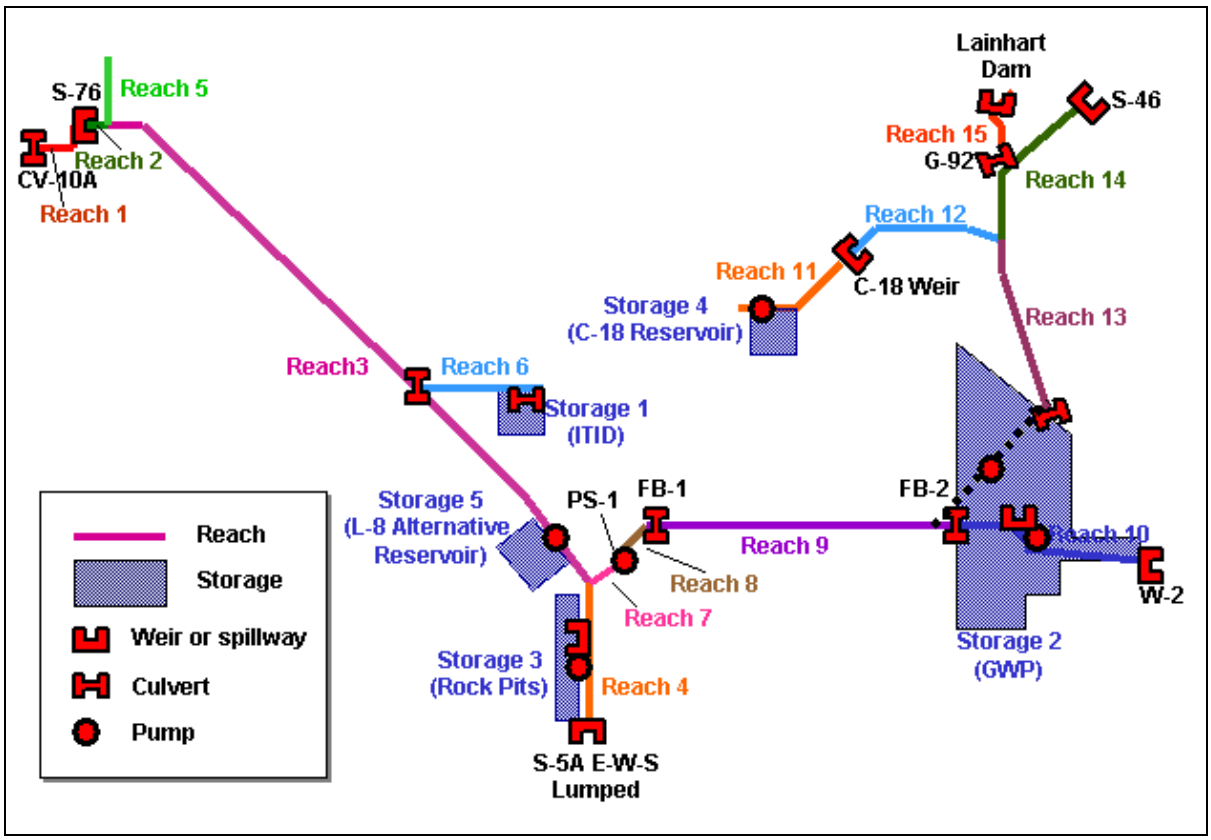

Fig. 4.3.5-5. Canal Reaches in the Model

Water storage area and reservoirs are considered as key components in a regional water management strategy. There are three existing water storage areas (Fig. 4.3.5-5): the Indian Trail Improvement District (ITID) impoundment area (Storage 1), the Grassy Waters Preserve (GWP) (Storage 2), and the Southern L-8 Reservoir (or Rock Pits) (Storage 3). The two proposed surface water reservoirs include the C-18 Reservoir (Storage 4) and the L-8 Alternative Reservoirs (Storage 5). The reservoir operations were simulated using the reservoir module in WASH123D. The connections between the reservoirs and canal reaches are by way of hydraulic structures and pump stations.

The Indian Trail Improvement District (ITID) impoundment area located at a sub-basin of the L-8 Basin (Fig. 4.3.5-1). The maximum storage of the area is around 3300 acre-feet at a water depth of 5 feet. The connection between the impoundment area and the L-8 Outfall Canal is by way of a culvert structure with riser. The riser is in the impoundment area and the culverts open to the L-8 Outfall Canal.

The Grassy Waters Preserve (GWP) formerly known as the City of West Palm Beach Water Catchment Area is an approximately 19 square mile impounded area that is predominantly wetland in nature. Currently, GWP is owned and maintained by the City of West Palm Beach and serves as a surface water storage reservoir for public water supply. Water from this wetland is discharged to the east through the M-Canal to Lake Mangonia and Clear Lake, and subsequently enters the City's water treatment plant in West Palm Beach.

The Southern L-8 Reservoir is proposed to use the abandoned rock mining pits to provide a combined above-ground and in-ground storage capacity of approximately 48,000 acre-feet. It is located immediately west of the L-8 Canal and near the junction of L-8 and C-51 Canals. An area of 1,200 acres may be available and the operation depth is 35 feet (20 feet in ground and 15 feet above ground). The purpose of this reservoir is to increase water supply availability, and attenuate discharge to Lake Worth Lagoon and provide compatible drainage benefits for northern Palm Beach County area. It will also provide flows to enhance hydroperiods in the Loxahatchee Slough, increase base flows to the Northwest Fork of the Loxahatchee River, and reduce high discharges to the Lake Worth Lagoon (SFWMD, 2002).

The C-18 Reservoir was modeled on a footprint of 1,000 acres or 2,000 acres with maximum depths ranging from 10 feet to 15 feet. The total storage volume ranges from 10,000 acre-feet to 30,000 acre-feet. The connection between the reservoir and C-18 Canal West Branch is by way of a pump station with a capacity of up to 100 cfs. This reservoir is designed for the purpose of catching and storing wet season water for use during the dry season to meet the minimum flow criteria to the Northwest Fork of the Loxahatchee River.

The L-8 Alternative Reservoir was placed near the junction of the L-8 Canal and the South L-8 Tieback Canal and west side of L-8 Canal. This reservoir was modeled with a foot print of 1,000 acres or 2,000 acres. Maximum depths ranging from 10 feet to 15 feet were evaluated. The total storage volume ranges from 10,000 acre-feet to 30,000 acre-feet. A pump station with a capacity of 100 cfs connected the reservoir to L-8 Canal.

For the purpose of calibration, the flow data recorded at several sites as described in Table 4.3.5-3 were downloaded from SFWMD's online database. Under the existing condition, the conveyance between the Grassy Waters Preserve (GWP) and the East Branch of C-18 Canal is severely constrained (< 10 cfs), thus the L-8 Canal system and C-18 Canal system can be considered as decoupled. Within this project, since the daily rainfall and evaporation data for the entire area were not available, the rainfall and evaporation input to the model was on a monthly basis. Thus it would be very difficult to calibrate the model against the daily field data but using monthly data as input. Therefore, one-year accumulative discharges through the three structures listed in Table 6.11 were used to calibrate the model.

Under the assumption that C-18 Canal system is isolated from the L-8 Canal system, the amount of water that enters the C-18 Canal system is thus divided among direct rainfall, surface runoff, and groundwater seepage. Water inflows to C-18 Canal system contributed by direct rainfall onto the canal and surface runoff from the thirty two sub-basins of the C-18 drainage area can be modeled or obtained from field data. The groundwater seepage is difficult to estimate without modeling. Though the three-dimensional groundwater module of WASH123D model is capable of precisely predicting the groundwater seepage to C-18 Canal, the time frame of the project would not allow us to do so (Wanielista, et al., 2004). Thus, the estimation of groundwater seepage became part of the calibration procedure. The outlet of the system consists of two structures: S-46 and G-92. The object of the calibration is to match the cumulative discharge and the base flow at structure G92.

Table 4.3.5-3 Surface water data for model calibration

Station/ Site	Interval	Description	Start Date	End Date
S46_S	Daily	At southwest fork of Loxahatchee River	11/8/1992	9/16/2002
G92_C	Daily	G-92 culvert from C-18 to west branch of Loxahatchee River	5/10/1988	1/26/2003
LNHRT	Daily	Lainhart Dam on Loxahatchee River	4/25/1995	9/17/2002

The year of 1995 was selected for calibration, since the rainfall and evaporation input was from 1965 through 1995 and there were more field data available in 1995. Table 4.3.5-4 gives the cumulative discharge at the structures.

Table 4.3.5-4 Measured cumulative flow in 1995

Station/Site	Start Date	End Date	Cumulated Discharge (acre-feet)
S46_S	1/1/1995	12/31/1995	124230
G92_C	1/1/1995	12/31/1995	59091
LNHRT	4/25/1995	12/31/1995	59920

Structure G-92 is a gated culvert; it diverts water from C-18 Canal to C-14 Canal. The structure is operated via remote telemetry from the SFWMD Operations Control Room under a joint agreement with the SIRWCD to permit conveyance of flows to the Northwest Fork of the Loxahatchee River through Lainhart Dam. In current simulation, since the operation rule of G-92 was not provided by SFWMD, the gate was set at fixed openings, as shown in Table 4.3.6-5, 12.5% for CASE A, and 15% for CASE B.

Table 4.3.5-5 Gate opening at Structure G-92

CASE	Gate Opening of G-92
A	12.5%
B	15%

The simulation results are shown in Table 4.3.5-6. The results indicate that when the gate opening of structure G-92 was 15%, the cumulative flow through the structure is very close to the field data. Therefore, the gate opening of 15% was chosen for a series of simulations. In 1995, the field data at Lainhart Dam starts on 4/25. The cumulative flows through the structures S-46, G-92 and Lainhart

Dam from 4/25/95 to 12/31/95 are displayed in Table 4.3.5-7. Though these numbers are not matched as well as for structure G-92, generally the model calibration is still acceptable.

Table 4.3.5-6 Cumulative flow through different structures

	Cumulative Flow through the Following Structures (acre-feet) (1/1/95 -12/31/95)		
	S-46	G-92	Lainhart Dam
Field Data	124230	59091	N/A
A	111795	52980	70507
B	104770	60027	77555

Table 4.3.5-7 Cumulative flow through Lainhart Dam compared with field data

	Cumulative Flow through the Lainhart Dam (acre-feet) (4/25/95 -12/31/95)
Field Data	59920
A	57244
B	63628

The goal of the project is to study the capability of water storage reservoirs of providing supplement water to the Northwest Fork of the Loxahatchee River to meet the minimum flow request in the dry season. The minimum flow request was tested at Lainhard Dam for both CASE A and B. The target minimum flows were set at 35 cfs, 65cfs, and 100 cfs. The percent of time the target flow was met under existing conditions in the year of simulation is shown in Table 4.3.5-8. The results are the same for both gate openings at structure G-92. The percent of time that the minimum flow of 35 cfs, 65cfs, and 100 cfs were met were 70%, 60%, and 54%, respectively. As indicated by the *Loxahatchee River Minimum Flows and Levels*, over the past decade, the 35 cfs and 65 cfs flow target for the Lainhart Dam, were met about 75% and 57% of the time. To compare with the field data, the percent of time was calculated again from 4/25/95 through 12/31/95. The results are displayed in Table 4.3.5-9. In simulation with both 12.5% and 15% gate openings, the simulated time percentage is higher than field data for 65 cfs and 100 cfs, but lower for 35 cfs.

Table 4.3.5-8 Percent of time the target minimum flow is met at Lainhart Dam

CASE	Percent of Time The Following Target Flow Is Met (1/1/95 -12/31/95)		
	≥ 35 (cfs)	≥ 65 (cfs)	≥ 100 (cfs)
1-A	70%	60%	54%

1-B	70%	60%	54%

Table 4.3.5-9 Percent of time the target minimum flow is met.
A comparison with field data

CASE	Percent of Time The Following Target Flow Is Met (4/25/95 -12/31/95)		
	≥ 35 (cfs)	≥ 65 (cfs)	≥ 100 (cfs)
Field Data	79%	60%	52%
1-A	72%	69%	67%
1-B	72%	69%	67%

Figure 4.3.5-6(a) shows the hydrograph at structure G-92 with a gate opening of 12.5% in 1995 obtained from CASE A in comparison with field flow data. The hydrograph at structure G-92 obtained from CASE B is displayed in Figure 4.3.5-6(b). In this case, the gate opening of G-92 was 15%. The data in Table 6.14 and 6.15 indicates that the larger gate opening allowed the passing of more water through structure G-92. But the Figure 4.3.5-6 shows that his only happens during the wet seasons, in the dry season, both openings pass the same amount of water. The large deviations between the simulation results and the field data can be attributed to the following two factors: 1) The rainfall data used for the simulation was on a monthly basis; 2) The operation rule the gate at structure G-92 was not clear, so the gate opening was fixed in the simulation. However, in both cases, the yearly cumulative flows were quite close to the field data as shown previously in Table 4.3.5-6.

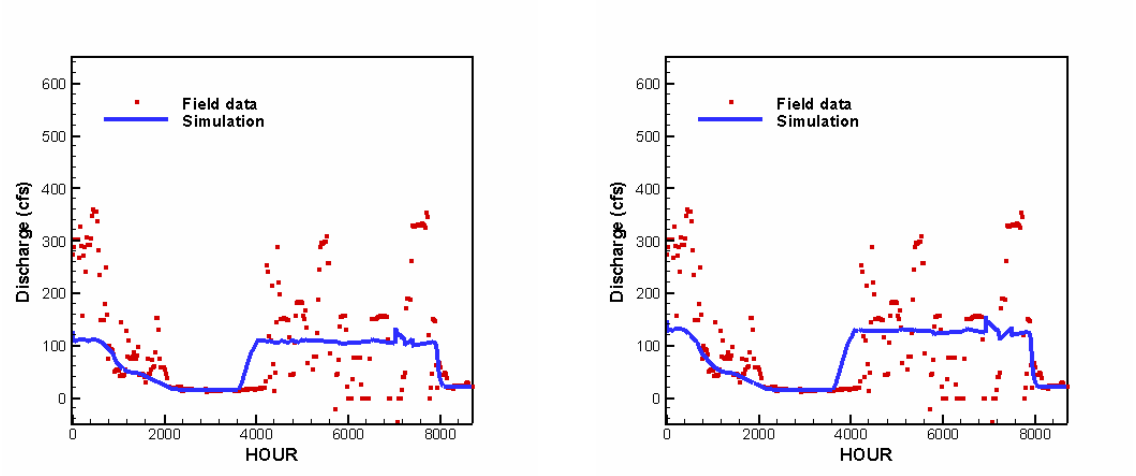

(a) CASE A (b) CASE B

Fig. 4.3.5-6. Hydrograph at structure G-92 from 1/1/95 through 12/1/95

The Lainhart Dam is an uncontrolled weir. The simulated hydrographs are displayed in Figures 4.3.5-7. Obviously the simulation results are in much better agreement with the field data than that of G-92 even though the input data was on monthly basis.

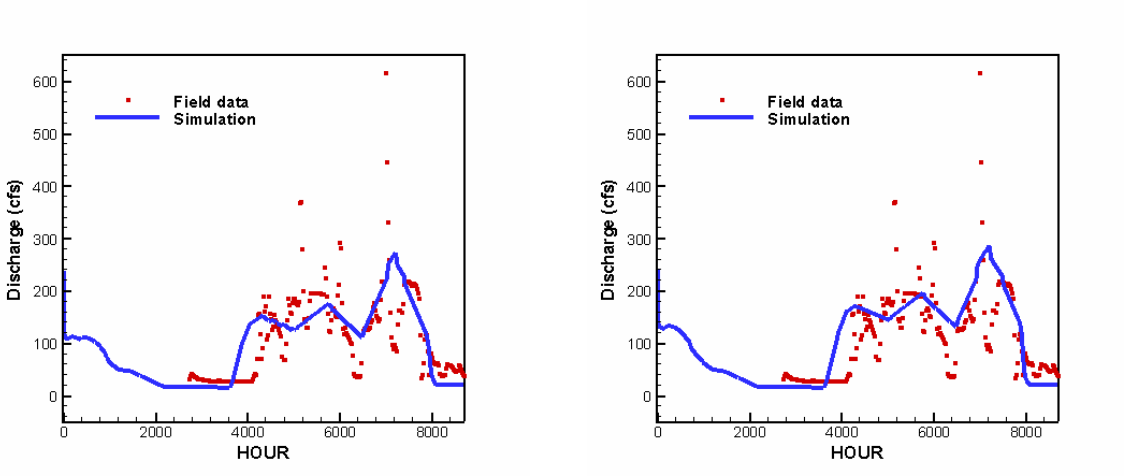

(a) CASE 1-A (b) CASE 1-B

Fig. 4.3.5-7. Hydrograph at Lainhart Dam from 1/1/95 through 12/1/95.

After successfully calibrate the model, various combinations of proposed reservoirs were investigated. The modeling of WASH123D coupled with an economic evaluation resulting in the recommendation of $2,500 per acre-ft of storage, which was in contrast to earlier studies, which estimated a cost of $5,500 per acre-ft. The study saved FDEP (Florida Department of Environmental Protection) of approximately $250 millions for the management.

4.3.6 Dade County Watershed Modeling.

This is a regional scale modeling effort for the South Florida wetlands. The Dade model domain extends from four miles west of the L-67 Extension dike to the western shore of Biscayne bay and from one mile north of the Tamiami canal south to Florida bay. Vertically, it extends from the land surface to the bottom of the surficial aquifer.

Some characteristics of this model are: (1) Strong interaction of overland flow/groundwater flow and canal flow in south Florida; (2) Complex hydraulic structure operations.

The 3-D finite element mesh for subsurface media (as shown in Figure 4.3.6-1) is complex: there are 37,760 global nodes, and 65,429 elements. There are 7 layers in vertical direction. And levees are incorporated as part of subsurface media.

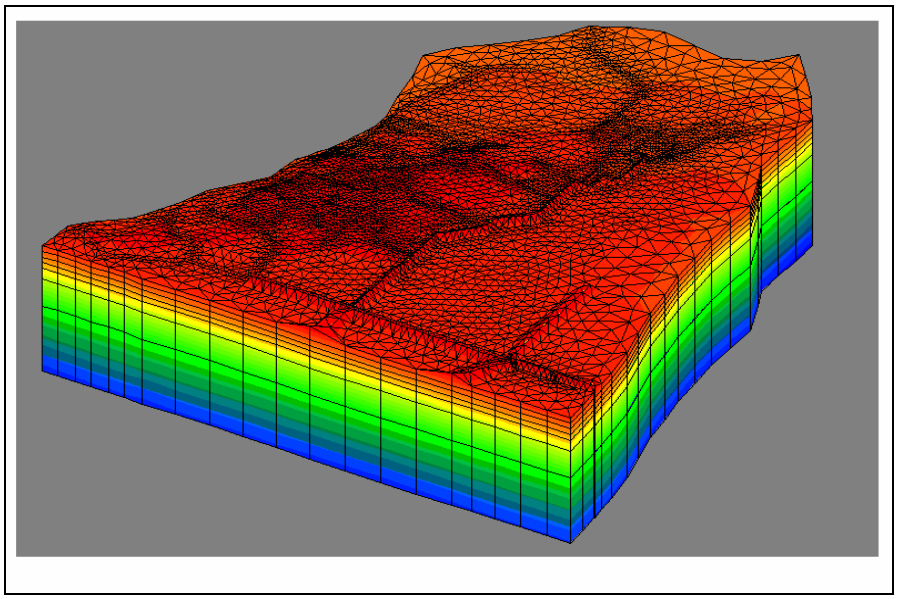

Fig. 4.3.6-1. 3-D Subsurface Media Finite Element Mesh

The boundary conditions for subsurface flow were determined from the SFWMM 2x2 model output for the northern boundary, and from structure operation records for the other sides of boundaries.

The 2-D overland flow domain consists of 4,720 nodes, and 9,347 triangular elements. Levees are included in the computation domain (Fig. 4.3.6-2). Boundary conditions were determined from structure operation records along the boundary.

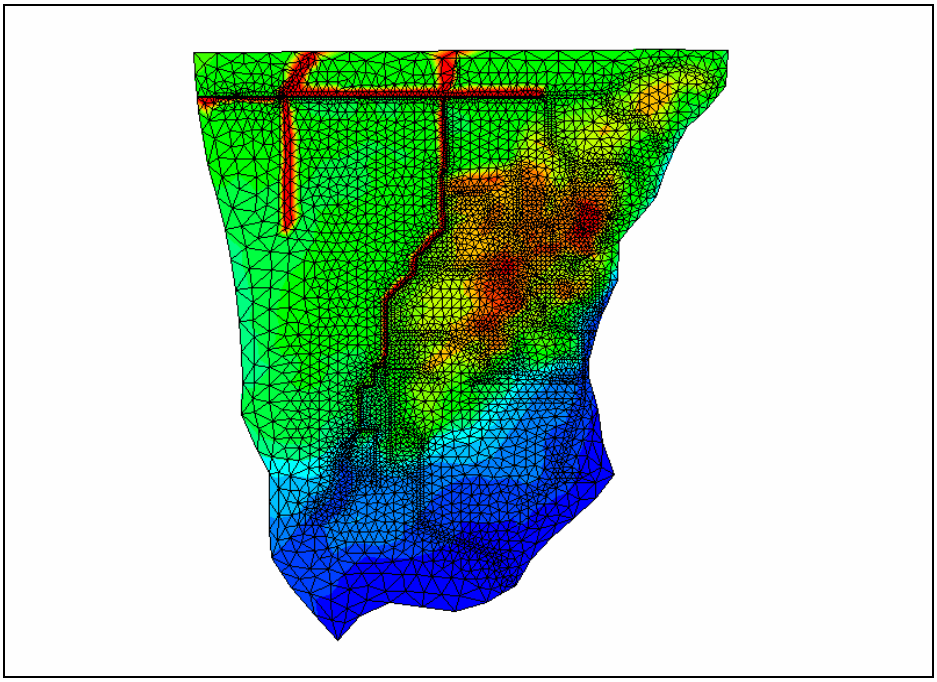

Fig. 4.3.6-2. 2-D Overland Regime Finite Element Mesh

The canal network as simplified in this simulation includes: Canal nodes: 560; Canal elements: 506; River reaches: 55; there are 20 canal junctions, and 11 interior Gates (Fig. 4.3.6-3).

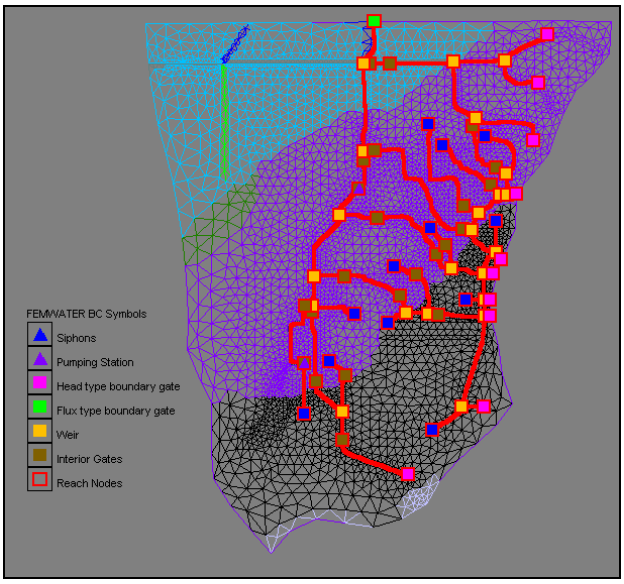

Fig. 4.3.6-3. Canal Network

The boundary conditions for subsurface flow were determined from the SFWMM 2x2 model output for the northern boundary, and from structure operation records for the other sides of boundaries.

The 1-D/2-D/3-D coupled flow simulation was first begun with a steady state of subsurface flow and the total head distribution of the steady state flow is shown in Figure 4.3.6-4. Then the steady state condition was used as the initial condition of the transient flow simulation.

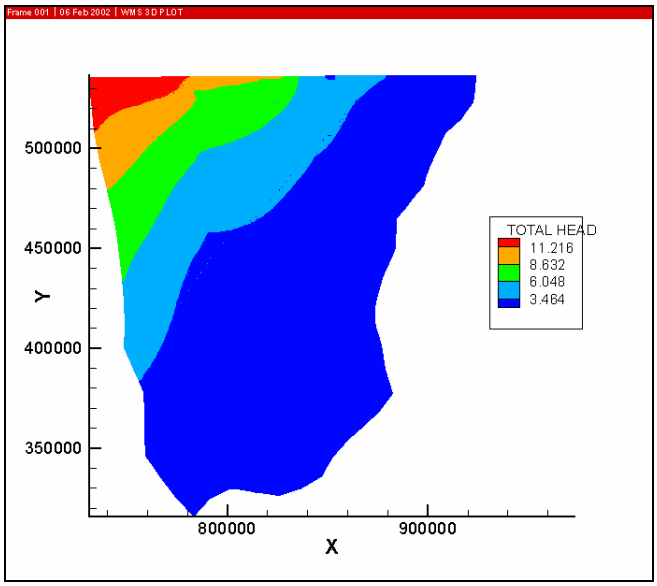

Fig. 4.3.6-4. Total Head at Steady State Subsurface Flow (feet)

Figure 4.3.6-5 and 4.3.6-6 depict the simulations result of a model run. Since the levee/dike are included as part of the subsurface media, it is demonstrated that the ground water flow from the northern boundary can bypass the less permeable levees via their underlying permeable media. It is also obvious that the canals recharge the ground water.

An animation showing the spatial-temporal distribution of water depth in surface runoff is attached in Appendix A (File Name: dade2ddepth.avi). Readers can visualize this move by clicking the file contained in the attached CD.

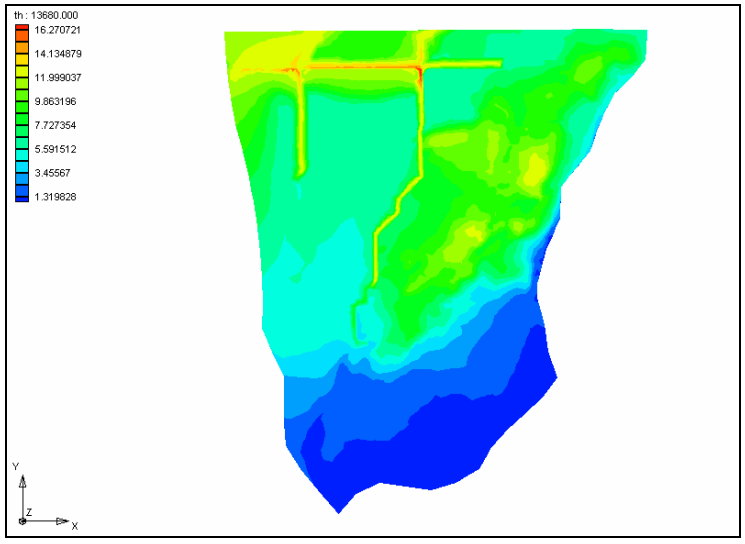

Fig. 4.3.6-5. Total Head Distribution (feet) at time=13,680 minutes (9.5 days)

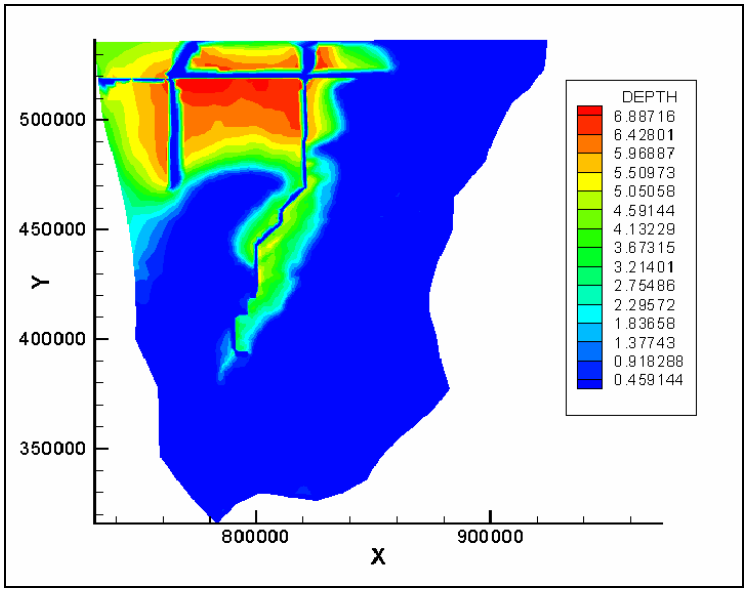

Fig. 4.3.6-6. Overland Water Depth (feet) at time = 7,000 minutes (4.86 days